STUDY ON CO2/O2-BLOWN COAL GASIFICATION IN TWO STAGE ENTRAINED FLOW GASIFIER

モハメド サイフル アラム

STUDY ON CO_2/O_2-BLOWN COAL GASIFICATION IN TWO

STAGE ENTRAINED FLOW GASIFIER

A Dissertation

Submitted to the Graduate School of Engineering

Department of Chemical Systems and Engineering

Kyushu University, Japan

In partial fulfillment of the requirements for the degree of

Doctor of Philosophy in Chemical Engineering

By

MD SAIFUL ALAM

September 2013

_____

Dr. Jun Fukai, Supervisor

Professor

Department of Chemical Engineering

Kyushu University, Japan

_____

Dr. Takayuki Watanabe, Advisory member

Professor

Department of Chemical Engineering

Kyushu University, Japan

_____

Dr. Jun-ichiro Hayashi, Advisory member

Professor

Institute for Materials Chemistry and Engineering

Kyushu University, Japan

ABSTRACT

Global energy consumption in 2030 is predicted to increase 1.4 times that in 2007, where about half of the increase will be contributed by Asia. It is also predicted that remaining years of exploitable global energy resources in sequences are: coal (122 years), uranium (100 years), natural gas (60 years) and oil (42 years). Presently, approximately 40% of electric power generation worldwide depends on coals. Because of limited exploitable oil resources and the risk for nuclear power plant, Japan now depends heavily on imported fossil fuels to meet its energy demand. The contribution of coal to total energy production is increasing day by day. However, the use of coal faces several challenges. The major one is the considerable emission of CO_2, which leads to climate change and air pollution.

Therefore, to reduce the CO_2 release into the atmosphere and to increase the gasification efficiency, attention is currently focused on coal gasification with CO_2/O_2 mixtures rather than with air (N_2/O_2). To implement the IGCC (Integrated gasification combined cycle) system efficiently and to mitigate the CO_2 emission problem, it is necessary to study CO_2/O_2-blown coal gasification. Moreover, the soot formation, which is of significant environmental concern, is still being neglected in the past studies.

A number of research programs are now under way all over the world to test and develop efficient and economical production of high heating value gas from coal. However, to date, there has been no published work investigating the coal gasification under $CO_2/O_2/N_2$ atmosphere in two stage entrained flow gasifier. In this study, numerical simulations of coal gasification including soot formation are conducted with the aim of describing the coal gasification behavior under $CO_2/O_2/N_2$ atmosphere in an effort to increase the syngas production. The numerical results obtained from this study are considered to be an important step towards better designs of gasifiers.

ACKNOWLEDGMENTS

DEDICATION

This work is dedicated to

My Parents

TABLE OF CONTENTS

1. INTRODUCTION

3. REACTION MECHANISM FOR NUMERICAL SIMULATION

4. MODELS FOR COAL GASIFICATION

5. COAL GASIFICATION UNDER N_2/O_2 AND $CO_2/O_2/N_2$ CONDITIONS & SOOT FORMATION

6. SENSITIVITY ANALYSIS

7. CONCLUSIONS

LIST OF FIGURES

LIST OF TABLES

NOMENCLATURE

a	absorption coefficient	$[m^{-1}]$
a_p	equivalent absorption coefficient	$[m^{-1}]$
A	surface area	$[m^2]$
A_s	surface area of surface material per unit length	$[m]$
A_p	surface area of coal particle	$[m^2]$
A_f	pre-exponential factor	$[m^3/kmol \cdot s]$, $[kg/m^2 \cdot s \cdot Pa]$, $[s^{-1}]$
$A_{f,k}$	pre-exponential factor for kth reaction	$[m^3/kmol \cdot s]$, $[kg/m^2 \cdot s \cdot Pa]$, $[s^{-1}]$
A_R	Magnussen constant for reactants	$[-]$
B_P	Magnussen constant for products	$[-]$
c_p	specific heat of gas	$[J/kg \cdot K]$
C_P	specific heat of coal particle	$[J/kg \cdot K]$
C_D	drag co-efficient	$[-]$
$C_{1\varepsilon}$	turbulence model constant	$[-]$
$C_{2\varepsilon}$	turbulence model constant	$[-]$
C_μ	turbulence model constant	$[-]$
d	diameter	$[m]$
d_p	diameter of coal particle	$[m]$
$\overline{d}_p$	mean diameter of coal particle	$[m]$
D	diffusion co-efficient	$[m^2/s]$
D_i	diffusion co-efficient of species i	$[m^2/s]$
D_k	diffusion co-efficient in kth reaction	$[m^2/s]$

D_l	diffusion rate constant	[-]
D_H	hydraulic diameter	[m]
E	energy	[J]
E_{ac}	activation energy	[J/kmol]
$E_{ac,k}$	activation energy for kth reaction	[J/kmol]
E_p	equivalent emission of coal particles	[W/m^3]
f_p	particle scattering factor	[-]
f_w	fraction of water present in coal particles	[-]
f_h	fraction of heat absorbed by coal particles	[-]
$\vec{F}$	force vector	[kg·m/s^2]
F_D	drag force	[kg·m/s^2]
g	gravitational acceleration	[m/s^2]
G	incident radiation	[W/m^2]
G_k	generation of turbulence kinetic energy due to velocity gradient	[kg/m·s^3]
h	heat transfer co-efficient	[W/m^2·K]
H	enthalpy	[J/kg]
H_i	enthalpy of species i	[J/kg]
$H_i^{\,0}$	enthalpy of species i at standard condition	[J/kg]
H_{comb}	height of combustor	[m]
I	number of species	[-]
I_{rad}	radiation intensity	[W/m^2]
I_t	turbulent intensity	[-]
$\hat{I}$	unit tensor	[-]
J	mass flux	[kg/m^2·s]
J_i	mass flux of species i	[kg/m^2·s]

k	turbulent kinetic energy	$[m^2/s^2]$
k_g	thermal conductivity of gas	$[W/m \cdot K]$
k_{kin}	reaction rate constant	[unit vary]
$k_{kin,f,k}$	forward reaction rate constant in kth reaction	[unit vary]
$k_{kin,b,k}$	backward reaction rate constant in kth reaction	[unit vary]
K	number of reactions	[-]
L	latent heat of water present in coal	[J/kg-coal]
m	mass	[kg]
m_p	mass of coal particle	[kg]
M	molecular weight	[kg/kmol]
M_i	molecular weight of species i	[kg/kmol]
n_p	number of coal particle	[-]
N	order of reaction	[-]
N_k	order of reaction for kth reaction	[-]
Nu	Nusselt number	[-]
p	pressure	[Pa]
P	wetted perimeter	[m]
Pr	Prandtl number	[-]
q	heat flux	$[J/m^2]$
$\vec{r}$	position vector	[m]
R	universal gas constant (8.314×10^3)	$[J/kmol \cdot K]$
R_i	source of chemical species i due to reaction	$[kg/m^3 \cdot s]$
$\hat{R}_{i,k}^{(A)}$	rate of production [Arrhenius] of species i in kth reaction	$[kmol/m^3 \cdot s]$
$\hat{R}_{i,k}^{(A,s)}$	rate of production [Arrhenius] of species i in kth surface reaction	$[kmol/m^2 \cdot s]$
$\hat{R}_{i,k}^{(R)}$	rate of production [Eddy dissipation] of reactant i in kth reaction	$[kmol/m^3 \cdot s]$

$\hat{R}_{i,k}^{\ (P)}$	rate of production [Eddy dissipation] of product i in kth reaction	[kmol/m^3·s]
$\overline{R}_k$	rate of particle surface species depletion in kth reaction	[kg/s]
$\widetilde{R}_k$	rate of particle surface species reaction per unit area in kth reaction	[kg/m^2·s]
Re_d	Reynolds number based on the particle diameter	[-]
Re_{D_H}	Reynolds number based on hydraulic diameter	[-]
s	path length	[m]
$\vec{s}$	direction vector	[m]
S	entropy	[J/kmol·K]
S_i	entropy of species	[J/kmol·K]
$S_i^{\ 0}$	entropy of species at standard condition	[J/kmol·K]
S_m	rate of mass added from coal particle	[kg/m^2·s]
$S_{h,reac}$	source of heat due to reaction	[W/m^2·s]
Sc_t	turbulent Schmidt number	[-]
t	time	[s]
T	temperature of gas	[K]
T_p	temperature of coal particle	[K]
T_{vap}	vaporization temperature of coal particle	[K]
u, v, w	velocity magnitude	[m/s]
u_p	velocity of coal particle	[m/s]
$\vec{v}$	velocity vector	[m/s]
V	volume	[m^3]
V_p	particle volume	[m^3]
X_i	molar concentration of species i	[kmol/m^3]
y^+	distance	[-]

Y_i	mass fraction of species i	[-]
Y_{carbon}	mass fraction of carbon in coal	[-]
Y_d	mass yield	[-]
$Y_{i,rel}$	relative mass fraction of species i	[-]
z	height of reactor	[m]

Greek letters

α_1	yield parameter for first step devolatilization	[-]
α_2	yield parameter for second step devolatilization	[-]
α_k	temperature exponent for kth reaction	[-]
ε	turbulent dissipation rate	[m^2/s^3]
ε_p	emissivity of coal particle	[-]
η	effectiveness factor	[-]
η', η''	rate exponent for reactants, products	[-]
v', v''	stochiometric co-efficient for reactants, products	[-]
θ_R	radiation temperature	[K]
μ	dynamic viscosity	[Pa·s]
μ_t	turbulent viscosity	[Pa·s]
ρ	density	[kg/m^3]
σ	Stefan-Boltzmann constant (5.669×10^{-8})	[W/m^2·K^4]
σ_k	turbulent Prandtl number for k	[-]
σ_ε	turbulent Prandtl number for ε	[-]
σ_s	scattering co-efficient	[m^{-1}]
σ_p	equivalent particle scattering factor	[m^{-1}]
$\omega_{i,g}$	rate of production of species i from gas all phase reactions	[kmol/m^3·s]
$\omega_{i,s}$	rate of production of species i from all surface phase reactions	[kmol/m^2·s]

$\omega_{con,i,k}$	contribution of species i from kth reaction	[-]
Ω	solid angle	[degree]
φ	refractive index	[-]
ϕ	spread parameter	[-]

Subscripts

a	ash
ac	activation
b	backward
con	contribution
f	forward
g	gas
i	species
h	heat
m	mass
P	product species
p	particles
R	reactant species
rad	radiation
rel	relative
ref	reference
s	surface
t	turbulent
w	water
0	initial stage

CHAPTER 1

INTRODUCTION

1.1 Background

1.1.1 Energy consumption and demand

Global energy consumption in 2030 is predicted to increase 1.4 times that in 2007, where about half of the increase will be contributed by Asia. The demand for fossil fuels such as oil, coal and natural gas will continue to increase along economic growth (Fig. 1-1). It is also predicted that remaining years of exploitable global energy resources (Fig. 1-2) in sequences are: coal (122 years), uranium (100 years), natural gas (60 years) and oil (42 years). These predictions are obtained as dividing the confirmed exploitable reserve by the annual production at 2007 [1]. Because of more exploitable coal resource compared to other resources, it is expected that coal will continue to play a significant role in meeting the future energy demand.
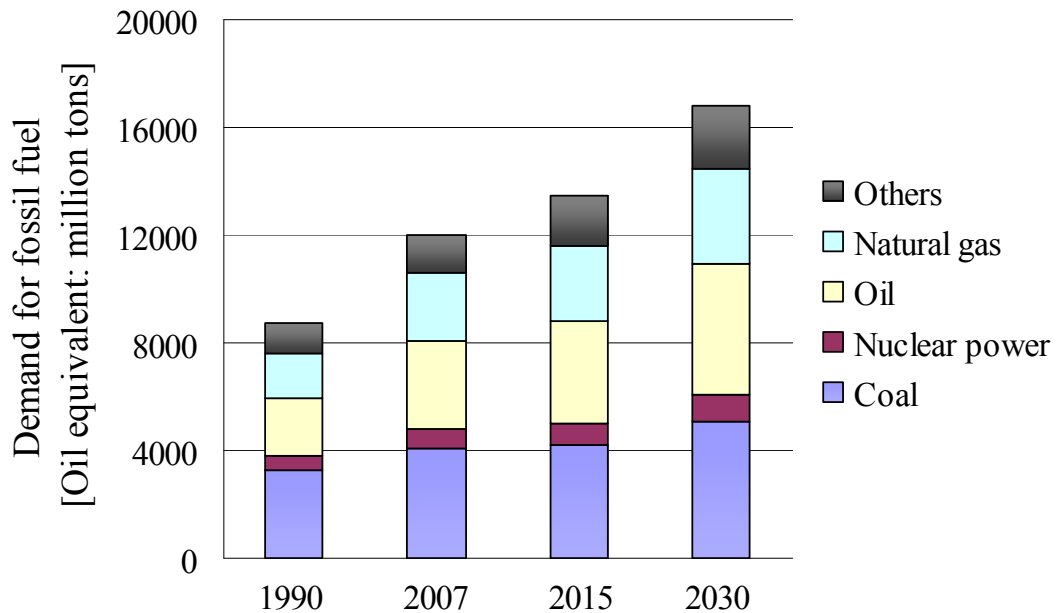
Figure 1-1 Predicted global energy demand in terms of oil equivalent (million tons) [1]
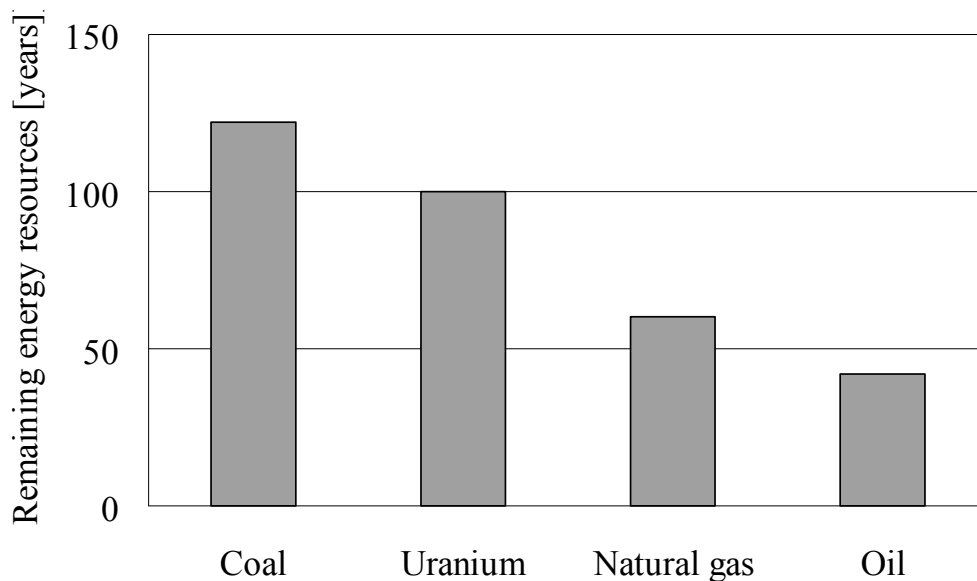
Figure 1-2 Remaining exploitable global energy resources in terms of years [1]

Coal, typically used as a base load source for power generation in Japan, remains an important fuel source and accounted for 22 percent of coal-fired generation in 2010 (Fig. 1-3). On the other hand, oil is the largest energy resource of fuel consumption, although its share of total energy consumption has declined from about 80 percent in the 1970s to 42 percent in 2010. Hydroelectric power and renewable energy comprise a relatively small percentage of total energy consumption in the country. Because of limited exploitable oil resources and the risk for nuclear power plant, Japan now depends heavily on imported fossil fuels to meet its energy demand [2]. Domestic coal production came to the end in 2002 and Japan imported 207 million short tons in 2010, mainly from Australia. However, new and clean coal technologies are being pursued in the power sector in an effort to meet the environmental targets.
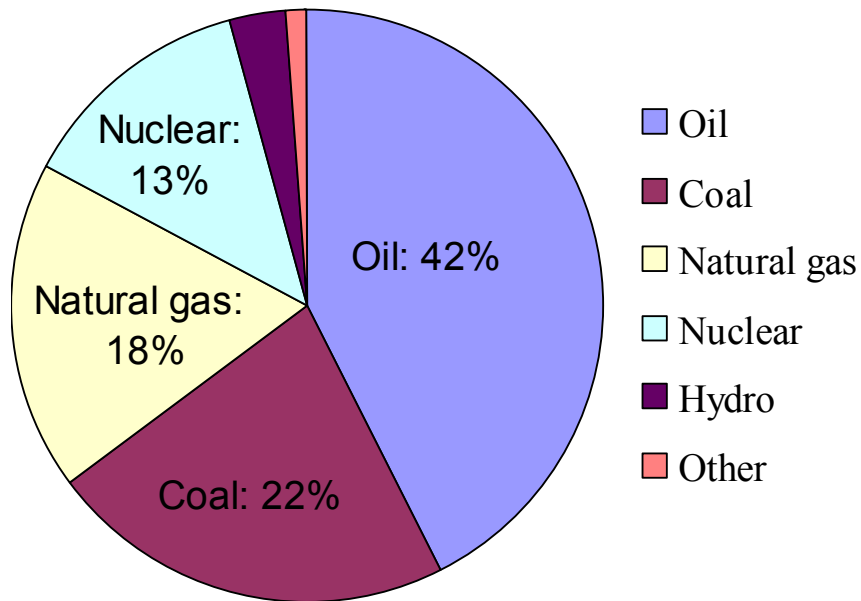
Figure 1-3 Total energy consumption in Japan by sector in 2010 [2]

1.1.2 Importance of coal and application

Coal has been acknowledged as the principal potential source of fuel for electrical utilities and a valuable raw material for industrial chemicals. Presently, approximately 40% of electric power generation worldwide depends on coals [3]. Continued utilization of coal is dependant on the technology available, and development of new processes with low environmental impact is required. A number of demonstration and near-commercial scale coal-fired integrated gasification combined cycle (IGCC) power plants are already operating around the world. It is predicted that coal will continue to play an important role in meeting the world's increasing energy demands in the foreseeable future.

1.1.3 CO_2 emission problem and mitigation

The contribution of coal to total energy production is increasing day by day. However, the use of coal faces several challenges. The major one is the considerable emission of CO_2, which leads to climate change and air pollution. CO_2 is considered to be a "greenhouse gas", which can lead to global warming [4-6]. CO_2 sequestration has been suggested as a means of reducing the amount of carbon dioxide being released into the atmosphere. CO_2 sequestration involves long-term storage of carbon dioxide in reservoirs to reduce its buildup in the atmosphere. Possible sequestration sites include geologic repositories, soils and biomass, and ocean depths. While the advantages, disadvantages, and overall effectiveness of these sequestration strategies are still being studied, they have one thing in common: nearly pure high-pressure carbon dioxide must be supplied in each case. This requires a technique to separate CO_2 from the remaining stack gases found in coal gasification. Schematic of Integrated Gasification Combined Cycle (IGCC) for conventional air (N_2/O_2) blown gasification and CO_2/O_2 gasification are shown in Fig. 1-4.
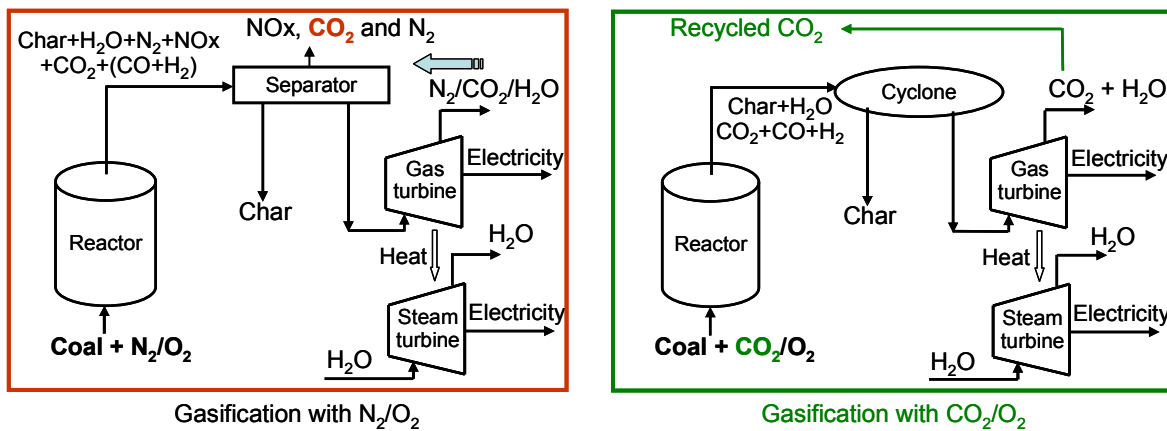
Figure 1-4 Schematic of Integrated Gasification Combined Cycle (IGCC)

In coal gasification with air (N_2/O_2), it is difficult to remove CO_2 efficiently, because the CO_2 concentration in the flue gas is only about 13%. For this reason, currently produced

CO_2 gas is simply released into the atmosphere together with other gas species. On the other hand, CO_2 concentration in the flue gas may be enriched up to 95% in coal gasification with CO_2/O_2 mixtures, and easy CO_2 recovery becomes possible without additional energy consumption [4]. The energy needed for the separation of CO_2 from stack gas, found in conventional coal gasification system, can be neglected in coal gasification with CO_2/O_2 mixtures, resulting in an increase of the gasification efficiency. The presence of much N_2 in conventional coal gasification system also leads to produce another pollutant, NO_x, at higher gasification temperatures. In contrast, NO_x formation will be reduced in CO_2/O_2 gasification condition.

Therefore, to reduce the CO_2 release into the atmosphere and to increase the gasification efficiency, attention is currently focused on coal gasification with CO_2/O_2 mixtures rather than air (N_2/O_2). However, there are several hurdles that must be crossed before widely implemented this process. The presence of higher CO_2 concentration than in a conventional air-fired gasification causes significant differences in gasification characteristics such as gas temperature, gas composition (especially syngas), carbon conversion, the radiating properties etc. [7-8].

1.2 Objectives of this study

A number of research programs are now under way all over the world to test and develop efficient and economical production of high heating value gas from coal. All studies are grouped into two types: coal combustion and coal gasification. Combustion is recognized as a complete combustion of coal where sufficient amount of O_2 is provided. On the other hand, gasification means a partial combustion of coal under insufficient O_2 atmosphere. To implement the IGCC system efficiently and to mitigate the CO_2 emission problem, it is necessary to study CO_2/O_2-blown coal gasification. Moreover, the soot formation, which is of significant environmental concern, is still being neglected in the past studies. Therefore, the

main objective of this study is to conduct numerical simulation of coal gasification under $CO_2/O_2/N_2$ gasification condition. This study will focus on the following topics:

a) Reduction of reactions mechanism of coal volatiles gasification.

b) Prediction of soot and syngas in coal volatiles gasification.

c) Prediction of soot and syngas in coal gasification under various gasification conditions.

1.3 Basics of gasification

1.3.1 Advantage of gasification over combustion

Gasification can be described as the conversion of any carbon-based feedstocks into a gaseous product with a useful chemical heating value. In IGCC system, gasification of carbon-based feedstocks is very important to produce turbine inlet gas having high chemical heating value. Gasification process can retain almost 70% of chemical energy which can be used to drive the turbine to produce more electricity. To understand the advantage of gasification over combustion, the reaction of carbon for two conditions is explained. When 1 kmol of carbon is burnt completely in adequate air or oxygen, it produces 393.77 MJ heat and carbon dioxide. This is combustion reaction (1-1).

$$C + O_2 \rightarrow CO_2 + 393.77 \text{ MJ/kmol} \tag{1-1}$$

Instead of burning it entirely, partial combustion or gasification of carbon can be obtained by restricting the oxygen supply. The carbon then produces 72% less heat than that in combustion, and the reaction (1-2) shown here produces a combustible gas, CO.

$$C + \frac{1}{2} O_2 \rightarrow CO + 110.53 \text{ MJ/kmol} \tag{1-2}$$

When the gasification product, CO, subsequently burns in adequate oxygen, it produces 283.24 MJ of the heat. Thus, CO retains 72% of the energy of the carbon, which can be used into the turbine as inlet in IGCC system.

$$CO + \frac{1}{2} O_2 \rightarrow CO_2 + 283.24 \text{ MJ/kmol} \tag{1-3}$$

However, in complete gasification system the energy recovery is 75 to 88% owing to the presence of hydrogen and other hydrocarbon [9].

1.3.2 Types of gasifier

For most purposes, gasifier types can be grouped into one of the three categories: moving bed gasifiers, fluidized bed gasifiers and entrained flow gasifiers. The gasifiers in each of these three categories share certain characteristic, which differentiate them from gasifiers in other categories. Some of these characteristics are summarized in Table 1-1.

Moving bed gasifiers (sometimes called fixed bed gasifiers, since although the feedstock is moving through the bed, the location of the bed itself is fixed in space) are characterized by a bed, in which the coal moves slowly downward under gravity as it is gasified, generally by a counter current manner. In such a counter current arrangement, the hot synthesis gas from the gasification zone is used to preheat and pyrolyze the downward flowing coal. The outlet temperature of the synthesis gas is generally low. An excessive amount of fine particles, particularly if the coal has strong caking properties, can block the passage of the upflowing syngas.

Fluid bed gasifiers offer extremely good mixing between feed and oxidant, which promotes both heat and mass transfer. The operation of fluid bed gasifiers is generally restricted to temperatures below the softening point of the ash, since agglomeration of soft ash particles will disturb the fluidization of the bed. Some attempts have been made to operate into the ash softening zone to promote a limited and controlled agglomeration of ash with the aim of increasing carbon conversion, but this mode of operation has so far not been successfully translated into commercial scale plants.

Entrained flow gasifiers operate with feed and blast in co-current flow. The residence time in this process is short (a few seconds). The feed is ground to a size of 200 μm or less to promote mass transfer and allow transport in the gas. Given the short residence time, high

temperatures are required to ensure a good conversion, and therefore all entrained flow gasifiers operate in the slagging range. An advantage of entrained flow gasifiers is that they do not have any specific technical limitations on the type of coal used. Additionally, the ash is produced in the form of an inert slag.

The majority of successful coal gasification processes that have been developed since 1950 are entrained flow slagging gasifiers operating at pressures of 275-1000 psig and at high temperatures of at least 24000 ^{0}F. Entrained flow gasifiers have become the preferred gasifiers for hard coals and have been selected for the majority of commercial-sized IGCC applications [9]. Entrained flow coal gasification has also been identified as a promising way of gas production, due to its high coal throughput, insensitivity to coal type and its simplicity in design and technology [10].

Table 1-1 Characteristics of different categories of gasification processes [10]

Category	Moving bed gasifiers		Fluidized bed gasifiers		Entrained flow gasifiers
Ash condition	Dry ash	Slagging	Dry ash	Agglomerating	Slagging
Feed characteristics					
Size	¼ - 2 inch	¼ - 2 inch	¼ - 2 inch	¼ - 2 inch	<200 μm
Acceptability of fines	Limited	Better than dry ash	Good	Better	Unlimited
Preferred coal rank	Any	High	Low	Any	Any
Operating characteristics					
Outlet gas temperature [^{0}F]	Low (800-1200)	Low (800-1200)	Moderate (1650-1900)	Moderate (1650-1900)	High (2300-2900)
Oxidant demand	Low	Low	Moderate	Moderate	High
Steam demand	High	Low	Moderate	Moderate	Low
Others	Hydrocarbon in gas	Hydrocarbon in gas	Lower carbon conversion	Lower carbon conversion	Pure gas, high carbon conversion

1.4 Past studies

1.4.1 Reduction of reaction mechanism

Different methodologies have been proposed for the reduction of detailed mechanisms, with different authors giving different meaning to reduction. Sensitivity analysis can be used for mechanism reduction that is, finding a smaller model that produces similar predictions for some of the variables (i.e., species concentrations and temperature). Such an analysis reveals which are the main control parameters in the model, which are the indirect effects of parameter changes and provides information about the structure of the model. Combustion of hydrogen is one of the simplest combustion processes. A typical hydrogen combustion mechanism consists of about 40 reactions of 8 reactive species. Turanyi [11] studied sensitivity analysis to reveal the main reactions in the detailed chemical mechanism of hydrogen combustion at homogeneous explosion and premixed laminar flame conditions. The computational singular perturbation (CSP) theory has also been studied to make reduced mechanism. Belcadi et al. [12] constructed a reduced mechanism with ten global reactions for methane combustion. In that study the fully automatic algorithm S-STEP, which is based on the computational singular perturbation (CSP) method, has been used to construct the reduced mechanism. A comparative study with the detailed mechanism GRI-3.0 showed that this reduced mechanism reproduces accurately the important parameters of combustion such as flame speed, flame temperature and mole fraction distributions of major species and pollutant species such as NOx and CO. Turanyi et al. [13] made a reduced mechanism for high temperature formaldehyde oxidation and high temperature propane pyrolysis by analyzing the rate of production (ROP) and the reduced mechanism gave a similar results to the detailed mechanism.

However, there is no works on reduction of reaction mechanism in coal volatiles gasification. Coal volatiles are generally composed of H_2, H_2O, CO, CO_2, hydrocarbon gases, hydrocarbon liquids, and polycyclic aromatic hydrocarbons (PAHs). These species are

assumed to participate in gasification reactions. The large number of species and reactions sometimes make difficulty to run the simulation especially for the complex flow system. Therefore, the number of species and reactions are decreased by analyzing the ROP to get a reduced mechanism small enough to use in CFD calculations.

1.4.2 Soot formation in coal volatiles gasification

Soot formation from coal is complex and might follow a different pathway to soot formation from simple hydrocarbon fuels. This is due to the fact that the molecules of coal volatiles, particularly PAH molecules, are much larger and more chemically diverse than those of simple hydrocarbon fuels. Chen et al. [14] found that the reaction pathways for soot generation from coal in secondary pyrolysis are irreversible. This includes direct conversion of PAHs to soot, and soot formation following production of light hydrocarbons from decomposing PAHs. Leung et al. [15] proposed the deduced reaction mechanism, which was validated with laminar ethylene and propane flames burning with a range of oxygen enriched and depleted air streams. In diffusion flames for ethylene–propane mixtures [16], soot and PAH concentration were increased when a small amount of propane was added to ethylene diffusion flames. Appel et al. [17] proposed the detailed chemical kinetic model in gas-phase reactions, aromatic chemistry, soot particle coagulation, soot particle aggregation and soot surface growth. Their detailed model was validated with laminar flames of C2-hydrocarbons. Richter et al. [18] developed the detailed mechanism of PAH and soot formation and tested in a premixed low-pressure benzene flame. This detailed mechanism was updated and validated with atmospheric pressure ethylbenzene and ethyl alcohol flames [19]. It is expected that these mechanisms could be implemented to predict the soot inside coal gasifiers using a computational method. According to these mechanism, initially, aromatic ring formation occurs during gas phase reactions of small hydrocarbons. Growth of the PAHs then occurs by their rapid polymerization. Finally, soot formation involving particle nucleation, particle

11

growth and oxidation occur. These main processes in the soot model are summarized in Fig. 1-5. Particle nucleation is the most important step in soot formation, that generates new condensed phase particles from a continuous gas phase. After particle nucleation, particle growth occurs when PAHs collide with each other. Soot particles grow continuously due to condensation of PAHs on the soot surface. Reactions at the surface of growing particles contribute considerably to the accumulated carbon mass. Oxidation of the PAHs and soot particles by heterogeneous surface reactions of molecular oxygen and hydroxyl radicals reduce the concentration of PAHs.
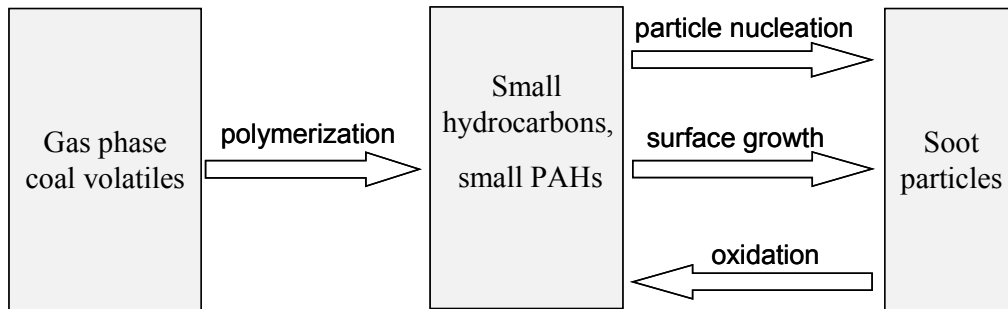
Figure 1-5 Schematic of soot model in coal volatiles gasification.

1.4.3 Coal gasification in two stage entrained flow gasifier

A comprehensive three-dimensional simulation model for two stage entrained flow coal gasifier with capacity of 200 T/D (pilot scale gasifier) was developed by Chen et al. [20-21] to simulate the gasification reaction and reactant mixing process using an extended coal gas mixture fraction model with the Multi Solids Progress Variables (MSPV). A series of numerical simulations were performed under various operating conditions for a 200 T/D two-stage air blown entrained flow gasifier developed in Japan for the IGCC process. Four mixture fractions of devolatilization, char-O_2, char-H_2O and char-CO_2 reactions are used to track the reaction products. The coal conversion, product gas composition, calorific value and gas temperature profiles throughout the gasifier were simulated. The results show that coal

devolatilization and char oxidation were responsible for most of the carbon conversion (up to 80%) in the two stage air blown entrained flow gasifier. The predicted carbon conversion was independent of devolatilization rate, sensitive to the chemical kinetics of heterogeneous reactions, and less sensitive to a change in coal particle diameter. It was found that the air ratio had a significant effect on gasifer performance with strong coal type dependence. Increasing air ratio leads to increased CO_2 and decreased CO and H_2 concentrations, and accordingly, had a strong effect on the heating value of the product gas. The effect of air/coal partitioning to the two stages, and the feed rate of recycle char was found to be limited.

In another study Chen et al. [22] predicted the gas flow field, gas temperature distributions, extent of burnout, and particle trajectories as well as particle concentration within a two stage air blown gasifier. It was found that the gas temperature generally decreased along the gasifier height and was related to particle concentration. The lower particle concentration in the combustor is responsible to the high combustor temperatures, and the high particle concentration in the reductor is the reason of the low gas temperatures. The local particle concentration was found to be sensitive to the swirl ratios for both the combustor and the reductor burners. In case of strong swirling ratio, particles were centrifuged to the wall of the combustor. On the other hand, lower swirling ratio resulted in more distributed particle in the combustor where they mostly burn out. However, in the reductor, particles were distributed in all volume except for an extremely high concentration region in the centre of the diffuser, caused by the collision of four directly aimed jets.

Watanabe et al. [23] studied the modeling of a coal gasification reaction, and prediction of gasification performance for a two stage entrained flow coal gasifier with a capacity of 2T/D (research scale gasifier). Influence of the air ratio on gasification performance, such as per pass carbon conversion efficiency, amount of product char, heating value of the product gas, and cold gas efficiency were presented. The trends of gas

temperature and product gas compositions with changing air ratios were also predicted accurately.

Silaen et al. [24] conducted numerical simulation of coal gasification process inside a generic two stage entrained flow coal gasifier. The effect of time scale in the stochastic particle tracking, turbulence models, devolatilization models and particle size were numerically investigated. It was reported that there was a large exit temperature difference about 640K (1779 K vs. 2426 K) between using smaller and larger particles (100 μm vs. 300 μm). Smaller particles produce more CO and less CO_2, which result in an increase in syngas heating value. They also reported that 3D results showed better gasification performance and syngas heating values than 2D cases due to longer residence time and more complete gasification process.

1.5 Structure of the thesis

Chapter 1 gives an introduction, background on coal gasification, the main objectives of this study, and past studies relating to coal gasification. Chapter 2 explains reaction mechanism of coal volatiles gasification under various operating conditions. The effects of temperature, pressure and CO_2/O_2 concentration on product gas concentration are discussed in detail. Chapter 3 compares the calculated results for the detailed reaction mechanism with those for the overall gas phase reactions mechanism including one step soot model under $CO_2/O_2/N_2$ condition. Chapter 4 explains all coal gasification models used in this study. Chapter 5 studies the numerical simulation of coal gasification under air (N_2/O_2) and $CO_2/O_2/N_2$ conditions. This chapter also predicts the soot formation by using one step soot model (proposed in Chapter 3) in coal gasification. Chapter 6 investigates the sensitivity analysis under various conditions to predict syngas and soot production in coal gasification. Chapter 7 concludes the main results obtained from this study of coal gasification.

References

[1] Ministry of Economy, Trade and Industry; "Energy in Japan 2010", pp. 13 and 14, Japan (2010).

[2] U.S. Energy Information Administration (EIA), Country Analysis Briefs (Japan), 4 June (2012).

[3] US Energy Information Administration (EIA), Annual energy outlook 2010 with projections to 2035 (2010).

[4] Okazaki K. and Ando T., "NOx reduction mechanism in coal combustion with recycled CO_2", *Energy*, 22 (2/3), 207-215 (1997).

[5] Chen J., Huang J., Chen C. and Guo J., "Emission characteristics of PAHs, benzene and phenol group hydrocarbons in O_2/RFG waste incineration processes", *Fuel*, 87, 2787-2797 (2008).

[6] Bachu S. and Adams J.J., "Sequestration of CO_2 in geological media in response to climate change: capacity of deep saline aquifers to sequester CO_2 in solution", *Energy Conversion Management*, 44, 3151–3175 (2003).

[7] Hecht E.S., Shaddix C.R., Molina A. and Haynesm B.S., "Effect of CO_2 gasification reaction on oxy-combustion of pulverized coal char", *Proceedings of the Combustion Institute*, 33, 1699-1706 (2011).

[8] Bejarano P.A. and Levendis Y.A., "Single-coal-particle combustion in O_2/N_2 and O_2/CO_2 environments", *Combustion and Flame*, 153, 270-287 (2008).

[9] Basu P., "Biomass gasification and Pyrolysis: Practical Design and Theory", Academic Press Publications (2010).

[10] Miller B.G. and Tillman D.A., "Combustion Engineering Issues for Solid Fuel Systems", Academic Press Publications (2008).

[11] Turanyi T., "Applications of sensitivity analysis to combustion chemistry", *Reliability Engineering and System Safety*, 57(1), 41–48 (1997).

[12] Belcadi A., Assou M., Affad E. and Chatri E., "Construction of a reduced mechanism for modelling premixed combustion of methane–air", *Combustion Theory and Modelling*, 11(4), 603–613 (2007).

[13] Turanyi T. and Berces T., "Reaction Rate Analysis of Complex Kinetic Systems", *International Journal of Chemical Kinetics*, 21, 83-99 (1989).

[14] Chen C.J., Castagnoli C. and Niksa S., "Coal Devolatilization during rapid transient heating: 2. Secondary pyrolysis", *Energy & Fuels*, 6, 264–271 (1992).

[15] Leung K.M., Lindstedt R.P. and Jones W.P., "A Simplified reaction mechanism for soot formation in nonpremixed flames", *Combustion and Flame*, 87, 289–305(1991).

[16] Hwang J.Y., Lee W., Kang H.G. and Chung S.H., "Synergistic effect of ethylene–propane mixture on soot formation in laminar diffusion flames", *Combustion and Flame*, 114, 370–80 (1998).

[17] Appel J., Bockhorn H. and Frenklach M., "Kinetic modeling of soot formation with detailed chemistry and physics: laminar premixed flames of C2 hydrocarbons", *Combustion and Flame*, 121, 122–36 (2000).

[18] Richter H., Granata S., Green W.H. and Howard J.B., "Detailed modeling of PAH and soot formation in a laminar premixed benzene/oxygen/argon low-pressure flame", *Proceeding of Combustion Institute*, 30, 1397–405 (2005).

[19] Ergut A., Granata S., Jordan J., Carlson J., Howard J.B. and Richter H., "PAH Formation in one-dimensional premixed fuel-rich atmospheric pressure ethylbenzene and ethyl alcohol flames", *Combustion and Flame*, 144, 757–72 (2006).

[20] Chen C., Masayuki H. and Toshinori K., "Numerical simulation of entrained flow coal gasifiers Part I: modeling of coal gasification in an entrained flow gasifier", *Chemical Engineering Science*, 55, 3861-3874 (2000).

[21] Chen C., Masayuki H. and Toshinori K., "Numerical simulation of entrained flow coal gasifiers Part II: effects of operating conditions on gasifier performance", *Chemical Engineering Science*, 55, 3875-3883 (2000).

[22] Chen C., Masayuki H. and Toshinori K., "Use of numerical modeling in the design and scale-up of entrained flow coal gasifiers", *Fuel*, 80, 1513-1523 (2001).

[23] Watanabe H. and Otaka M., "Numerical simulation of coal gasification in entrained flow coal gasifier", *Fuel*, 85, 1935-1943 (2006).

[24] Silaen A. and Wang T., "Effect of turbulence and devolatilization models on coal gasification simulation in an entrained-flow gasifier", *International Journal of Heat and Mass Transfer*, 53, 2074–2091 (2010).

CHAPTER 2

REACTION MECHANISM UNDER $CO_2/O_2/N_2$ GASIFICATION CONDITION

2.1 Introduction

Computational Fluid Dynamics (CFD) plays a key role to explain the different coal chemistry steps including devolatilisation, volatile combustion and reforming, char oxidation and char gasification. Various investigators have demonstrated that coal consists roughly of two portions that differ greatly in reactivity: a highly reactive portion, possibly corresponding in some way to the amount of volatile matter present, and a portion of relatively low reactivity, residual carbonaceous matter-coke. As the particle heats up, the volatile components of the coal will evaporate and diffuse into the gas stream. Coal volatiles are generally composed of H_2, H_2O, CO, CO_2, hydrocarbon gases, hydrocarbon liquids, and polycyclic aromatic hydrocarbons (PAHs). PAHs are products of primary pyrolysis and precursors of soot in secondary pyrolysis. Soot formation during gasification of coal volatiles is a very complicated process involving homogeneous gas phase and heterogeneous surface phase reactions.

This chapter focuses on the study of coal volatiles gasification under various operating conditions. A reduced reaction mechanism is obtained from the detailed reaction mechanism by analyzing the rate of production (ROP). The prediction of soot in coal volatiles gasification under enriched CO_2 condition is numerically studied using a detailed reaction mechanism with soot. The effects of CO_2/O_2 mixtures are evaluated under $CO_2/O_2/N_2$ gasification condition in an effort to increase syngas production and decrease soot and CO_2 emission.

2.2 Experimental

The experimental work was conducted in the laboratory of Professor Jun-ichiro Hayashi. Figure 2-1 shows a simple diagram of the Drop Tube Furnace (DTF) experimental set-up. Coals were subjected to the rapid pyrolysis at 700 °C. The coal sample was fed into inner tube of the DTF at a rate of about 0.2g/min together with the flow of N_2 at a flow rate of 1000 N mL/min. The feeding time for coal was about 15 min. The lower end of the inner tube was closed by a sintered quartz filter plate. The temperature of the inner tube was electrically heated around 700 °C. Coals were heated up when passed to the inner tube and the volatiles were formed from the rapid pyrolysis of coal at 700 °C. The volatiles were immediately swept out of the inner tube by the N_2 flow, while the char particles were left over the filter plate. The mixed gas flow rate ($N_2/O_2/CO_2$) to the furnace was maintained at 500/0/0, 490/10/0 and 470/10/20 N mL/min in case of pyrolysis (N_2), partial oxidation (N_2/O_2) and CO_2/O_2 gasification ($N_2/O_2/CO_2$) conditions, respectively. The temperature of mixed gas was increased to reforming temperature at 1000 °C before entering into the furnace. The volatiles and mixed gas were then mixed in the furnace. The pressure inside the DTF was kept at 0.1 MPa during the experiment. Products gas from the furnace flows through a filter to remove particulates and any potential tars, and sent to online Gas Chromatography (GC) for gas species analysis.
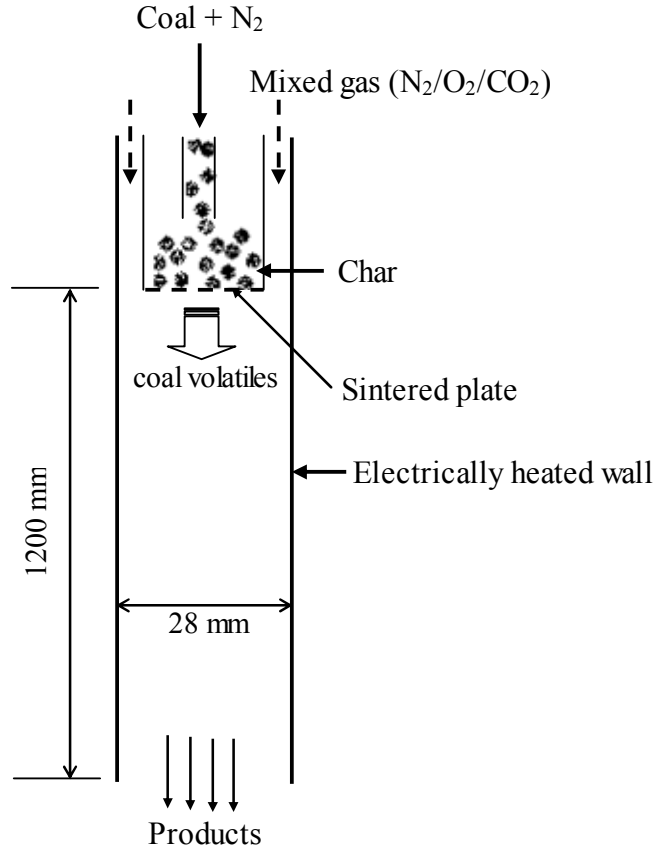
Figure 2-1 A simple diagram of the DTF set-up

2.3 Mathematical model

The Plug Flow Reactor (PFR) model for multiple reactions of coal volatiles is developed under conditions of pyrolysis (N_2), partial oxidation (N_2/O_2) and CO_2/O_2 gasification ($N_2/O_2/CO_2$). For K number of reactions involving I number of chemical species, the general reaction can be represented as:

$$\sum_{i=1}^{I} \upsilon'_{i,k} \chi_i \underset{k_{kin,b,k}}{\overset{k_{kin,f,k}}{\rightleftharpoons}} \sum_{i=1}^{I} \upsilon''_{i,k} \chi_i \quad (k=1, 2, 3,\ldots, K) \tag{2-1}$$

where

I = number of species

K = number of reactions

χ_i = chemical symbol for ith species

$\upsilon_{i,k}^{'}$ = stoichiometric coefficients for ith reactant species in kth reaction

$\upsilon_{i,k}^{''}$ = stoichiometric coefficients for ith product species in kth reaction

$k_{kin,f,k}$ = forward rate constant for kth reaction

$k_{kin,b,k}$ = backward rate constant for kth reaction

The forward rate constant, $k_{kin,f,k}$, for the kth reaction is assumed to follow the Arrhenius equation as follows:

$$k_{kin,f,k} = A_{f,k} T^{\alpha_k} \exp\left(-\frac{E_{ac,k}}{RT}\right)$$ (2-2)

where

$A_{f,k}$ = pre-exponential factor for kth reaction

α_k = temperature exponent for kth reaction

$E_{ac,k}$ = activation energy for kth reaction

T = gas temperature

R = universal gas constant

The backward rate constant, $k_{kin,b,k}$, is related to the forward rate constant as follows:

$$k_{kin,b,k} = \frac{k_{kin,f,k}}{\exp\left(\frac{\Delta S_k^0}{R} - \frac{\Delta H_k^0}{RT}\right)\left(\frac{P}{RT}\right)^{\sum\limits_{i=1}^{I} \upsilon_{i,k}^{''} - \upsilon_{i,k}^{'}}}$$ (2-3)

where

ΔS_k^0 = change of standard state molar entropy in kth reaction

ΔH_k^0 = change of standard state molar enthalpy in kth reaction.

P = pressure

The rate of gas phase reaction resulting from both forward and backward reaction as follows:

$$\hat{R}_{i,k}^{(A)} = (\upsilon_{i,k}^{''} - \upsilon_{i,k}^{'}) \left(k_{kin,f,k} \prod_{i=1}^{I} [X_i]^{\eta_{i,k}^{'}} - k_{kin,b,k} \prod_{i=1}^{I} [X_i]^{\eta_{i,k}^{''}} \right) \tag{2-4}$$

where

$\hat{R}_{i,k}^{(A)}$ = molar rate of creation or destruction for ith species in kth reaction

X_i = molar concentration of ith species

$\eta_{i,k}^{'}$ = rate exponents for ith reactant species in kth reaction

$\eta_{i,k}^{''}$ = rate exponents for ith product species in kth reaction

The total molar rate of creation or destruction, $\omega_{i,g}$, of the species i from K number of reactions can be written as:

$$\omega_{i,g} = \sum_{k=1}^{K} \hat{R}_k^{(A)} \quad (i = 1, 2, 3, \ldots, I) \tag{2-5}$$

Similarly, for the surface phase reactions, the total molar rate of creation or destruction, $\omega_{i,s}$ of the ith species can be written as:

$$\omega_{i,s} = \sum_{k=1}^{K} \hat{R}_{i,k}^{(A,s)} \quad (i = 1, 2, 3, \ldots, I) \tag{2-6}$$

where $\hat{R}_{i,k}^{(A,s)}$ represents the molar rate of creation or destruction for the ith species in the kth surface reaction (similar to Eq. (2-4)).

The PFR is assumed to be complete mixing perpendicular to the direction of flow (i.e. the radial direction) and no mixing in the direction of flow. The equation for conservation governing the behavior of PFR model is given as follows:

$$\rho u A \frac{dY_i}{dx} + Y_i A_s \sum_{i=1}^{I} \omega_{i,s} M_i = M_i \left(\omega_{i,s} A_s + \omega_{i,g} A \right) \tag{2-7}$$

where

ρ = density

u   = axial velocity

x   = axial distance

A   = cross-sectional flow area

A_s = surface area of surface species per unit length

M_i = molecular weight of species *i*

Y_i = mass fraction of species *i*

The conservation Eq. (2-7) simply states that the mass of species can change as a result of generation or consumption of species by gas phase and surface phase reactions. The system of governing equation described above is solved using Chemkin for modeling multiple reactions in the PFR and analyzing the species mass fractions along the reactor.

2.4 Reaction mechanism

Two reaction mechanisms under conditions of without soot and with soot, illustrated in Fig. 2-2, are considered in the calculation. The chemical species are arranged in the order of molecular weight. Some of the aromatic species produced during pyrolysis are listed in Table 2-2. During gasification, these species undergo a chemical change to produce BIN1, BIN2, BIN3 and so on. BIN is considered as a class of aromatic species with molecular weight in the range of 300 to 153,600. BINs 1 to 3 are conceptually treated as intermediate aromatic species, while BINs 4 to 10 are considered as soot. This is consistent with the definition of nascent soot particles as species with a molecular weight of about 2000 [1]. The chemical formula and molecular weight of BINs are shown in Table 2-1. All aromatic species except soot will be referred here after as Polycyclic Aromatic Hydrocarbons (PAHs). The reaction mechanism without soot consist of 255 species (molecular weight range: 2~300) and 1095 elementary chemical reactions. While the reaction mechanism with soot consists of 276 species (molecular weight range: 2~153600) and 3793 elementary chemical reactions.

Species	*M*
H_2	2
CH_4	16
H_2O	18
CO	28
CO_2	44
....	....
C_6H_6	78
C_7H_8	92
$C_{10}H_8$	128
....	....
BIN1	300
BIN2	600
BIN3	1200
BIN4	2400
BIN5	4800
....	....
BIN10	153600

Detailed reaction mechanism without soot
Species: 256
Reactions: 1095

Detailed reaction mechanism with soot
Species: 276
Reactions: 3793

Aromatic

Initial

Intermediate

Soot
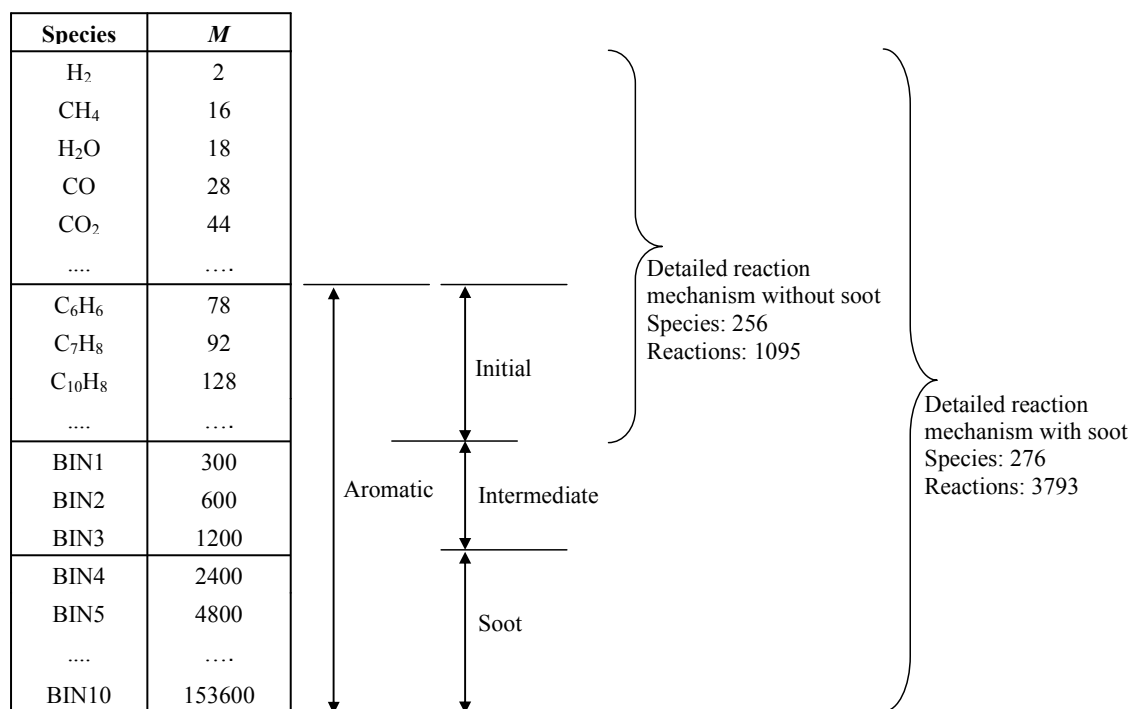
Figure 2-2 Illustration of reaction mechanism considered in calculation

Table 2-1 Chemical formula and molecular weight of BINs

BIN	Chemical formula	Molecular weight	wt% of C
1	$C_{24}H_{12}$	300	96.000
2	$C_{48}H_{24}$	600	96.000
3	$C_{96}H_{48}$	1,200	96.000
4	$C_{193}H_{84}$	2,400	96.500
5	$C_{388}H_{144}$	4,800	97.000
6	$C_{778}H_{264}$	9,600	97.250
7	$C_{1560}H_{480}$	19,200	97.500
8	$C_{3124}H_{912}$	38,400	97.625
9	$C_{6256}H_{1728}$	76,800	97.750
10	$C_{12528}H_{3264}$	153,600	97.875

2.5 Calculation conditions

The kinetic mechanism, Formation and Consumption of PAH and their Radicals in Premixed Rich Low Pressure Benzene Flames, taken from MIT combustion research website [2], is implemented to carry out the simulation. The simulation is conducted inside a reactor of 28 mm in diameter and 1200 mm in length. The temperature and pressure maintained in the reactor are 1273–1573 K and 0.1–2 MPa, respectively. The inlet gas velocity is 0.66 m/s. Total of 53 species (H_2, CH_4, H_2O, CO, CO_2, 10 other aliphatic compounds, 37 initial aromatic species and inert N_2) are considered as inlet. The corresponding inlet boundary species (mass fraction) are shown in Table 2-2. The chemical formula and structure of initial aromatic species are shown in Table 2-3.

Table 2-2 Mass fraction of inlet species

Species	Pyrolysis (N_2)	Partial Oxidation (N_2/O_2)	CO_2/O_2 Gasification ($N_2/O_2/CO_2$)
N_2	0.965800	0.958500	0.938600
O_2	0.000000	0.007354	0.007299
H_2	0.000502	0.000502	0.000498
CO	0.002849	0.002846	0.002825
CO_2	0.002239	0.002237	0.022410
H_2O	0.009643	0.009634	0.009563
CH_4	0.002132	0.002130	0.002114
C_2H_4	0.000573	0.000573	0.000568
C_2H_6	0.000359	0.000359	0.000356
C_3H_6	0.000435	0.000434	0.000431
C_3H_8	0.000121	0.000121	0.000120
CH_3OH	0.000022	0.000022	0.000022
CH_3CHO	0.000006	0.000006	0.000006
C_4H_8	0.000396	0.000395	0.000392
C_5H_6	0.000255	0.000255	0.000253
CH_3COCH_3	0.000322	0.000322	0.000319

Table 2-2 Mass fraction of inlet species (Continued)

	Species	Pyrolysis (N$_2$)	Partial Oxidation (N$_2$/O$_2$)	CO$_2$/O$_2$ Gasification (N$_2$/O$_2$/CO$_2$)
	C$_6$H$_6$	0.000678	0.000678	0.000673
	C$_7$H$_8$	0.000906	0.000905	0.000898
	C$_6$H$_5$OH	0.000955	0.000954	0.000947
	INDENE	0.000031	0.000031	0.000031
I	C$_{10}$H$_8$	0.000184	0.000184	0.000183
N	A2CH3-2	0.000117	0.000117	0.000116
I	A2CH3-1	0.000122	0.000122	0.000121
T	BIPHEN	0.000024	0.000024	0.000024
I	A2R5	0.000038	0.000038	0.000038
A	HA2R5	0.000038	0.000038	0.000038
L	FLUORENE	0.000088	0.000088	0.000087
	A3	0.000077	0.000077	0.000076
A	A3L	0.000056	0.000056	0.000055
R	A3CH2R	0.000056	0.000056	0.000055
O	A3R5	0.000056	0.000056	0.000055
M	A3LR5	0.000056	0.000056	0.000055
A	PYRENE	0.000113	0.000113	0.000112
T	BENZNAP	0.000056	0.000056	0.000055
I	FLTHN	0.000562	0.000561	0.000557
C	CPCDPYR	0.000562	0.000561	0.000557
	CPCDFLTH	0.000562	0.000561	0.000557
S	BGHIF	0.000562	0.000561	0.000557
P	A4	0.000562	0.000561	0.000557
E	A4L	0.000562	0.000561	0.000557
C	CHRYSEN	0.000562	0.000561	0.000557
I	BGHIFR	0.000562	0.000561	0.000557
E	COR	0.000562	0.000561	0.000557
S	DCPCDFG	0.000562	0.000561	0.000557
	BAPYR	0.000562	0.000561	0.000557
	BEPYREN	0.000562	0.000561	0.000557
	PERYLEN	0.000562	0.000561	0.000557
	BBFLUOR	0.000562	0.000561	0.000557
	BKFLUOR	0.000562	0.000561	0.000557
	ANTHAN	0.000562	0.000561	0.000557
	BGHIPER	0.000562	0.000561	0.000557
	INPYR	0.000562	0.000561	0.000557
	CPBPER	0.000562	0.000561	0.000557

Table 2-3 Chemical formula and structure of initial aromatic species
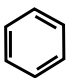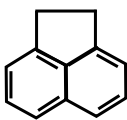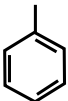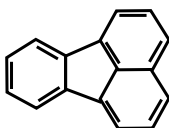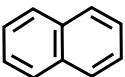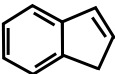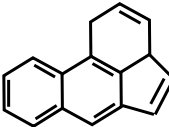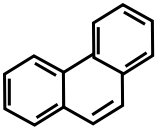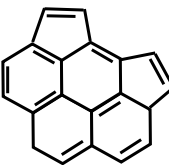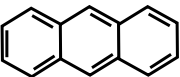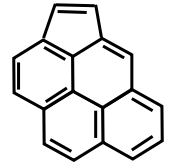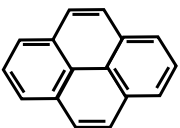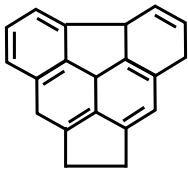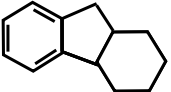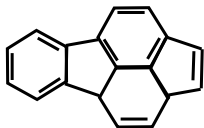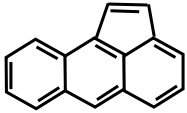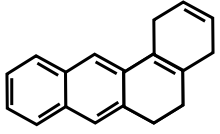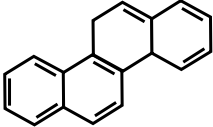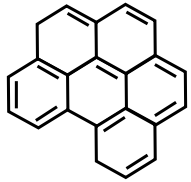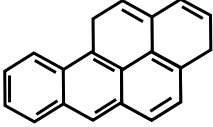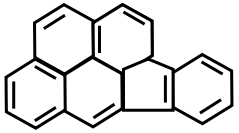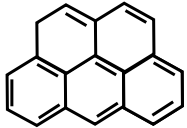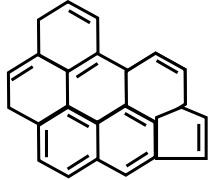
Species	Structure	Species	Structure
C_6H_6 Benzene		$C_{12}H_8$ (A2R5) Acenaphthylene	
C_7H_8 Toluene		$C_{16}H_{10}$ (FLTHN) Fluranthene	
$C_{10}H_8$ Napthalene		$C_{20}H_{10}$ (COR) Corannulene	
C_9H_8 INDENE		$C_{16}H_{10}$ A3R5 Acephenantrene	
$C_{14}H_{10}$ (A3) Phenanthrene		$C_{20}H_{10}$ (DCPCDFG) Dicyclopentapyrene-cdfg	
$C_{14}H_{10}$ (A3L) Anthracene		$C_{18}H_{10}$ (CPCDPYR) Cyclopenta[cd]pyrene	
$C_{16}H_{10}$ Pyrene		$C_{20}H_{10}$ (BGHIFR) Cyclopenta[cd]benzofluoranthene	
$C_{13}H_{10}$ Fluorene		$C_{18}H_{10}$ (CPCDFLTH) Cyclopenta[cd]fluoranthene	

Table 2-3 Chemical formula and structure of initial aromatic species (Continued)

Species	Structure	Species	Structure
$C_{16}H_{10}$ (A3LR5) Aceanthrylene		$C_{18}H_{12}$ (A4) Tetraphene benzo[a]anthracene	
$C_{18}H_{12}$ Chrysene		$C_{22}H_{12}$ (BGHIPER) Benzoperylene	
$C_{20}H_{12}$ (BAPYR) Benzo[a]pyrene		$C_{22}H_{12}$ (INPYR) Indeno[1,2,3-cd]pyrene	
$C_{22}H_{12}$ (ANTHAN) Anthracene		$C_{24}H_{12}$ (CPBPER) Cyclopentabenzoperylene	

2.6 Results and discussion

2.6.1 Comparison between experiment and calculation

The calculations using a detailed reaction mechanism without soot (256 species and 1095 chemical reactions) and a detailed reaction mechanism with soot (276 species and 3793 chemical reactions) for coal volatiles gasification are carried out under pyrolysis (N_2), partial oxidation (N_2/O_2) and CO_2/O_2 gasification ($N_2/O_2/CO_2$) conditions at 1273K and 0.1MPa in a plug flow reactor. Figure 2-3 compares the relative outlet concentrations of species for experiment and calculations. The relative concentration of species i is calculated as follows:

$$Y_{i,rel} = \frac{Y_{i,j}}{\min[Y_{i,pyrolysis}, Y_{i,partial\ oxidation}, Y_{i,CO_2/O_2\ gasification}]} \qquad (2\text{-}8)$$

where

j = pyrolysis, partial oxidation or CO_2/O_2 gasification

$Y_{i,pyrolysis}$ = outlet mass fraction of species i obtained from pyrolysis

$Y_{i,partial\ oxidation}$ = outlet mass fraction of species i obtained from partial oxidation

$Y_{i,CO_2/O_2\ gasification}$ = outlet mass fraction of species i obtained from CO_2/O_2 gasification

CO_2/O_2 gasification condition provides the lowest concentration of H_2 in experiment and calculations. The concentration of H_2 from pyrolysis is 1.25 times higher than that from CO_2/O_2 gasification condition. In contrast, maximum CO concentration can be achieved if the gasification occurs under CO_2/O_2 condition. CH_4 concentration from pyrolysis is higher than that from partial oxidation or CO_2/O_2 gasification condition. In partial oxidation or CO_2/O_2 gasification, CH_4 reacts with available O_2 or H_2O, resulting in a decrease in CH_4 concentration; in both experiment and calculation.
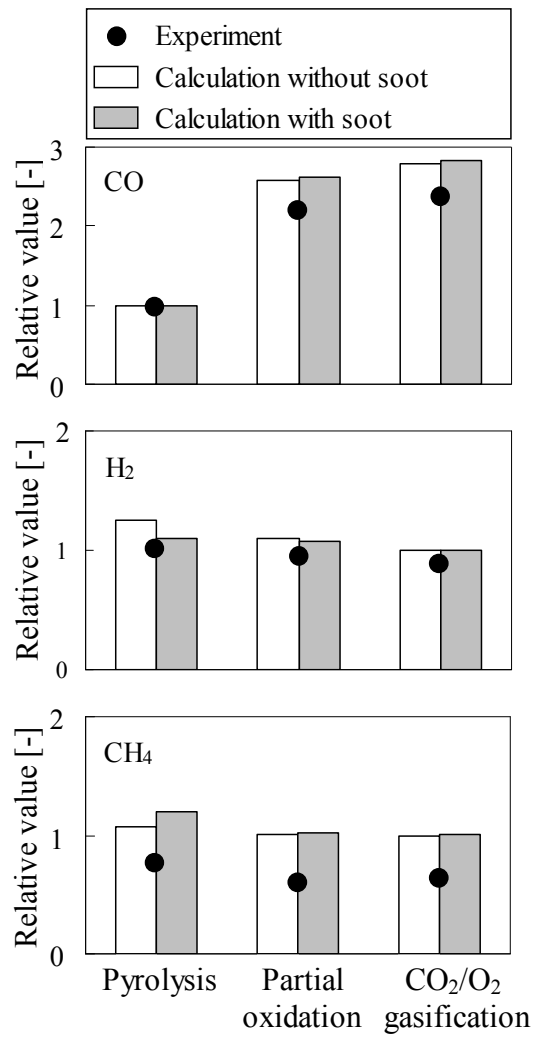
Figure 2-3 Comparison between experimental and calculated results

2.6.2 Reduction of reaction mechanism without soot

The term "reduced mechanism" here means a mechanism with a smaller number of species than the original "detailed mechanism". The ROP analysis is studied to make a reduced mechanism under $CO_2/O_2/N_2$ gasification condition. ROP analysis determines the contribution of each reaction to the net production or destruction rates of a species. The percentage of the contribution of the kth reaction to the formation or consumption of a species i is calculated as:

$$\omega_{con,i,k} = \frac{\hat{R}_{i,k}^{(A)}}{\omega_{i,g}} \times 100 \qquad (2\text{-}9)$$

where

$\omega_{con,i,k}$ = contribution of species i from kth reaction

$\hat{R}_{i,k}^{(A)}$ = rate of production [Arrhenius] of species i in kth reaction

$\omega_{i,g}$ = rate of production of species i from all gas phase reactions

To make a reduced mechanism from the detailed mechanism (255 species and 1095 reactions), the following steps are taken:

    (a) Determine five reactions for each species having the smallest value of $\omega_{con,i,k}$.

    (b) Remove the corresponding reactions.

    (c) Continue the step (a) and (b) for several times.

    (d) Calculate the number of reactions involved for each species.

    (e) If any species involved in less than three reactions, remove that species and the corresponding reactions.

    (f) Repeat the procedure from step (a) to (e).

To check if there is any significant reaction or species has been eliminated, the mechanism obtained after every step is compared with the detailed mechanism.

In Table 2-4, the corresponding number of species and reactions are shown for different progressive reduced mechanism (RM) under $CO_2/O_2/N_2$ gasification condition. In Fig. 2-4, the outlet species concentrations are shown for different reaction mechanisms. The outlet concentration of H_2, CO, CO_2 and PAH are found to be similar for RM1 to RM5. RM5 contains 12 inlet compound species and 165 elementary chemical reactions, which are listed in Tables 2-5 and 2-6. RM6 is made after removing some of the reactions, which are marked by underline in Table 2-6. However, RM6 shows large deviations although it consists of equal number of species with RM5 (Fig. 2-4). The calculated concentration of species for the RM5 is then compared with those for the detailed reaction mechanism in Figs. 2-5 and 2-6. It is found that the species concentration profiles for the RM5 are very similar to those for the detailed reaction mechanism under various operating conditions.

Table 2-4 Number of species and reactions involved in different reduced mechanism

No.	Name	Number of reactions	Number of species		
			Inlet	Intermediate	Total
0	Detailed mechanism without soot	1095	53	202	255
1	RM1	700	51	184	235
2	RM2	502	44	149	193
3	RM3	299	28	70	98
4	RM4	212	17	59	76
5	RM5	165	12	34	46
6	RM6	147	12	34	46
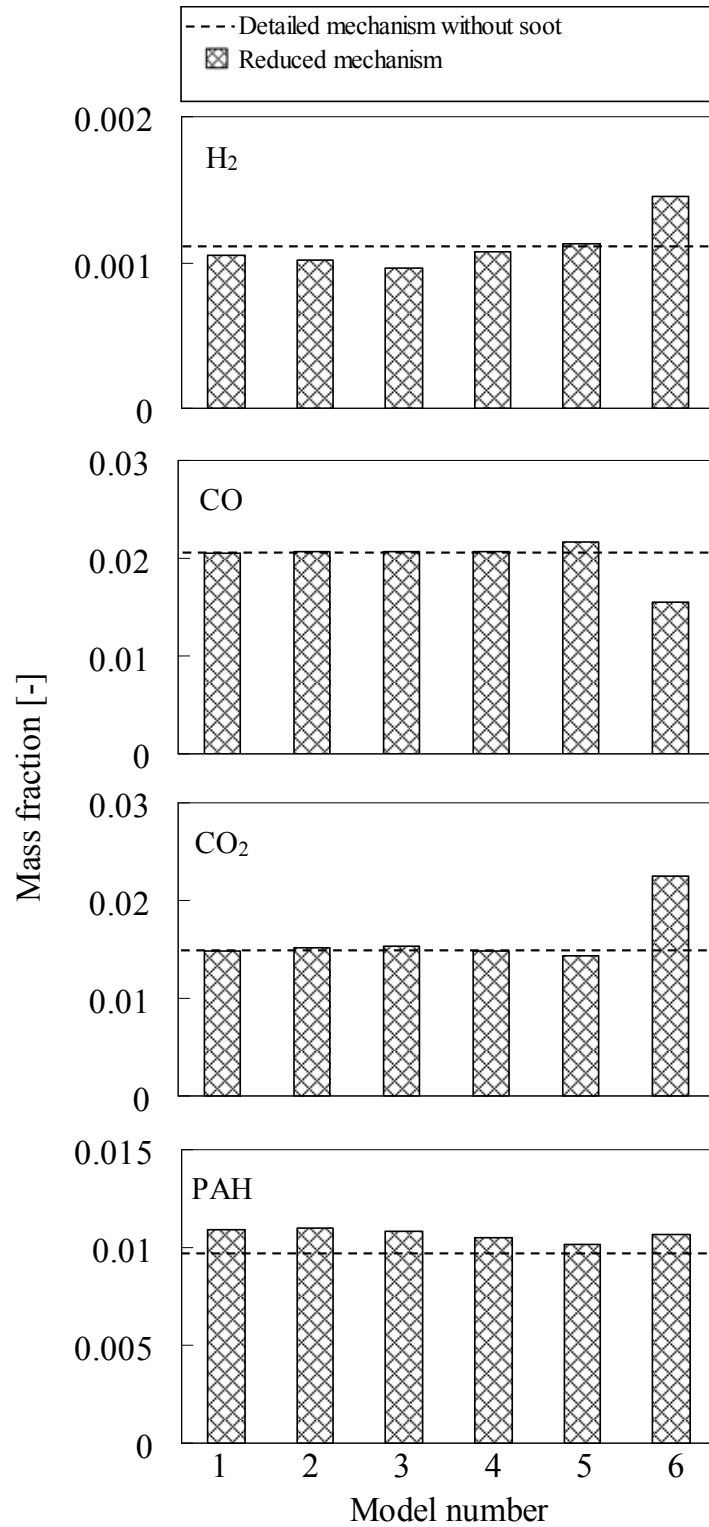
Figure 2-4 Comparison of reduced mechanism with detailed mechanism without soot

Table 2-5 Species involved in RM5

Inlets species (12)	CO, CO$_2$, H$_2$, H$_2$O, O$_2$, CH$_4$, C$_2$H$_6$, C$_2$H$_4$, C$_6$H$_6$, C$_6$H$_5$OH, C$_{10}$H$_8$ and N$_2$
Intermediate species (34)	C$_2$H$_2$ C$_2$H$_3$ C$_2$H$_5$ C$_3$H$_4$ C$_3$H$_5$ C$_4$H$_4$ C$_5$H$_4$O C$_5$H$_5$ C$_5$H$_6$ CH$_2$CHCHCH CH$_2$CHCHO CH$_2$CO CH$_2$O CH$_2$OH CH$_3$ CH$_3$O H H$_2$CCCCH H$_2$CCCH H$_2$O$_2$ HCCO HCH HCO HO$_2$ O C$_6$H$_4$O$_2$ OH C$_{10}$H$_7$ C$_{10}$H$_7$O C$_{10}$H$_7$OH C$_6$H$_5$ C$_6$H$_5$O C$_6$H$_5$OH and C$_7$H$_7$

Table 2-6 Reactions involved in RM5

Reaction	A_f [m^3/kmol·s]	α [-]	E_{ac} [J/kmol]
H$_2$+OH=H$_2$O+H	2.14×10^{05}	1.5	1.44×10^{07}
H$_2$+O$_2$=OH+OH	1.70×10^{10}	0	2.01×10^{08}
H+O$_2$=OH+O	1.91×10^{11}	0	6.90×10^{07}
H+O$_2$+M=HO$_2$+M	1.41×10^{15}	-0.8	0.00×10^{00}
H+O+M=OH+M	6.02×10^{13}	-0.6	0.00×10^{00}
OH+OH=O+H$_2$O	1.23×10^{01}	2.6	-7.89×10^{06}
O+HO$_2$=OH+O$_2$	1.74×10^{10}	0	-1.68×10^{06}
O+H$_2$=OH+H	5.13×10^{01}	2.7	2.64×10^{07}
O+OH+M=HO$_2$+M	1.00×10^{14}	0	0.00×10^{00}
HO$_2$+H=OH+OH	1.40×10^{11}	0	4.51×10^{06}
HO$_2$+HO$_2$=H$_2$O$_2$+O$_2$	2.00×10^{09}	0	0.00×10^{00}
H$_2$O$_2$+M=OH+OH+M	1.21×10^{14}	0	1.91×10^{08}
HCO+O$_2$=CO+HO$_2$	3.30×10^{10}	-0.4	0.00×10^{00}
HCO+M=H+CO+M	2.50×10^{11}	0	7.06×10^{07}
CO+OH=CO$_2$+H	6.32×10^{03}	1.5	-2.09×10^{06}
CO+HO$_2$=CO$_2$+OH	6.03×10^{10}	0	9.64×10^{07}
CH$_2$O+H=HCO+H$_2$	2.19×10^{05}	1.8	1.26×10^{07}
CH$_2$O+O=HCO+OH	1.80×10^{10}	0	1.29×10^{07}
CH$_2$O+HO$_2$=HCO+H$_2$O$_2$	4.40×10^{03}	2	5.04×10^{07}
HCH+O$_2$=CO$_2$+2H	1.60×10^{09}	0	4.20×10^{06}
HCH+O$_2$=CH$_2$O+O	5.00×10^{10}	0	3.78×10^{07}
HCH+OH=CH$_2$O+H	2.50×10^{10}	0	0.00×10^{00}
HCH+CH$_3$O=CH$_3$+CH$_2$O	1.81×10^{10}	0	0.00×10^{00}
CH$_3$+M=HCH+H+M	2.72×10^{33}	-5.3	4.92×10^{08}
CH$_3$+H=HCH+H$_2$	6.03×10^{10}	0	6.34×10^{07}
CH$_3$+O=CH$_2$O+H	7.17×10^{10}	0	0.00×10^{00}
CH$_3$+O=CH$_3$O	1.78×10^{11}	-2.1	2.53×10^{06}
CH$_3$+O$_2$=CH$_3$O+O	7.26×10^{08}	0.4	1.15×10^{08}
CH$_3$+OH=CH$_3$O+H	8.93×10^{08}	0	5.49×10^{07}
CH$_3$+OH=HCH+H$_2$O	7.50×10^{03}	2	2.10×10^{07}
CH$_3$+HO$_2$=CH$_3$O+OH	1.81×10^{10}	0	0.00×10^{00}
CH$_3$+CH$_2$O=CH$_4$+HCO	7.77×10^{-05}	6.1	8.27×10^{06}
CH$_3$+CH$_3$=C$_2$H$_5$+H	8.92×10^{08}	0	4.98×10^{07}
CH$_2$OH+M=CH$_2$O+H+M	1.67×10^{21}	-2.5	1.44×10^{08}
CH$_2$OH+O=CH$_2$O+OH	1.00×10^{10}	0	0.00×10^{00}
CH$_2$OH+O$_2$=CH$_2$O+HO$_2$	2.41×10^{11}	0	2.10×10^{07}

Table 2-6 Reactions involved in RM5 (Continued)

Reaction	A_f [m^3/kmol·s]	α [-]	E_{ac} [J/kmol]
CH$_3$O+M=CH$_2$O+H+M	5.42×10^{10}	0	5.67×10^{07}
CH$_3$O+O=CH$_2$O+OH	1.00×10^{10}	0	0.00×10^{00}
CH$_3$O+O$_2$=CH$_2$O+HO$_2$	6.30×10^{07}	0	1.09×10^{07}
CH$_4$+H=CH$_3$+H$_2$	1.48×10^{11}	0	5.71×10^{07}
CH$_4$+OH=CH$_3$+H$_2$O	1.57×10^{04}	1.8	1.17×10^{07}
CH$_4$+O=CH$_3$+OH	6.92×10^{05}	1.6	3.57×10^{07}
HCCO+O$_2$=2CO+OH	1.46×10^{09}	0	1.05×10^{07}
CH$_2$CO+M=HCH+CO+M	3.60×10^{12}	0	2.49×10^{08}
CH$_2$CO+O=HCO+HCO	2.00×10^{10}	0	9.63×10^{06}
CH$_2$CO+H=HCCO+H$_2$	5.00×10^{10}	0	3.36×10^{07}
CH$_2$CO+O=HCCO+OH	1.00×10^{10}	0	3.36×10^{07}
CH$_2$CO+OH=HCCO+H$_2$O	7.50×10^{09}	0	8.40×10^{06}
CH$_2$CO+OH=CH$_2$O+HCO	2.80×10^{10}	0	0.00×10^{00}
CH$_2$CO+OH=CH$_3$O+CO	2.80×10^{10}	0	0.00×10^{00}
C$_2$H$_2$+H$_2$=C$_2$H$_4$	1.41×10^{38}	-9.1	2.15×10^{08}
C$_2$H$_2$+OH=CH$_2$CO+H	2.18×10^{-01}	4.5	-4.20×10^{06}
HO$_2$+C$_2$H$_2$=CH$_2$CO+OH	6.03×10^{06}	0	3.34×10^{07}
C$_2$H$_2$+O=HCH+CO	1.40×10^{03}	2.1	6.56×10^{06}
C$_2$H$_2$+O=HCCO+H	5.80×10^{03}	2.1	6.56×10^{06}
C$_2$H$_3$=C$_2$H$_2$+H	2.74×10^{19}	-4.1	1.56×10^{08}
C$_2$H$_3$+O=CH$_2$CO+H	3.00×10^{10}	0	0.00×10^{00}
C$_2$H$_3$+O=C$_2$H$_2$+OH	3.00×10^{10}	0	0.00×10^{00}
2HCH=C$_2$H$_3$+H	7.12×10^{18}	-3.9	1.03×10^{07}
CH$_2$OH+C$_2$H$_2$=C$_2$H$_3$+CH$_2$O	7.30×10^{08}	0	3.78×10^{07}
C$_2$H$_3$+O$_2$=CH$_2$O+HCO	4.58×10^{13}	-1.4	4.26×10^{06}
C$_2$H$_3$+O$_2$=C$_2$H$_2$+HO$_2$	1.34×10^{03}	1.6	-1.61×10^{06}
C$_2$H$_3$+CH$_3$=C$_2$H$_2$+CH$_4$	1.99×10^{10}	0	0.00×10^{00}
HCH+C$_2$H$_3$=CH$_3$+C$_2$H$_2$	1.81×10^{10}	0	0.00×10^{00}
C$_2$H$_4$+H=C$_2$H$_3$+H$_2$	5.07×10^{04}	1.9	5.44×10^{07}
C$_2$H$_4$+H=C$_2$H$_5$	8.42×10^{05}	1.5	4.16×10^{06}
HCH+CH$_3$=C$_2$H$_4$+H	4.20×10^{10}	0	0.00×10^{00}
CH$_3$O+C$_2$H$_3$=CH$_2$O+C$_2$H$_4$	2.41×10^{10}	0	0.00×10^{00}
C$_2$H$_3$+CH$_2$OH=C$_2$H$_4$+CH$_2$O	3.01×10^{10}	0	0.00×10^{00}
C$_2$H$_4$+O=CH$_3$+HCO	1.60×10^{06}	1.2	3.13×10^{06}
C$_2$H$_4$+OH=CH$_3$+CH$_2$O	1.05×10^{09}	0	-3.85×10^{06}
C$_2$H$_4$+CH$_3$=C$_2$H$_3$+CH$_4$	4.16×10^{09}	0	4.67×10^{07}
C$_2$H$_4$+C$_2$H$_2$=2C$_2$H$_3$	2.41×10^{10}	0	2.87×10^{08}
C$_2$H$_5$+O=C$_2$H$_4$+OH	5.00×10^{10}	0	0.00×10^{00}
C$_2$H$_5$+O=CH$_2$O+CH$_3$	1.61×10^{10}	0	0.00×10^{00}
HCH+CH$_3$=C$_2$H$_5$	2.53×10^{17}	-3.5	8.53×10^{06}
C$_2$H$_5$+O$_2$=C$_2$H$_4$+HO$_2$	1.92×10^{04}	1	-8.55×10^{06}
C$_2$H$_5$+HO$_2$=CH$_3$+CH$_2$O+OH	2.40×10^{10}	0	0.00×10^{00}
HCH+C$_2$H$_5$=CH$_3$+C$_2$H$_4$	1.81×10^{10}	0	0.00×10^{00}
C$_2$H$_6$+CH$_3$=C$_2$H$_5$+CH$_4$	5.50×10^{-04}	4	3.49×10^{07}
C$_2$H$_6$+O=C$_2$H$_5$+OH	3.00×10^{04}	2	2.15×10^{07}
C$_2$H$_6$+HO$_2$=C$_2$H$_5$+H$_2$O$_2$	2.95×10^{08}	0	6.27×10^{07}
C$_2$H$_4$+C$_2$H$_5$=C$_2$H$_3$+C$_2$H$_6$	6.32×10^{-01}	3.1	7.56×10^{07}

Table 2-6 Reactions involved in RM5 (Continued)

Reaction	A_f [m³/kmol·s]	α [-]	E_{ac} [J/kmol]
C₂H₃+C₂H₅=C₂H₆+C₂H₂	4.82×10⁰⁸	0	0.00×10⁰⁰
H₂CCCH+O₂=CH₂CO+HCO	3.00×10⁰⁷	0	1.20×10⁰⁷
HCH+C₂H₂=H₂CCCH+H	1.20×10¹⁰	0	2.77×10⁰⁷
H₂CCCH+OH=CH₂CHCHO	3.01×10¹⁰	0	0.00×10⁰⁰
HCO+C₂H₃=CH₂CHCHO	1.81×10¹⁰	0	0.00×10⁰⁰
C₃H₅+O=CH₂CHCHO+H	6.03×10¹⁰	0	0.00×10⁰⁰
C₃H₄=H₂CCCH+H	2.30×10⁰⁹	0	2.93×10⁰⁸
C₃H₄+OH=HCO+C₂H₄	1.00×10⁰⁹	0	0.00×10⁰⁰
C₃H₄+CH₃=H₂CCCH+CH₄	2.00×10⁰⁹	0	3.23×10⁰⁷
C₃H₄+H=C₂H₂+CH₃	2.00×10¹⁰	0	1.01×10⁰⁷
C₂H₃+HCH=C₃H₄+H	3.00×10¹⁰	0	0.00×10⁰⁰
C₃H₄+O=CH₂O+C₂H₂	9.00×10⁰⁹	0	7.85×10⁰⁶
C₃H₄+O=HCO+C₂H₃	9.00×10⁰⁹	0	7.85×10⁰⁶
C₃H₄+OH=CH₂CO+CH₃	3.37×10⁰⁹	0	-1.28×10⁰⁶
C₃H₄+H=H₂CCCH+H₂	3.00×10⁰⁴	2	2.10×10⁰⁷
C₃H₄+OH=H₂CCCH+H₂O	2.00×10⁰⁴	2	4.20×10⁰⁶
C₃H₄+H=C₃H₅	1.20×10⁰⁸	0.7	1.26×10⁰⁷
C₃H₅+C₂H₃=C₃H₄+C₂H₄	2.41×10⁰⁹	0	0.00×10⁰⁰
C₃H₅+C₂H₅=C₃H₄+C₂H₆	9.64×10⁰⁸	0	-5.50×10⁰⁵
C₂H₃+CH₂OH=C₃H₅+OH	1.21×10¹⁰	0	0.00×10⁰⁰
C₂H₄+HCH=C₃H₅+H	3.19×10⁰⁹	0	2.22×10⁰⁷
CH₃+C₂H₂=C₃H₅	1.40×10⁰¹	2.2	6.93×10⁰⁷
C₂H₃+CH₃=C₃H₅+H	7.20×10¹⁰	0	0.00×10⁰⁰
H₂CCCCH+O₂=CH₂CO+HCCO	1.00×10⁰⁹	0	0.00×10⁰⁰
C₂H₂+C₂H₂=C₄H₄	1.89×10⁵⁵	-13.6	2.64×10⁰⁸
C₂H₃+C₂H₃=C₄H₄+2H	7.83×10⁰⁹	0	0.00×10⁰⁰
C₂H₃+C₂H₂=C₄H₄+H	1.91×10¹²	-0.7	4.41×10⁰⁷
H₂CCCH+HCH=C₄H₄+H	4.00×10¹⁰	0	0.00×10⁰⁰
C₄H₄+H=H₂CCCCH+H₂	3.00×10⁰⁴	2	2.10×10⁰⁷
C₄H₄+C₂H₃=C₂H₄+H₂CCCCH	5.00×10⁰⁸	0	6.85×10⁰⁷
C₂H₃+C₂H₂=CH₂CHCHCH	3.45×10⁴²	-11.1	6.71×10⁰⁷
CH₂CHCHCH+M=C₄H₄+H+M	1.00×10¹¹	0	1.26×10⁰⁸
CH₂CHCHCH+O₂=C₄H₄+HO₂	1.20×10⁰⁸	0	0.00×10⁰⁰
C₅H₅+H=C₅H₆	2.71×10⁶⁰	-14.8	8.84×10⁰⁷
C₅H₅=H₂CCCH+C₂H₂	2.79×10⁷⁶	-18.3	5.50×10⁰⁸
C₅H₅+O=CH₂CHCHCH+CO	7.27×10¹⁰	-0.3	1.97×10⁰⁶
C₅H₅+O=C₅H₄O+H	6.71×10¹⁰	0	1.68×10⁰⁵
C₅H₄O+H=CH₂CHCHCH+CO	2.10×10⁵⁸	-13.3	1.71×10⁰⁸
C₅H₆+H=C₅H₅+H₂	2.80×10¹⁰	0	9.49×10⁰⁶
C₅H₆+H=C₃H₅+C₂H₂	6.60×10¹¹	0	5.18×10⁰⁷
C₅H₆+O=C₅H₅+OH	4.77×10⁰¹	2.7	4.65×10⁰⁶
C₅H₆+O₂=C₅H₅+HO₂	4.00×10¹⁰	0	1.56×10⁰⁸
C₅H₆+HO₂=C₅H₅+H₂O₂	1.10×10⁰¹	2.6	5.42×10⁰⁷
C₅H₆+CH₃=C₅H₅+CH₄	1.80×10⁻⁰⁴	4	0.00×10⁰⁰
C₅H₆+C₂H₃=C₅H₅+C₂H₄	1.20×10⁻⁰⁴	4	0.00×10⁰⁰
C₃H₅+C₅H₅=C₅H₆+C₃H₄	1.00×10⁰⁹	0	0.00×10⁰⁰
C₆H₅+O₂=C₆H₅O+O	2.39×10¹⁸	-2.6	1.85×10⁰⁷

Table 2-6 Reactions involved in RM5 (Continued)

Reaction	$A_f[\text{m}^3/\text{kmol·s}]$	α [-]	E_{ac} [J/kmol]
$C_6H_5+HO_2=C_6H_5O+OH$	5.00×10^{10}	0	4.20×10^{06}
$H_2CCCH+H_2CCCH=C_6H_6$	3.00×10^{09}	0	0.00×10^{00}
$\underline{C_4H_4+C_2H_3=C_6H_6+H}$	1.90×10^{09}	0	1.05×10^{07}
$\underline{C_3H_4+H_2CCCH=C_6H_6+H}$	2.20×10^{08}	0	8.40×10^{06}
$C_6H_6+H=C_6H_5+H_2$	3.23×10^{04}	2.1	6.65×10^{07}
$C_6H_6+O=C_6H_5+OH$	2.00×10^{10}	0	6.18×10^{07}
$C_6H_6+O=C_6H_5O+H$	2.40×10^{10}	0	1.96×10^{07}
$C_6H_6+OH=C_6H_5+H_2O$	2.11×10^{10}	0	1.92×10^{07}
$\underline{C_6H_5+CH_4=C_6H_6+CH_3}$	6.00×10^{09}	0	5.17×10^{07}
$C_6H_6+OH=C_6H_5OH+H$	1.59×10^{16}	-1.8	5.38×10^{07}
$C_6H_5O+H=C_6H_5OH$	4.43×10^{57}	-13.2	1.26×10^{08}
$C_6H_5O=C_5H_5+CO$	2.51×10^{08}	0	1.84×10^{08}
$C_6H_5OH=C_5H_6+CO$	1.00×10^{09}	0	2.55×10^{08}
$C_6H_5OH+O=C_6H_5O+OH$	2.81×10^{10}	0	3.09×10^{07}
$C_6H_5OH+HO_2=C_6H_5O+H_2O_2$	3.00×10^{10}	0	6.30×10^{07}
$C_6H_5OH+C_2H_3=C_2H_4+C_6H_5O$	6.00×10^{09}	0	0.00×10^{00}
$C_6H_5OH+C_6H_5=C_6H_6+C_6H_5O$	4.91×10^{09}	0	1.85×10^{07}
$C_6H_5O+C_5H_6=C_5H_5+C_6H_5OH$	3.16×10^{08}	0	3.36×10^{07}
$C_6H_5+O_2=C_6H_4O_2+H$	3.00×10^{10}	0	3.78×10^{07}
$C_6H_4O_2=C_5H_4O+CO$	1.00×10^{09}	0	1.68×10^{08}
$C_6H_5+CH_3=C_7H_7+H$	4.44×10^{30}	-5.5	1.02×10^{08}
$C_4H_4+H_2CCCH=C_7H_7$	5.39×10^{48}	-12.2	2.99×10^{07}
$C_7H_7+HO_2=C_6H_5+CH_2O+OH$	5.00×10^{09}	0	0.00×10^{00}
$\underline{2C_5H_5=C_{10}H_8+2H}$	5.00×10^{09}	0	3.36×10^{07}
$\underline{C_7H_7+H_2CCCH=C_{10}H_8+H+H}$	3.00×10^{09}	0	0.00×10^{00}
$C_{10}H_8+CH_3=C_{10}H_7+CH_4$	2.00×10^{09}	0	6.33×10^{07}
$C_{10}H_7+O_2=C_{10}H_7O+O$	2.39×10^{18}	-2.6	1.85×10^{07}
$C_{10}H_8+OH=C_{10}H_7OH+H$	1.59×10^{16}	-1.8	5.38×10^{07}
$C_{10}H_7O+H=C_{10}H_7OH$	4.43×10^{57}	-13.2	1.26×10^{08}
$C_{10}H_8+H=C_{10}H_7+H_2$	3.23×10^{04}	2.1	6.65×10^{07}
$C_{10}H_8+OH=C_{10}H_7+H_2O$	2.11×10^{10}	0	1.92×10^{07}
$CH_2CHCHCH+C_2H_2=C_6H_6+H$	1.90×10^{04}	1.5	2.06×10^{07}
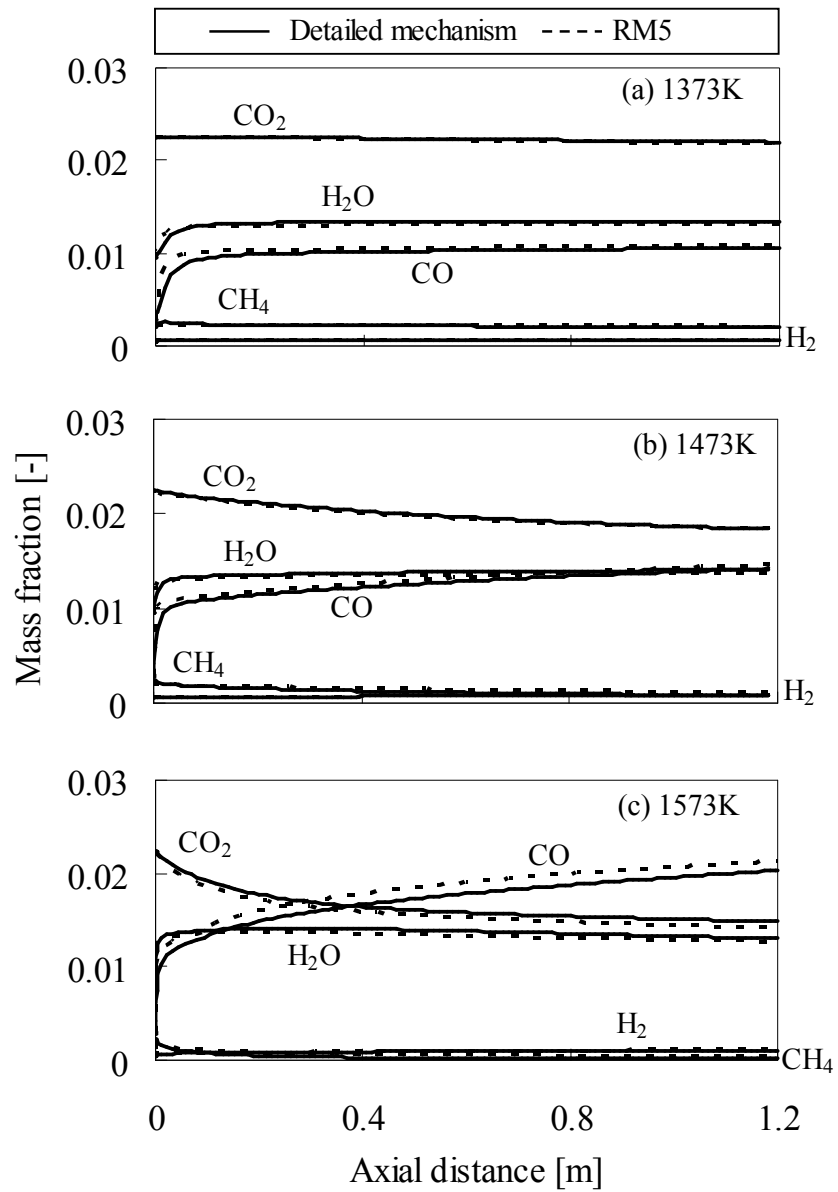
Figure 2-5 Comparison of species concentration profiles at 0.1 MPa
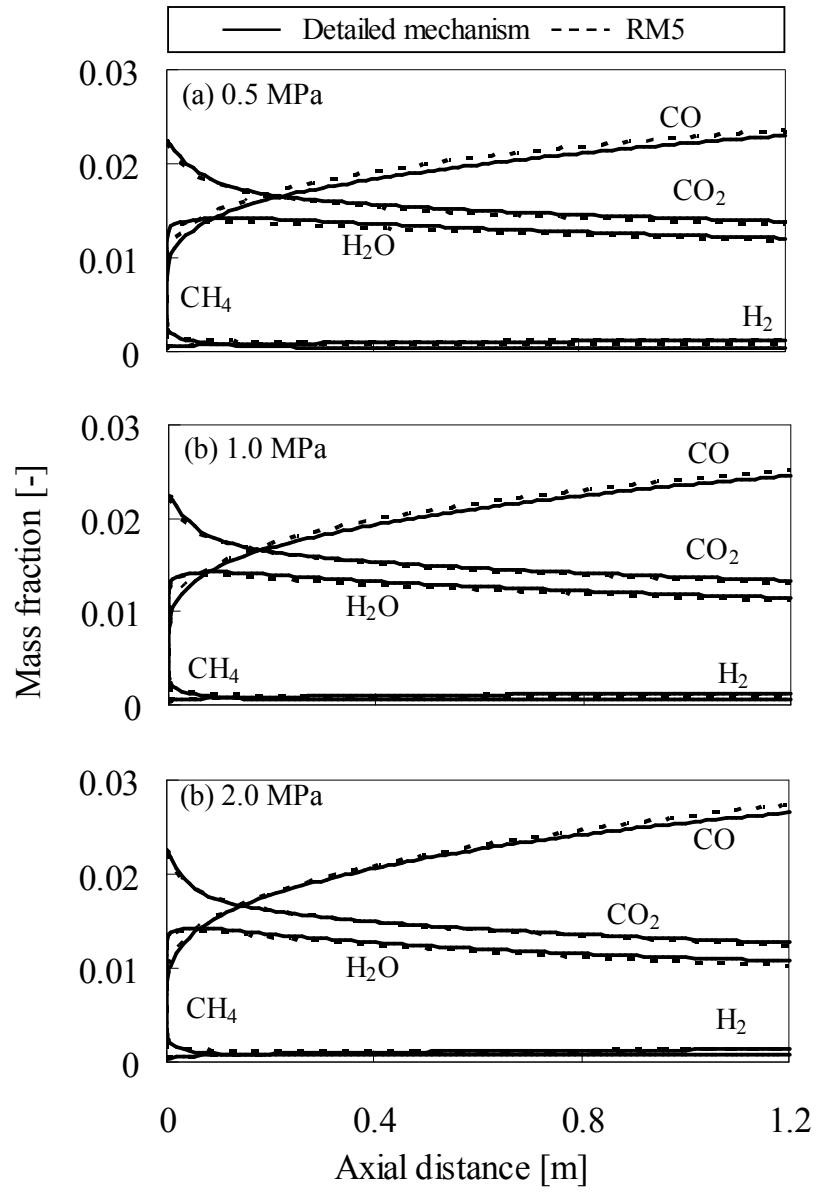
Figure 2-6 Comparison of species concentration profiles at 1573K

2.6.3 Main reaction pathways

All inlet species (CO, CO_2, H_2, H_2O, O_2, CH_4, C_2H_6, C_2H_4, C_6H_6, C_6H_5OH and $C_{10}H_8$) are placed in the main reaction pathways. Every two species are connected with an arrow line. The arrow indicates the way that the reaction proceeds . Some pairs of species such as CH_4 and O_2, CH_4 and CO_2, C_2H_6 and CO etc. have no reaction with each other and therefore they are not connected. The contribution of each reaction to the total rate of production or consumption of each species is investigated. The reactions having the highest contribution for every two connecting species are summarized in Table 2-7.

The main reaction pathways in coal volatiles gasification is shown in Fig. 2-7. It shows that aliphatic hydrocarbons C_2H_4 and C_2H_6 mainly contribute to the production of CH_4 and H_2 (MR6, MR7, MR8, MR10). Whereas aromatic compounds C_6H_6 and C_6H_5OH affect the CO production. C_6H_6 reacts with available OH radical to produce C_6H_5OH (MR11). The dissociation of C_6H_5OH then produces CO (MR14). The forward rates of reactions are dominant for all reactions mentioned in main reaction path except MR1 and MR2. Under higher temperature, reverse reaction of MR1 and MR2 become dominant, resulting in a significant increase in syngas (CO and H_2) concentration.

The reaction mechanism with soot illustrated in Fig. 2-2 consists of 3793 elementary chemical reactions. Among them about 70% of the reactions are similar to MSR1 and MSR2.

$$PAH/PAH^* + PAH/PAH^* = PAH/PAH^* + H/H_2 \hspace{3cm} \text{(MSR1)}$$

$$PAH/PAH^* + O/OH = PAH/PAH^* + CO + H/H_2 \hspace{2.5cm} \text{(MSR2)}$$
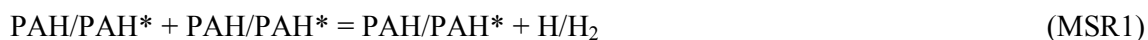
where PAH* means a PAH radical entity.

Reaction MSR1, which involves reactions of PAH* with PAH and between PAH*, is the dominant formation pathway of soot nuclei. This process is repeated producing higher molecular weight PAH, that forms soot particle. In contrast, oxidation by oxygen or hydroxyl radicals in reaction MSR2 depletes PAH and soot.

The main reaction pathways is extended considering the soot formation mechanism and shown in Fig. 2-8. In this reaction pathways, all aromatic compounds are represented as PAH molecules except C_6H_6. The species $C_{10}H_8$ shown in Fig. 2-7 is combined with PAH molecules in Fig. 2-8. MR11, MR16 and MR17 are integrated to MSR1. Therefore, these reactions are omitted from the reaction pathways. The contribution of MR14 compared to MSR1 and MSR2 is also very small in soot formation mechanism. C_6H_6 is directly related to CH_4 and H_2O formation (MR9 and MR12). C_6H_6 is also responsible to produce higher PAH molecules by similar reaction to MSR1. It is also found that oxidation of PAHs/soot (MSR2) can play a major role to produce CO and H_2. More explanation of this reaction pathways is explained in the next analysis of coal volatiles gasification under various operating conditions.

Table 2-7 Main reactions in coal volatiles gasification

ID	Reactions	A_f[m^3/kmol·s]	α [-]	E_{ac} [J/kmol]
MR1	$H_2+OH=H_2O+H$	2.14×10^{05}	1.5	1.44×10^{07}
MR2	$CO+OH=CO_2+H$	6.32×10^{03}	1.5	-2.09×10^{06}
MR3	$HCCO+O_2=2CO+OH$	1.46×10^{09}	0	1.05×10^{07}
MR4	$CH_4+OH=CH_3+H_2O$	1.57×10^{04}	1.8	1.17×10^{07}
MR5	$CH_4+H=CH_3+H_2$	1.48×10^{11}	0	5.71×10^{07}
MR6	$C_2H_4+CH_3=C_2H_3+CH_4$	4.16×10^{09}	0	4.67×10^{07}
MR7	$C_2H_4+C_2H_5=C_2H_3+C_2H_6$	6.32×10^{-01}	3.1	7.56×10^{07}
MR8	$C_2H_6+CH_3=C_2H_5+CH_4$	5.50×10^{-04}	4	3.49×10^{07}
MR9	$C_6H_5+CH_4=C_6H_6+CH_3$	6.00×10^{09}	0	5.17×10^{07}
MR10	$C_2H_4+H=C_2H_3+H_2$	5.07×10^{04}	1.9	5.44×10^{07}
MR11	$C_6H_6+OH=C_6H_5OH+H$	1.59×10^{16}	-1.8	5.38×10^{07}
MR12	$C_6H_6+OH=C_6H_5+H_2O$	2.11×10^{10}	0	1.92×10^{07}
MR13	$C_6H_6+H=C_6H_5+H_2$	3.23×10^{04}	2.1	6.65×10^{07}
MR14	$C_6H_5OH=C_5H_6+CO$	1.00×10^{09}	0	2.55×10^{08}
MR15	$C_{10}H_8+CH_3=C_{10}H_7J1+CH_4$	2.00×10^{09}	0	6.33×10^{07}
MR16	$C_{10}H_8+H=C_{10}H_7J1+H_2$	3.23×10^{04}	2.1	6.65×10^{07}
MR17	$C_{10}H_8+OH=C_{10}H_7J1+H_2O$	2.11×10^{10}	0	1.92×10^{07}
MSR1	PAH/PAH* + PAH/PAH* = PAH/PAH* + H/H$_2$			
MSR2	PAH/PAH* + O/OH = PAH/PAH* + CO + H/H$_2$			

Note:

MR = main reaction, MSR = main soot reaction

Typical reactions of MSR1 and MSR2 are as follows:

MSR1: $C_{10}H_8 + C_6H_5 = C_{16}H_{10}$ (FLTHN) + H + H$_2$

$C_{14}H_{10}$ (A3) + $C_{12}H_9$ = 1.083BIN1 + 2.50H$_2$ + H

MSR2:   0.005BIN5 + OH = 0.00513BIN4 + CO + 1.308H

0.001BIN10 + O = 0.000159BIN9 + CO + 0.245H
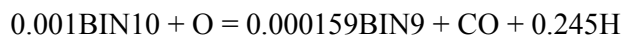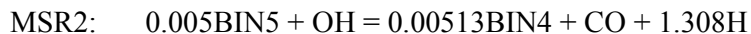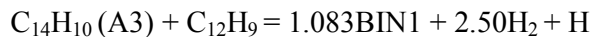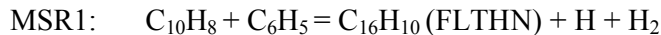
BIN is a class of PAH with molecular weight in the range of 300 to 153,600. BINs 1 to 3 are conceptually treated as intermediate PAHs, while BINs 4 to 10 are considered as soot.
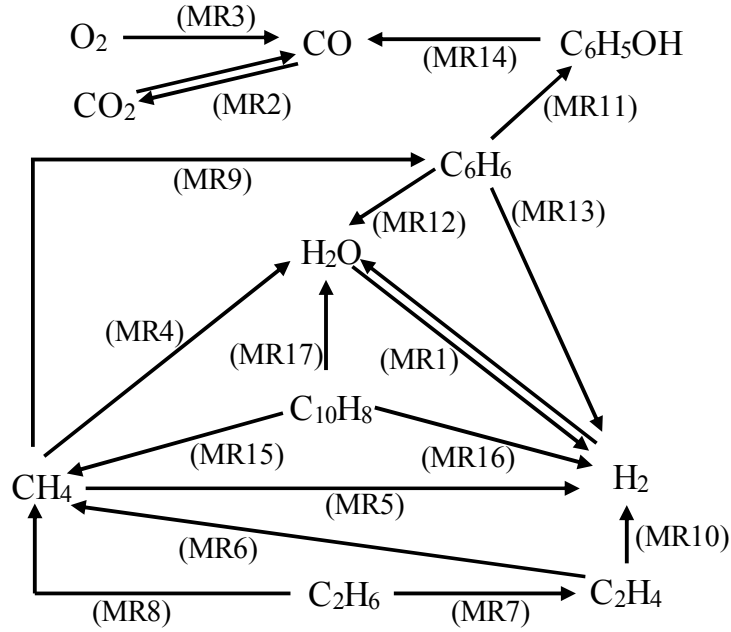
Figure 2-7 Main reaction path ways under condition of without soot formation
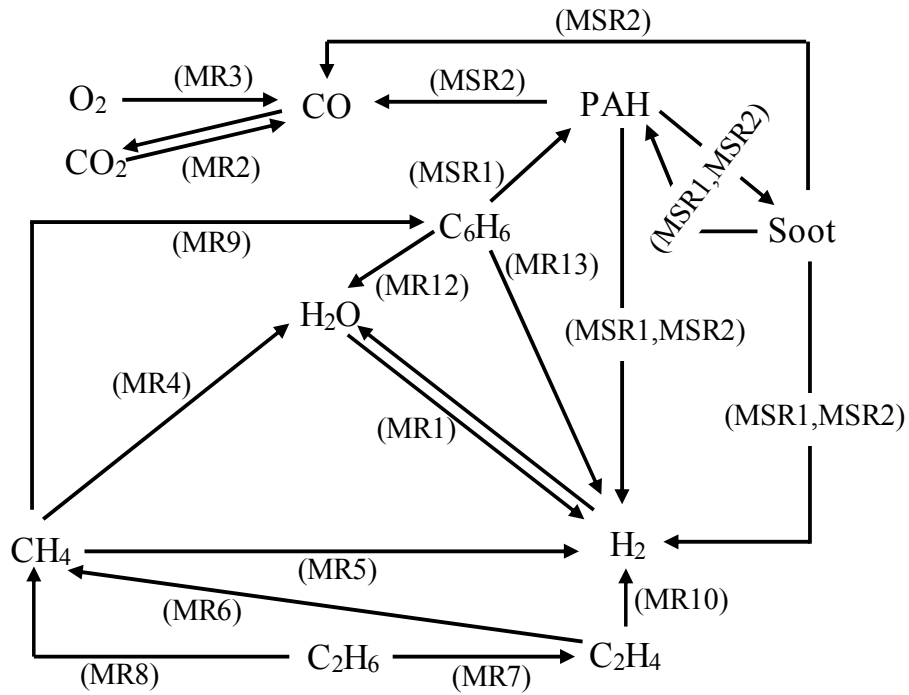
Figure 2-8 Main reaction pathways under condition of soot formation

2.6.4 Soot formation: Effect of temperature and pressure

Using the detailed reaction mechanism with soot (species 276 and reactions 3793), different concentration profiles are observed for species H_2, H_2O, CH_4, CO, CO_2 and PAHs/soot at 1273 K and 0.1 MPa under pyrolysis (N_2), partial oxidation (N_2/O_2), and CO_2/O_2 gasification conditions (Fig. 2-9). Partial oxidation and CO_2/O_2 gasification conditions produce similar concentration profiles and the following changes in concentration are observed. The mass fraction of CH_4 decreases as it reacts with hydroxyl/oxygen radicals to form hydrocarbon radicals and H_2O (MR4, Fig. 2-8). H_2O and CO mass fractions increase due to interaction between CO_2 and H_2. Due to reactions MR4 and MR12 (Fig. 2-8), H_2O also increases. CO and H_2 also increase because of the oxidation of PAHs/soot (MSR2). In addition, CO_2/O_2 gasification provides more CO_2, which produces CO and OH radical and also contributes to the CO mass fraction increase. The mass fractions of PAHs decreased as they are involved in soot formation and PAHs/soot oxidation (MSR1 & MSR2). The concentration profiles of PAHs and soot are very similar under partial oxidation and CO_2/O_2 gasification conditions. Compared with partial oxidation and CO_2/O_2 gasification, the pyrolysis condition produces less CO and more PAHs/soot because a lack of O_2 led to minimal soot oxidation.
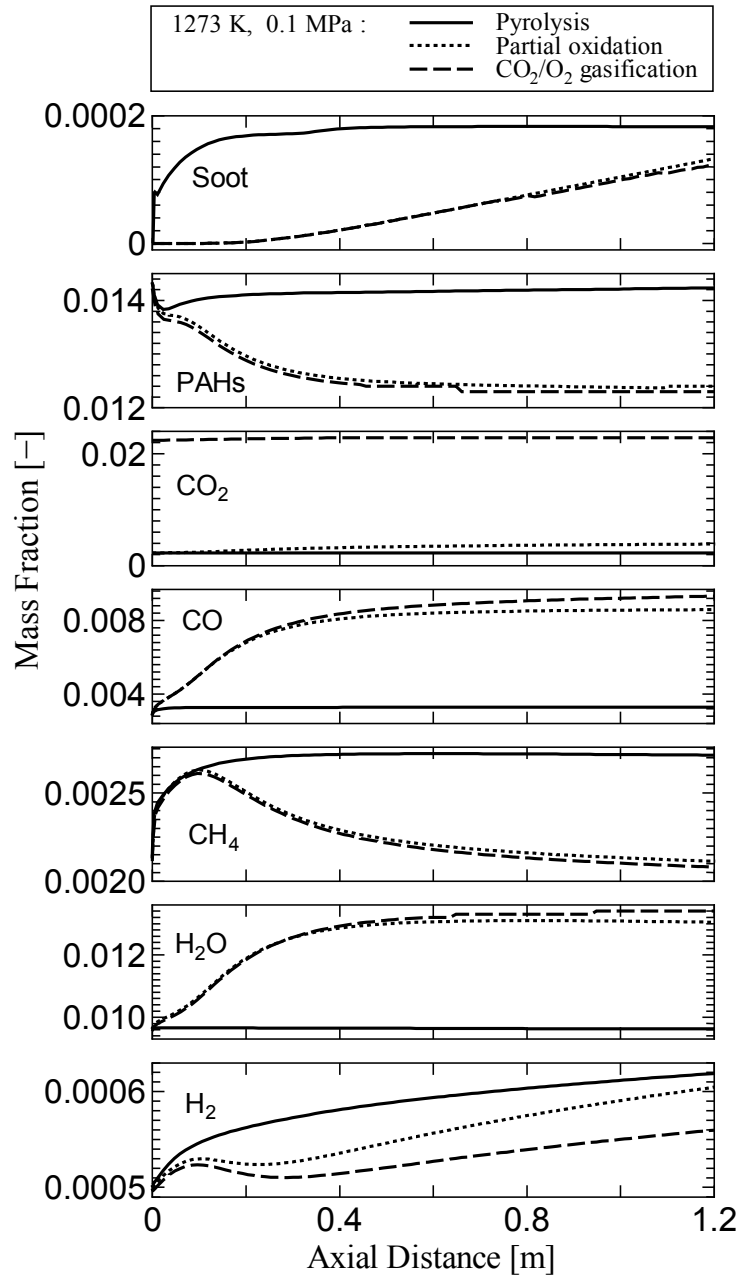
Figure 2-9 Species concentration profiles under various gasification conditions

The effects of reaction temperature on product mass fractions are investigated from 1273–1873 K at a constant pressure (0.1 MPa) under CO_2/O_2 gasification condition (Fig. 2-10). The mass fractions of H_2 and CO increase and that of CO_2 decreases with increasing reaction temperature. The CO_2 mass fraction is considerably lower at higher temperatures. Reverse reaction of MR2 (Fig. 2-8) becomes dominant at higher temperatures, which contributes to reduction of CO_2. With increasing reaction temperature, the mass fraction of PAHs decreases rapidly. This is occurred due to oxidation of PAHs (MSR2), which produces CO and H_2, at a high reaction temperature.

At a high constant pressure (2 MPa) under CO_2/O_2 gasification condition (Fig. 2-11), with increasing the reaction temperature, the mass fractions of H_2 and CO increase and those of CO_2 and PAHs decrease. Comparison between Figs. 2-10 and 2-11 indicates that 2 MPa results in more H_2 and CO and less CO_2 and PAHs than 0.1 MPa.

The effects of pressure on product mass fractions are investigated from 0.1–2 MPa at 1473K and 1673K under CO_2/O_2 gasification condition (Figs. 2-12 and 2-13). With increasing pressure, the mass fractions of H_2 and CO increase. On the other hand, the mass fractions of CO_2 and PAHs reduce with increasing pressure. However, the effect of pressure on product concentration appears smaller when the temperature is high (1673K).
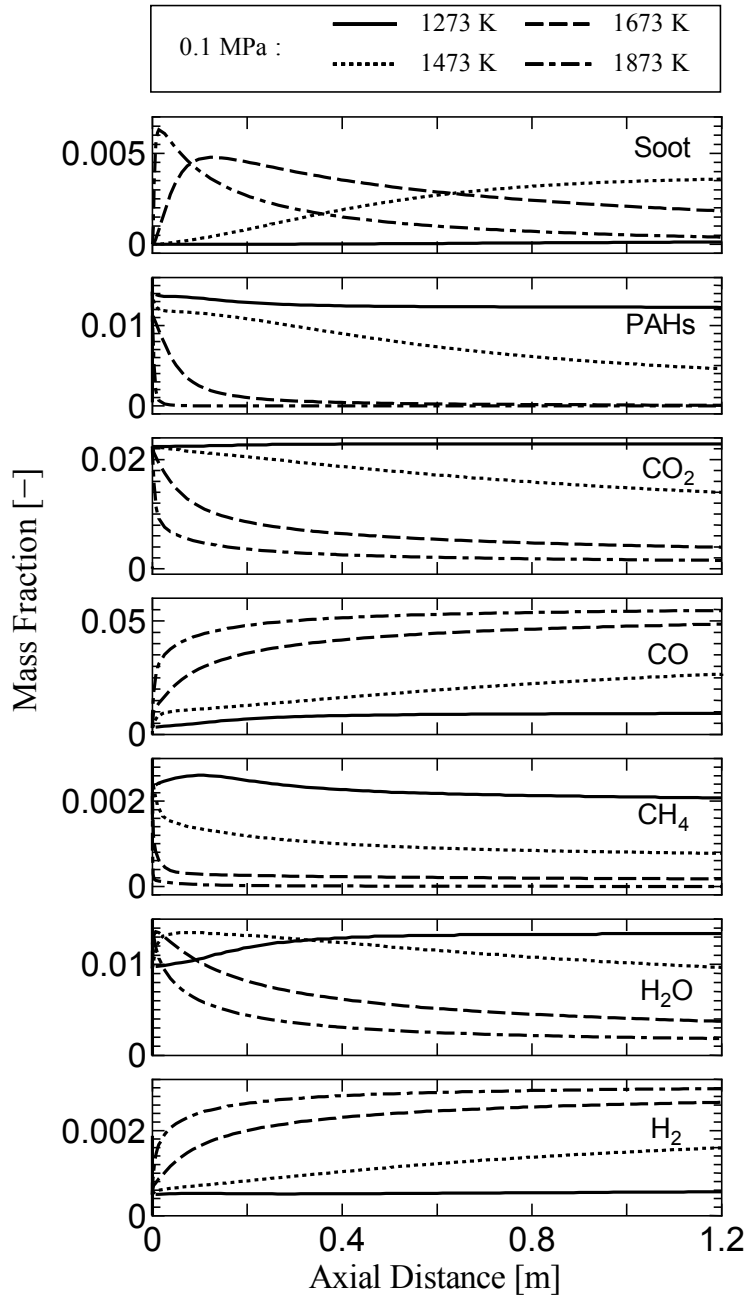
Figure 2-10 Comparison of species concentration profiles at 0.1 MPa
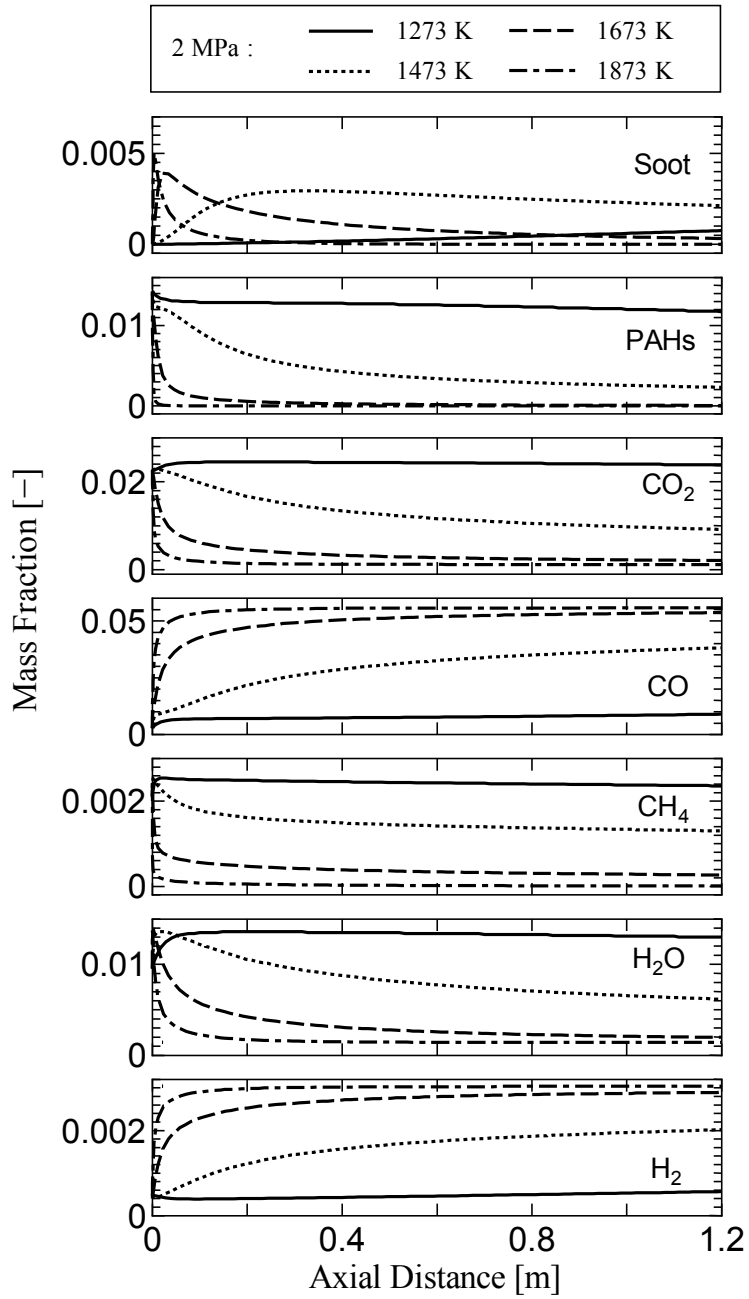
Figure 2-11 Comparison of species concentration profiles at 2 MPa

48
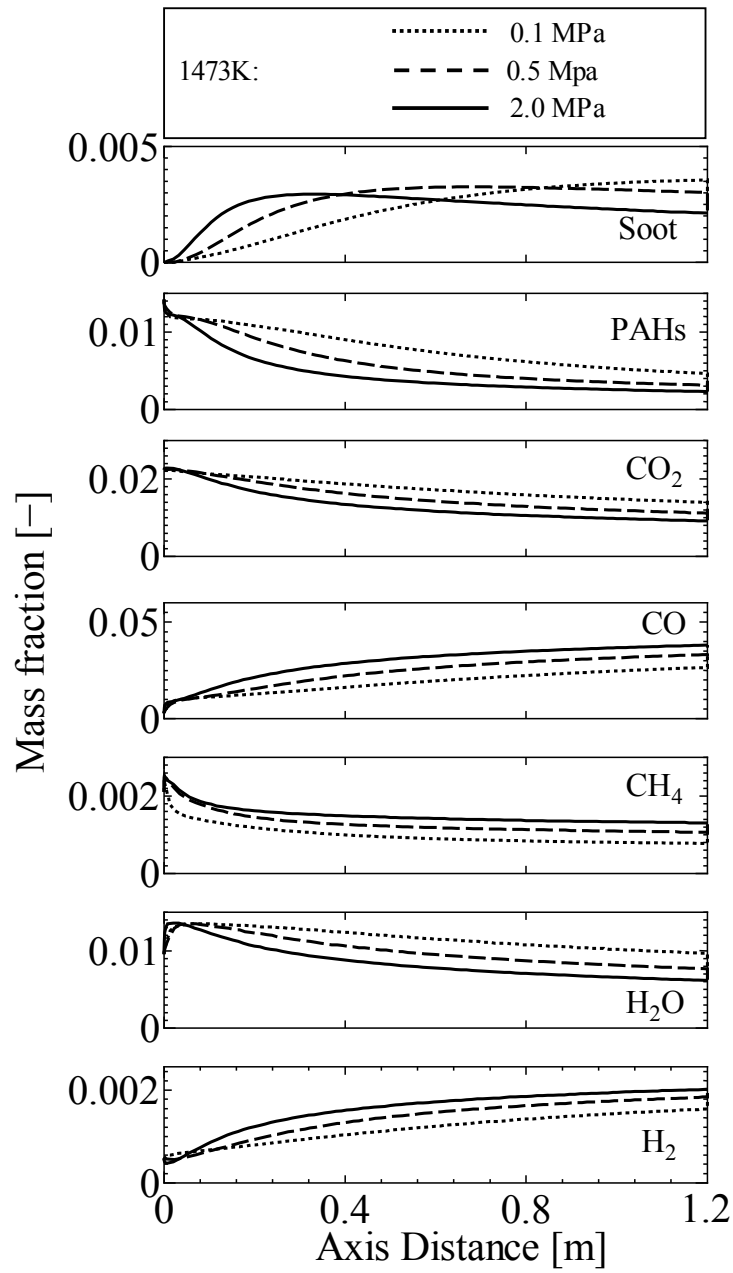
Figure 2-12 Comparison of species concentration profiles at 1473 K

49
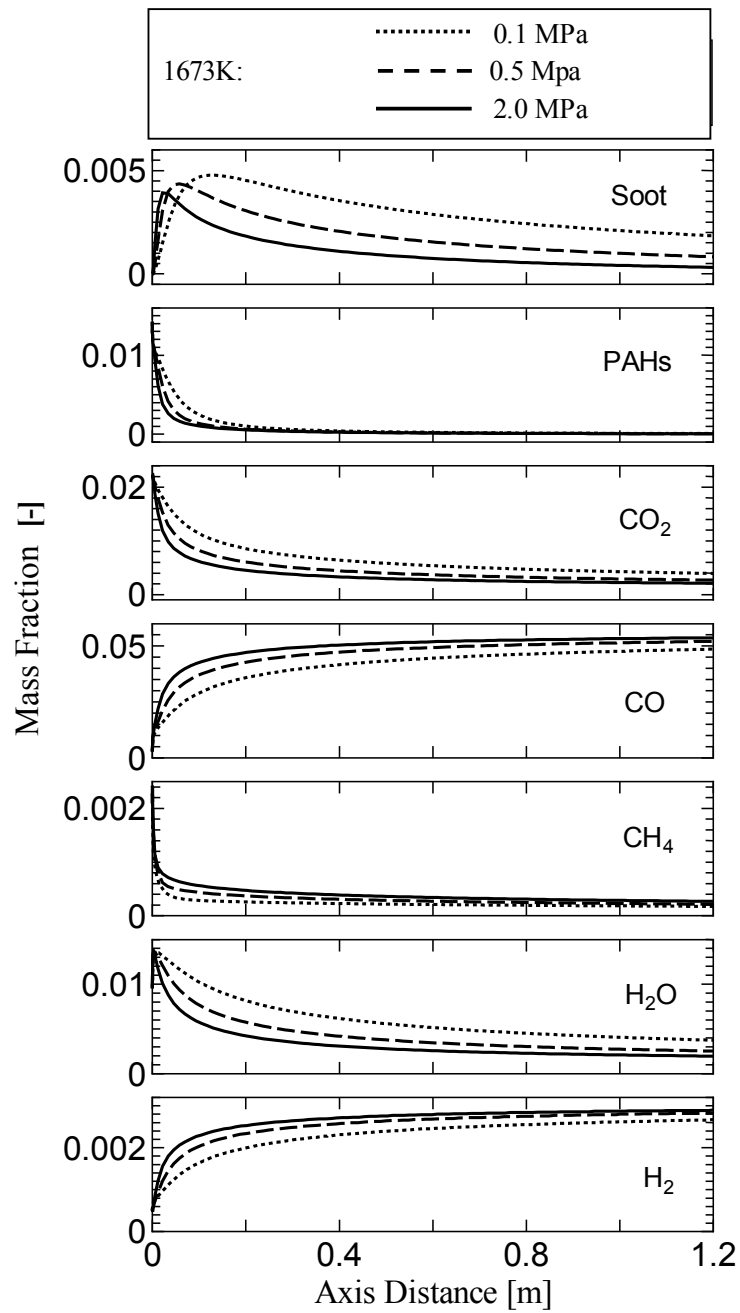
Figure 2-13 Comparison of species concentration profiles at 1673 K

50

Under CO_2/O_2 gasification condition, the effect of the inlet CO_2 mass fraction on the product mass fractions is examined (Figs. 2-14 and 2-15). Mass fraction profiles are obtained along the axis of the reactor at 1473K and 1673 K at constant pressure of 0.1 MPa with inlet CO_2 mass fractions of 0.02241 and 0.2241. An increase in inlet CO_2 mass fraction increases production of CO and reduces production of soot compared to lower inlet CO_2 mass fraction. At 1473K, PAHs concentration does not change with increasing CO_2 mass fraction, indicating formation of large PAHs doest not advance at that temperature. However, with an inlet CO_2 mass fraction of 0.2241 the production of soot reduces to almost zero at 1673K (Fig. 2-15). In comparison, with an inlet CO_2 mass fraction of 0.02241 some soot is still present at the outlet of the reactor. With the high inlet CO_2 mass fraction, the reverse reaction of MR2 (Fig. 2-8) dominates and produces more CO and OH radical. This reaction also consumes hydrogen radical and reduces the H_2 concentration. Reaction MR3 (Fig. 2-8) also contributes to CO production. Production of H_2 is lower with the CO_2 inlet mass fraction of 0.2241 than with the CO_2 inlet mass fraction of 0.02241 due to reaction MR1 (Fig. 2-8). Reactions MR1, MR4 and MR19 become important with high CO_2 inlet, which results in an increase in H_2O concentration. In addition, reaction MR3 forms hydroxyl radical, which participates in further oxidation of soot/PAHs.
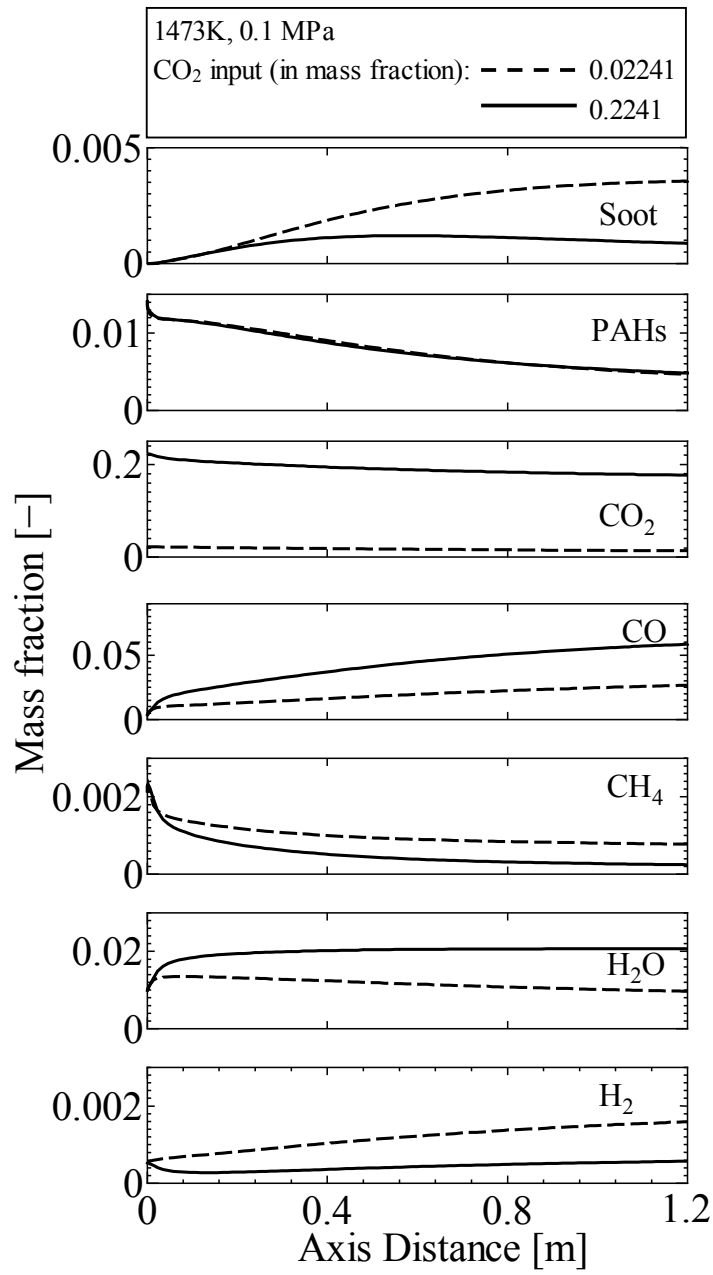
Figure 2-14 Effect of CO_2 inlet on species concentration profiles at 1473K
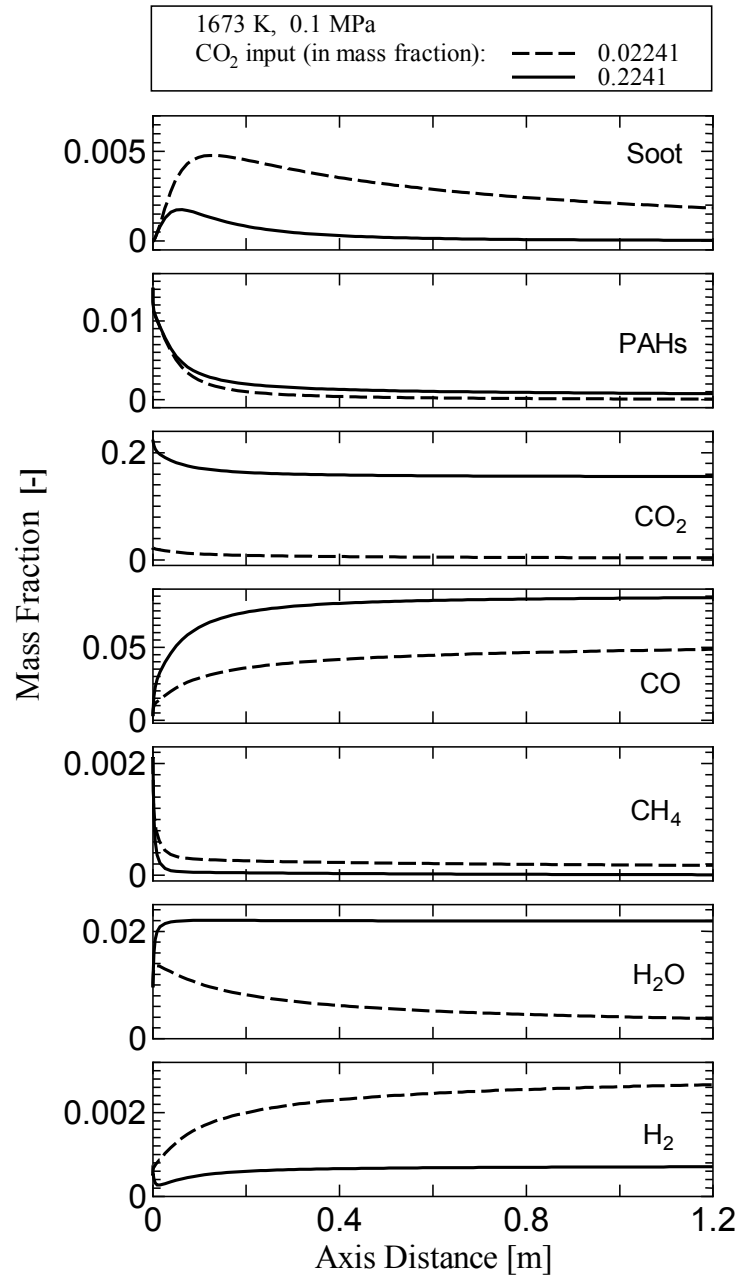
Figure 2-15 Effect of CO_2 inlet on species concentration profiles at 1673K

The effects of CO_2 and O_2 inlet mass fraction are investigated from 1273–1673 K at a constant pressure (0.1 MPa) under $CO_2/O_2/N_2$ gasification condition (Fig. 2-16). Increasing the O_2 inlet from a mass fraction of 0.007 to 0.07 while maintaining the CO_2 inlet mass fraction of 0.02 results in complete elimination of PAHs and soot at outlet of the reactor at all temperatures. In contrast, increasing the CO_2 inlet from a mass fraction of 0.02 to 0.2 alone does not result in PAHs/soot reduction at lower temperatures (1273 and 1473 K, Fig. 2-16) or almost completely eliminate PAHs/soot at a high temperature (1673 K, Fig. 2-16). This is due to the domination of small hydrocarbon addition reactions with PAHs/soot rather than PAHs/soot oxidation at lower temperatures. At lower temperatures the oxidizing species of oxygen and hydroxyl radicals are insufficient to continually oxidize PAHs/soot. Consequently, a high temperature is required to eliminate PAHs/soot if the CO_2 inlet is high.
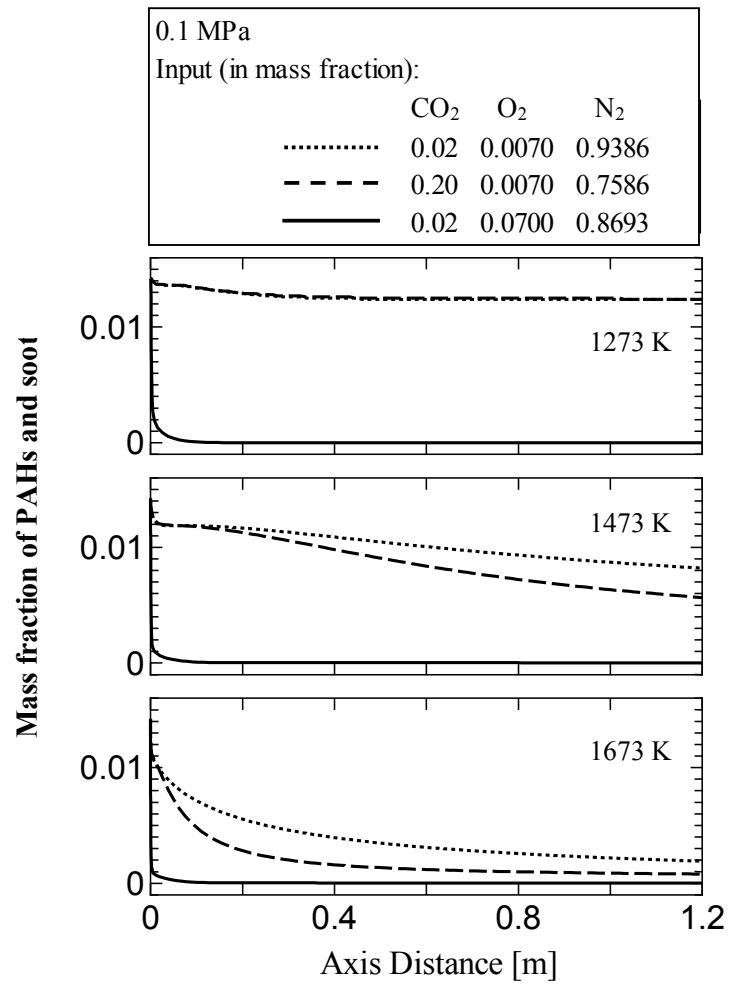
Figure 2-16 Effect of CO_2/O_2 inlet on total PAHs and soot concentration at 0.1MPa

2.7 Chapter conclusions

The following conclusions are made from this chapter:

a) Reaction mechanism of coal volatiles gasification in a Plug Flow Reactor is numerically investigated. The calculated results are compared with the experimental result at a temperature of 1273K and pressure of 0.1 MPa under conditions of without soot and with soot formation, which show a satisfied agreement.

b) The detailed reaction mechanism without soot (255 species and 1095 elementary reactions) is reduced by using the rate of production analysis. The calculated results for the reduced mechanism RM5 (46 chemical species and 165 elementary chemical reactions) are found to be similar to those for the detailed mechanism under various operating conditions. Main reaction pathways of coal volatiles gasification under conditions of without soot and with soot are predicted using the reduced mechanism.

c) Higher temperatures result in an increase in CO and H_2 concentrations, and a decrease in PAHs and soot concentrations compared to lower temperatures. CO_2 inlet mass fraction shows a large effect on PAHs/soot reduction at higher temperatures. At lower temperatures, O_2 input becomes important in reducing PAHs/soot. If the target of CO_2 inlet is high, higher temperatures provide in eliminated PAHs/soot and increased CO.

References

[1] Richter H., Granata S., Green W.H. and Howard J.B., "Detailed modeling of PAH and soot formation in a laminar premixed benzene/oxygen/argon low-pressure flame", *Proceeding of the Combustion Institute*, 30, 1397–405 (2005).

[2] Massachusetts Ins. of Tech., Combustion Research Website (http://web.mit.edu).

CHAPTER 3

REACTION MECHANISM FOR NUMERICAL SIMULATION

3.1 Introduction

The motivation behind the development of reduced mechanism is the demand for a speedup in computational time for complex simulations of gasification phenomena. By reducing the number of species involved in the gasification process, the overall central processing unit (CPU) time and memory requirement are considerably reduced. This is because the reduction of the number of differential equations that need to be solved is also reduced. For the most complex system (complex geometry), as for a computational fluid dynamics (CFD) computation, a reduced mechanism is not an option but a necessity to take into account [1]. In previous chapter, reaction mechanisms in coal volatiles gasification are numerically investigated using a simple tubular reactor. The reaction mechanisms, consisting of many elementary reactions and species including radical, is very difficult to implement into CFD especially for complex coal gasification process. Therefore, this chapter focuses on the reaction mechanism that includes only overall reactions. The numerical results are compared with the detailed mechanism discussed in Chapter 2.

3.2 Gas phase reactions

In coal gasification, most of the research works are focused on some limited gas phase reactions only. These reactions are assumed as the main reactions occurred in the coal gasification process. Therefore, an overall gas phase reactions mechanism shown in Table 3-1 is considered in present calculation. This mechanism consists of five overall reactions and six chemical species (CO, CO_2, H_2, H_2O, CH_4 and O_2).

Table 3-1 Overall gas phase reactions

		ΔH [MJ/kmol]	A_f [m³/kmol·s]	E_a [J/kmol]	References
$CO + \frac{1}{2}O_2 \rightarrow CO_2$	(R1)	- 283.24	2.2×10^{12}	1.67×10^8	[2, 3]
$CO + H_2O \leftrightarrow CO_2 + H_2$	(R2)	- 41.10	2.75×10^2	8.38×10^7	[2, 3]
$CH_4 + H_2O \leftrightarrow CO + 3H_2$	(R3)	+ 206.00	4.4×10^{11}	1.68×10^8	[2, 3]
$CH_4 + \frac{1}{2}O_2 \leftrightarrow CO + 2H_2$	(R4)	- 35.70	3.0×10^8	1.26×10^8	[2, 3]
$H_2 + \frac{1}{2}O_2 \rightarrow H_2O$	(R5)	- 242.00	6.8×10^{15}	1.68×10^8	[2, 3]

3.2.1 Mathematical model

The Plug Flow Reactor (PFR) model for five overall reactions shown in Table 3-1 is used to conduct the calculation under $CO_2/O_2/N_2$ gasification condition. The PFR is assumed to be complete mixing perpendicular to the direction of flow (i.e. the radial direction) and no mixing in the direction of flow. The equation for conservation governing the behavior of PFR model is given as follows:

$$\rho u A \frac{dY_i}{dx} + Y_i A_s \sum_{i=1}^{I} \omega_{i,s} M_i = M_i \left(\omega_{i,s} A_s + \omega_{i,g} A \right) \tag{2-7}$$

The details of the model is introduced in section 2.3.

3.2.2 Calculation conditions

The simulation is conducted inside a PFR of 28 mm in diameter and 1200 mm in length. The temperature and pressure maintained in the reactor are 1273–1573 K and 0.1–2 MPa, respectively. The inlet gas velocity is 0.66 m/s. The inlet gas compositions are shown in Table 3-2.

Table 3-2 Mass fractions of inlet species for overall gas phase reactions mechanism

Species	Mass fraction [-]
O_2	0.007299
CO_2	0.022410
CO	0.002825
H_2	0.000498
H_2O	0.009563
CH_4	0.018805
N_2	0.938600

3.2.3 Results and discussion

The calculations using overall gas phase reactions mechanism (Table 3-1) for coal volatiles gasification are carried out under various operating conditions. Figures 3-1 and 3-2 show the comparison of calculated results between overall gas phase reactions mechanism and RM5 (From Chapter 2). Overall gas phase reactions mechanism overestimates the CO and H_2 concentration of RM5. At a higher pressure (2.0 MPa), the forward reaction of R3 becomes dominant under calculated condition, resulting in a decrease in CH_4 and H_2O concentration. As the gas mixture is assumed as an ideal gas mixture, an increase in system pressure causes the reaction to shift to the side with the larger moles of gas. Therefore, forward rate of reactions R3 ($CH_4 + H_2O \leftrightarrow CO + 3H_2$) and R4 ($CH_4 + \frac{1}{2}O_2 \leftrightarrow CO + 2H_2$) tend to increase at higher pressures resulting in a decrease in CH_4 concentration and an increase in CO concentration. In contrast, since RM5 mechanism consists only elementary reactions where the number of moles in left side and right side are same, the effect of pressure at constant temperature is not significant. This makes a large deviation in species concentration between overall reactions mechanism and RM5 at higher pressures.
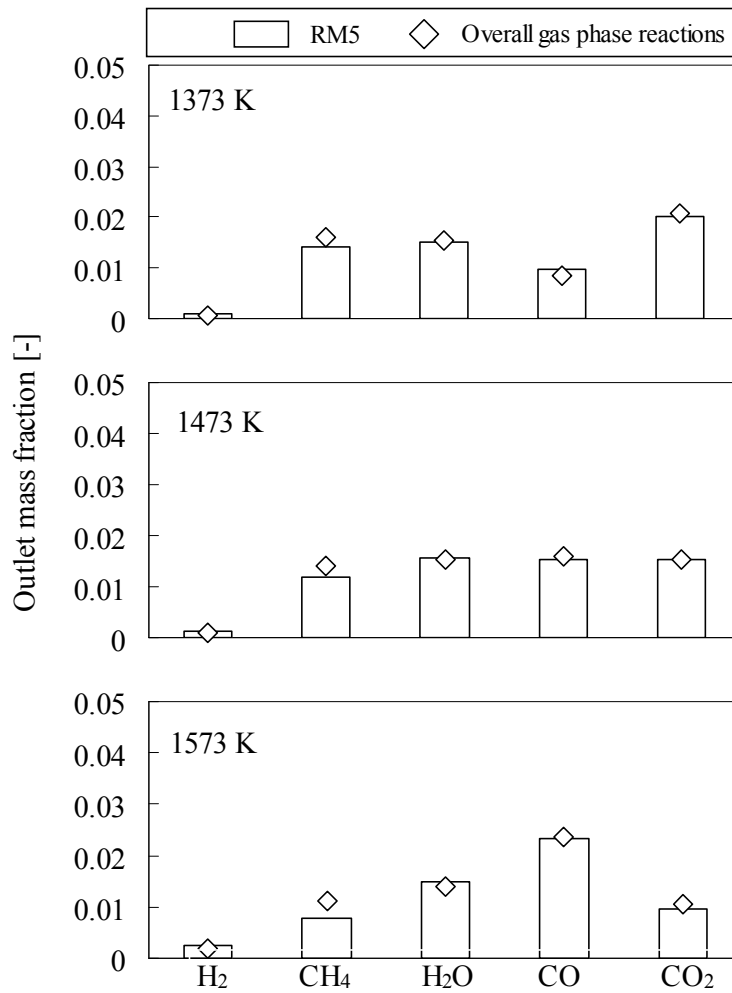
Figure 3-1 Comparison between overall gas phase reactions and RM5 mechanism at 0.1 MPa
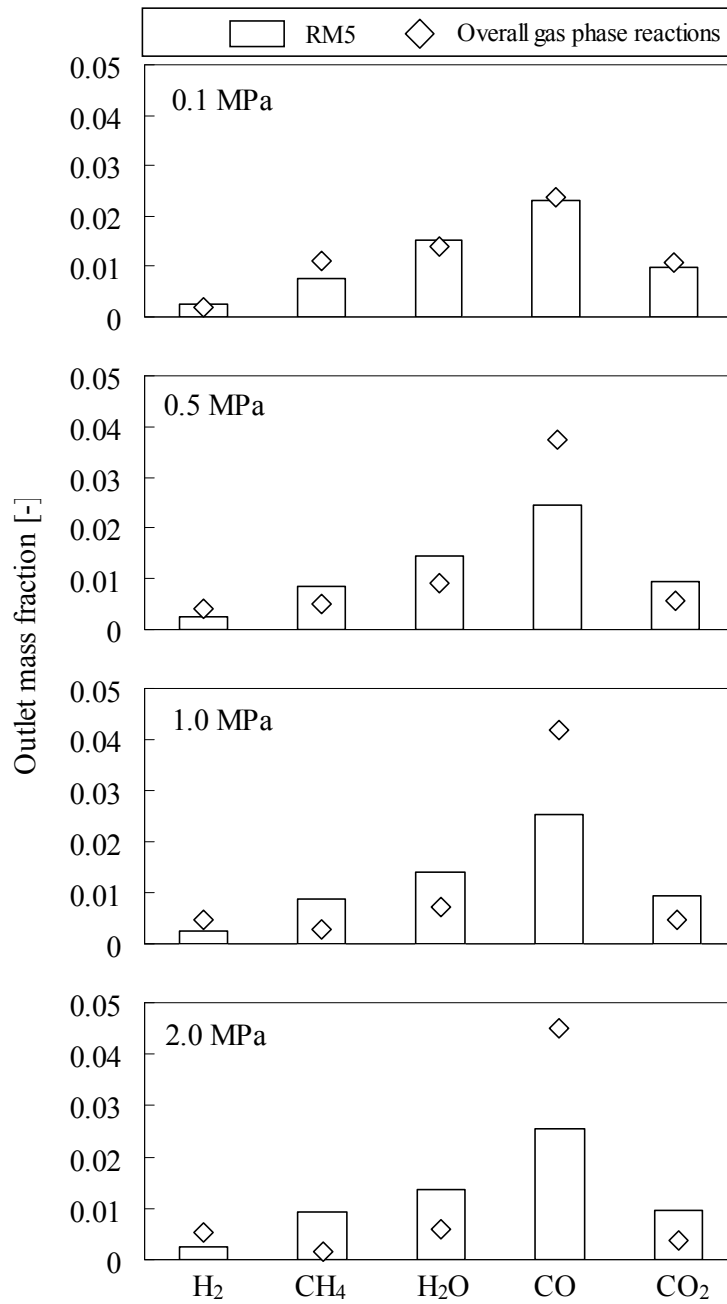
Figure 3-2 Comparison between overall gas phase reactions and RM5 mechanism at 1573 K

3.3 One step soot model

The reaction mechanism with soot illustrated in Fig. 2-2 consists of 3793 elementary chemical reactions. Among them about 70% of the reactions are similar to MSR1 and MSR2. An overall soot formation reactions mechanism (Table 3-3) referred here after "One step soot model" following the above mentioned two general reactions is implemented in the calculation of soot formation. It is assumed that all aromatics compounds are released as benzene (C_6H_6) during coal devolatilization. A high molecular weight species coronene ($C_{24}H_{12}$) is produced from benzene similar to the reaction MSR1. The species $C_{24}H_{12}$ will be considered as soot in this study. Two oxidation reactions of PAH (C_6H_6) and soot with oxygen are considered to be equivalent to the reaction MSR2.

Table 3-3 One step soot model

		ΔH [MJ/kmol]	A_f [kg/m^2·s·Pa]	E_a [J/kmol]	References
Formation of soot					
$4C_6H_6 \rightarrow C_{24}H_{12} + 6H_2$	(R6)	- 9.15	1.50×10^{10}	4.70×10^5	[4, 5]
PAH/soot oxidation					
$C_6H_6 + 4.5O_2 \rightarrow 6CO + 3H_2O$	(R7)	- 746.00	2.00×10^9	3.10×10^7	[4, 5]
$C_{24}H_{12} + 15O_2 \rightarrow 24CO + 6H_2O$	(R8)	- 2357.00	2.00×10^9	3.10×10^7	[4, 5]

One step soot model is proposed here with the aim of implementing it in the coal gasification simulation where turbulent flow becomes dominant. In coal gasification process, turbulence slowly mixes fuel and oxidizer into the reaction zone where they burn quickly. In such cases, kinetic rate of reaction can be neglected. Therefore, simulation of coal volatiles gasification under turbulent flow condition is conducted inside a simple tubular reactor. The calculated results obtained from overall gas phase reactions mechanism with one step soot model are compared with those from the detailed reaction mechanism with soot (discussed in Chapter 2).

3.3.1 Mathematical model

The time-averaged steady-state Navier-Stokes equations as well as the mass and energy conservation equations are solved for tubular type reactor. Both the finite rate and the eddy dissipation models are used to calculate the rate of R1-R8 reactions. Turbulence is calculated using the standard k–ε model, while Discrete Ordinates (DO) radiation model is used to calculate the radiation energy. The details of the model is introduced in sections 4.3.1 and 4.4.2.

3.3.2 Calculation conditions

Calculations are carried out using overall gas phase reactions mechanism (Table 3-1) with one step soot model (Table 3-3) . The calculation conditions for various types of flow are shown in Table 3-4. Inlet mass fraction of species is shown in Table 3-5. In one step soot model, all aliphatic compounds are lumped into a single component CH_4, while all aromatic compounds are considered as C_6H_6.

Table 3-4 Calculation conditions for overall gas phase reactions mechanism with one step

soot model

Parameters	Detailed mechanism with soot (Plug flow condition)	Overall gas phase + one step soot model (Re=25,000)	Overall gas phase + one step soot model (Re=100,000)
Number of reactions [-]	3793	8	8
Number of species [-]	276	8	8
Reynolds number [-]	250	25,000	100,000
Reactor length [m]	1.2	12	48
Reactor diameter [m]	0.028	0.28	0.28
Inlet gas velocity [m/s]	0.66	6.6	26.4
Temperature [K]	1473 or 1673	1473 or 1673	1473 or 1673
Pressure [MPa]	0.1 or 2.0	0.1 or 2.0	0.1
Residence time [s]	1.818	1.818	1.818

Table 3-5 Mass fractions of inlet species for overall gas phase reactions mechanism with

one step soot model

Species	Mass fraction [-]
O_2	0.007299
CO_2	0.022410
CO	0.002825
H_2	0.000498
H_2O	0.009563
CH_4	0.004586
C_6H_6	0.014220
N_2	0.938600

3.3.3 Results and discussion

The outlet concentrations of soot, PAH and other smaller gas species are shown in Figs. 3-3 and 3-4. It is found that soot and PAH decrease with increasing the gas temperature because of large extent of oxidation reaction. At higher temperatures, the production of soot from PAH molecules also increase, resulting in an increase in H_2 concentration. Syngas concentration increases and soot concentration decreases with increasing the Reynolds number. This suggests that at higher turbulent conditions soot formation and soot oxidation become dominant. Formation of soot increases the production of H_2, while soot oxidation increases the CO concentration. In contrast, PAH concentration remains unchanged under two turbulent conditions. Trends of outlet species concentration under various turbulent conditions are found to be similar, in both: overall gas phase reactions with one step soot model and detailed reaction mechanism with soot. Thus, the overall gas phase reactions mechanism with one step soot model is proposed to use in the simulation of coal gasification in Chapters 5 and 6.
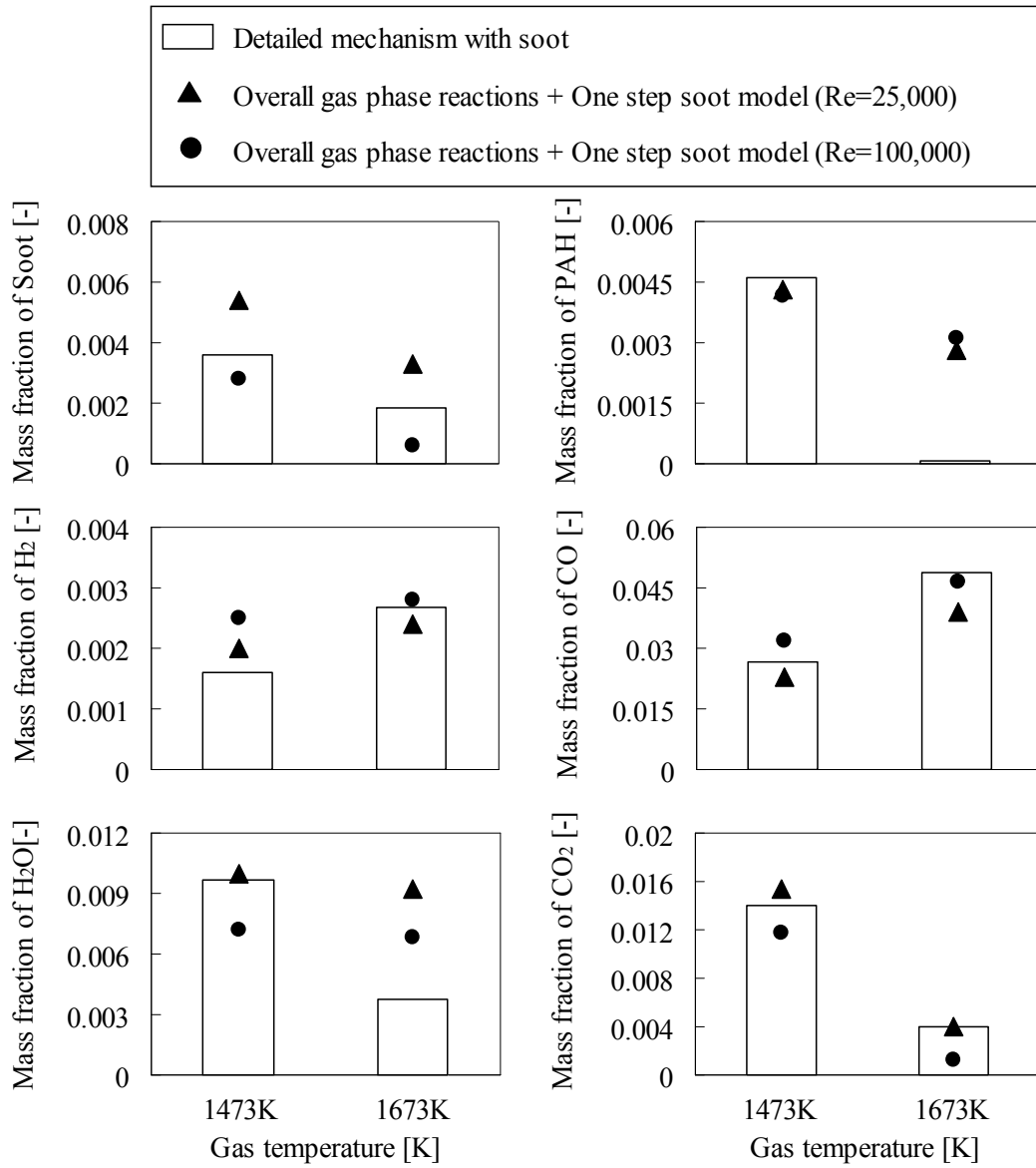
Figure 3-3 Comparison of outlet gas species concentration between detailed mechanism with

soot and overall gas phase reactions with one step soot model at 0.1MPa
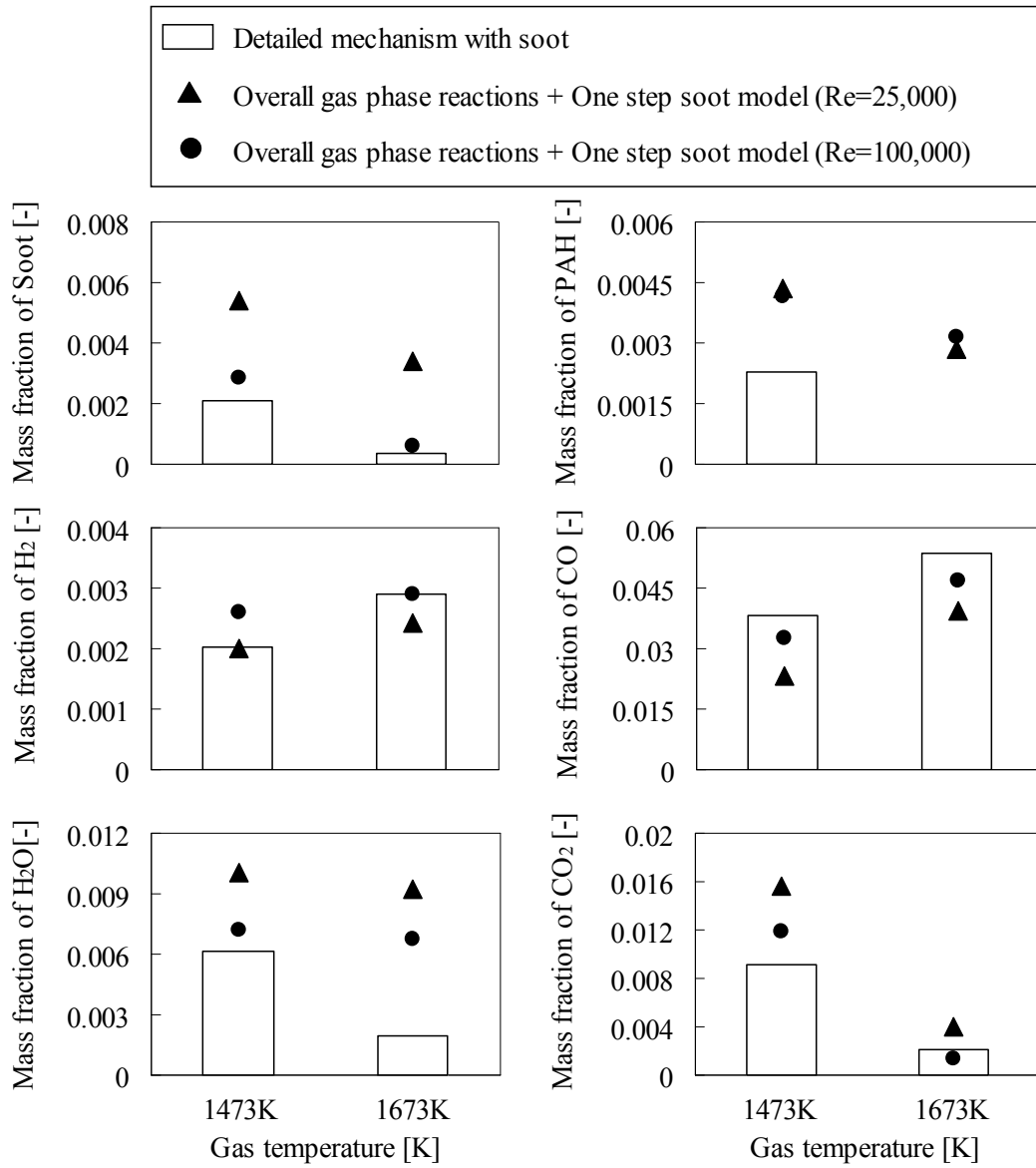
Figure 3-4 Comparison of outlet gas species concentration between detailed mechanism with

soot and overall gas phase reactions with one step soot model at 2.0 MPa

3.4 Chapter conclusions

Overall gas phase reactions mechanism with one step soot model is used to study the coal volatiles gasification in $CO_2/O_2/N_2$ atmosphere under two turbulent conditions. The calculated trends of species concentration show a reasonable agreement with those of the detailed mechanism with soot. Therefore, one step soot model is proposed to implement it in the simulation of coal gasification for predicting soot in a two stage entrained flow coal gasifier.

References

[1] Belcadi F., Assou M., Affad E. and Chatri E., "Construction of a reduced mechanism for modelling premixed combustion of methane-air", *Combustion theory and modelling*, 11(4), 603-613 (2007).

[2] Watanabe H. and Otaka M., "Numerical simulation of coal gasification in entrained flow coal gasifier", *Fuel*, 85, 1935-1943 (2006).

[3] Silaen A. and Wang T., "Effect of turbulence and devolatilization models on coal gasification simulation in an entrained-flow gasifier", *International Journal of Heat and Mass Transfer*, 53, 2074–2091 (2010).

[4] Massachusetts Ins. of Tech., Combustion Research Website (http://web.mit.edu).

[5] Kazakov A., Wang H. and Frenklach M., "Detailed modeling of soot formation in laminar premixed ethylene flames at a pressure of 10 bar", *Combustion and Flame*, 100, 111-120 (1995).

CHAPTER 4

MODELS FOR COAL GASIFICATION

4.1 Introduction

Development and application of comprehensive, multidimensional, computational gasification model are increasing at a significant pace across the world. Development of fossil-fuel combustion/gasification technology in the past was largely empirical in nature, being based primarily on years of accumulated experience in the operations of utility furnaces and on data obtained from sub-scale test facilities. Empirically based experience and data have limited applicability when considering changes in process parameters for improving combustion/gasification efficiencies or mitigating pollutant formation.

Gasification modeling technology can take many forms, but the type that will be considered here will be referred to as a comprehensive gasification model. The term "comprehensive" is used to signify that sub-models for all pertinent physico-chemical mechanisms have been assembled into an integrated model with a solution approach that can adequately simulate the overall combustion/gasification process of interest. In case of modeling coal gasification, the framework for the solution approach is based on computational fluid dynamics (CFD) using numerical solutions of multidimensional, differential equations for conservation of mass, energy, and momentum. Other sub-models are coupled within this framework to account for gaseous species mixing and chemical reactions, coal particle devolatilization and char oxidation/gasification, and radiant energy transport. Information available from model predictions can include temperature distributions, gas composition, velocity, particle trajectories, particle size distributions, soot formation, and so forth.

The main objective of this chapter is to introduce various models and sub-models that are used in the simulation of coal gasification.

4.2 Computational domain

The coal gasifier (Fig. 4-1) considered here consists of a combustor stage and a reductor stage. Coal and char are injected into the combustor stage with O_2-rich gas mixtures. The gasifier has two levels of injectors that are positioned axisymmetrically at combustor and reductor stage. The combustor injectors are placed similar to a tangential firing system to create swirling flow inside the gasifier. The reductor injectors are directed towards the center of the gasifier.

The gasifier is an up-flow reactor consisting of a combustor and a reductor. 50 to 60 wt% of the pulverized coal and the recycled char, with about 80 wt% of the total gasifying agents are tangentially injected into the combustor. The remaining part of the pulverized coal with about 20 wt% of the total gas is injected into the reductor. In the combustor, the pulverized coal is devolatailized and reacts with O_2 rapidly to produce a high-temperature combustion gas, which is simultaneously used to drive the endothermic char-H_2O and char-CO_2 reactions. In the reductor, the coal is devolatailized under O_2-lean conditions to produce mainly hydrogen and carbon monoxide [1].

A three dimensional mesh consisting of 247,818 computational cells is used with the small cell size being around 2 mm and the largest one around 10 mm. The near wall y^+ value is 250, which is appropriate ($30 > y^+ > 300$) to apply the standard wall functions in the standard k-ε turbulence model.
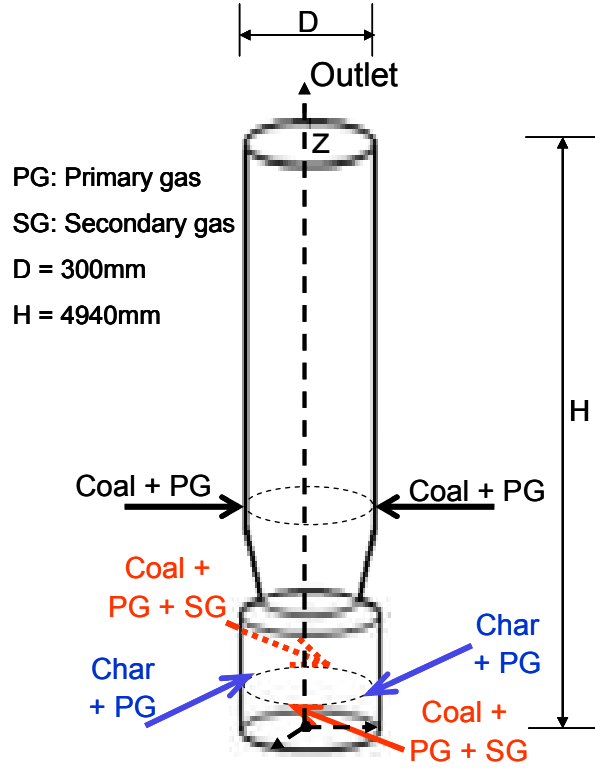
Figure 4-1 A schematic of two stage entrained flow coal gasifier adopted from CRIEPI experiment [2].

4.3 Governing equations

4.3.1 Gas phase

For the fluid phase, the time-averaged steady-state Navier-Stokes equations as well as the mass and energy conservation equations are solved for two stage entrained flow coal gasifier shown in Fig. 4-1 [2]. The governing equations for the conservation of mass, momentum, energy and species in 3D Cartesian coordinates are given as:

Continuity: $\nabla \cdot (\rho \vec{v}) = S_m$ (4-1)

Momentum: $\nabla \cdot (\rho \vec{v} \vec{v}) = -\nabla p + \nabla \cdot (\bar{\bar{\tau}}) + \rho \vec{g} + \vec{F}$ (4-2)

Energy: $\nabla \cdot (\vec{v}(\rho E + p)) = -\nabla \cdot \left(\sum_i H_i J_i \right) + I_{rad} + S_{h,reac}$ (4-3)

Species: $\nabla \cdot \left(\rho \vec{v} Y_i\right) = -\nabla \cdot \vec{J}_i + R_i + S_i$ (4-4)

where

ρ = density

$\vec{v}$ = velocity vector

S_m = source of mass added to the gas phase from the coal

$\rho\vec{g}$ = gravitational body force

$\vec{F}$ = external body forces that arise from interaction with the coal

p = pressure

H_i = enthalpy of gas species i

J_i = mass flux of species i

I_{rad} = energy term due to radiation

$S_{h,reac}$ = energy term due to chemical reaction

Y_i = mass fraction of species i

R_i = rate of production of species i by chemical reaction

S_i = source of species i from the coal

∇ $= \dfrac{\partial}{\partial x}\vec{i} + \dfrac{\partial}{\partial y}\vec{j} + \dfrac{\partial}{\partial z}\vec{k}$ (4-5)

$\bar{\bar{\tau}}$ $= \mu\left[\left(\nabla\vec{u} + \nabla\vec{u}^T\right) - \dfrac{2}{3}\nabla\cdot\vec{u}\hat{I}\right]$ (4-6)

A standard k–ε model [3-5] is used to solve the turbulence. The standard k-ε model is a semi-empirical turbulent model which was developed using the assumption that the fluid flow is fully turbulent, and the effects of molecular viscosity are negligible. The turbulence kinetic energy, k, and its rate of dissipation, ε, are obtained from the following transport equations:

$$\frac{\partial}{\partial x_i}\left(\rho k u_i\right) = \frac{\partial}{\partial x_j}\left[\left(\mu + \frac{\mu_t}{\sigma_k}\right)\frac{\partial k}{\partial x_j}\right] + G_k - \rho\varepsilon \tag{4-7}$$

$$\frac{\partial}{\partial x_i}\left(\rho \varepsilon u_i\right) = \frac{\partial}{\partial x_j}\left[\left(\mu + \frac{\mu_t}{\sigma_\varepsilon}\right)\frac{\partial \varepsilon}{\partial x_j}\right] + C_{1\varepsilon}G_k\frac{\varepsilon}{k} - C_{2\varepsilon}\rho\frac{\varepsilon^2}{k} \tag{4-8}$$

where G_k represents the generation of turbulence kinetic energy due to the mean velocity gradient and μ_t is the turbulent viscosity. G_k and μ_t are calculated as:

$$G_k = -\overline{\rho u_i' u_j'} \frac{\partial u_j}{\partial x_i} \tag{4-9}$$

$$\mu_t = \frac{\rho C_\mu k^2}{\varepsilon} \tag{4-10}$$

The k-ε model with the following model constants: $C_{1\varepsilon}=1.44$, $C_{2\varepsilon}=1.92$, $C_\mu=0.09$, $\sigma_k=1.0$, $\sigma_\varepsilon=1.3$ are used for the flow predictions [4,5].

In the coal gasification, coal particles scatter, as well as emit and absorb radiative flux. Thus absorption, emission and scattering need to be taken into account for the radiant energy balance. The Discrete Ordinates (DO) radiation model is used to solve the radiative heat transfer equation. The DO radiation model solves the radiative transfer equation (RTE) for a finite number of discrete solid angles, each associated with a vector direction fixed in the global Cartesian system (x, y, z). The DO radiation model considers the RTE in the direction as a field equation. This equation is written as:

$$\frac{dI_{rad}(\vec{r},\vec{s})}{ds} = -\left(a + a_p + \sigma_p\right)I_{rad}(\vec{r},\vec{s}) + E_p + a\varphi^2\frac{\sigma T^4}{\pi} + \frac{\sigma_s}{4\pi}\int_0^{4\pi} I_{rad}(\vec{r},\vec{s}')\Phi(\vec{s}.\vec{s}')d\Omega \tag{4-11}$$

where

I_{rad} = radiation intensity

$\vec{r}$ = position vector

$\vec{s}$ = direction vector

$\vec{s}'$ = scattering direction vector

a = absorption coefficient

T = temperature

Φ = phase function used to characterize the nature of the scattering media

φ = refractive index of the medium

Ω = solid angle

E_p = equivalent emission of the coal particles

a_p = equivalent absorption coefficient

σ_p = equivalent particle scattering coefficient

Integration of RTE results in an expression for the conservation of radiant energy, which provides the radiant energy source term, I_{rad}, for the energy equation.

4.3.2 Solid phase

In discrete phase modeling, coal particles of known properties are injected into the gasifier and tracked in a Lagrangian fashion throughout the computational domain. The dispersed phase is solved by tracking coal particles through the calculated flow field. The trajectory of a discrete phase particles is predicted by integrating the force balance on the particles. The force balance equates the particles inertia with the forces acting on the particles, and can be written as:

$$\frac{du_p}{dt} = F_D(u - u_p) + \frac{g(\rho_p - \rho)}{\rho_p} \tag{4-12}$$

$F_D(u–u_p)$ is the drag force per unit particle mass and

$$F_D = \frac{18\mu}{\rho_p d_p^2} \frac{C_D \, \mathrm{Re}_d}{24} \tag{4-13}$$

Re_d is the relative Reynolds number, which is defined as:

$$\mathrm{Re}_d = \frac{\rho d_p |u_p - u|}{\mu} \tag{4-14}$$

where

u_p = particle velocity

g = gravitational acceleration

ρ_p = particle density

μ = dynamic viscosity

C_D = drag coefficient

d_p = particle diameter

Devolatilization starts when the temperature of coal particle reaches to devolatilization temperature (T_{vap} = 400K). Particle heat balance during the devolatilization process is given as:

$$m_p C_p \frac{dT_p}{dt} = hA_p(T - T_p) + \frac{dm_p}{dt} L + A_p \varepsilon_p \sigma (\theta_R^{\,4} - T_p^{\,4}) \qquad (4\text{-}15)$$

where

m_p = particle mass

C_p = particle specific heat

T_p = particle temperature

h = heat transfer coefficient

A_p = particle surface area

T = temperature

L = latent heat of water in coal

ε_p = particle emissivity

σ = Stefan-Boltzmann constant

θ_R = radiation temperature

After the volatile species of the coal particle has evolved completely, a surface reaction begins. The char surface reaction consumes the oxidant species (O_2, CO_2 or H_2O) in the gas phase. The surface reaction also consumes or produces energy, in an amount determined by the heat of reaction. During surface reaction, the following heat balance equation is used:

$$m_p C_p \frac{dT_p}{dt} = hA_p(T - T_p) - f_h\left(\frac{dm_p}{dt}\right)\Delta H + A_p \varepsilon_p \sigma (\theta_R^{\,4} - T_p^{\,4}) \qquad (4\text{-}16)$$

where

ΔH = heat released by the corresponding surface reaction

f_h = fraction of heat absorbed by coal particle

The heat transfer coefficient, h, is evaluated using the correlation of Ranz and Marshall [6,7] as follows:

$$\frac{hd_p}{k_g} = 2.0 + 0.6\,\mathrm{Re}_d^{1/2}\,\mathrm{Pr}^{1/3} \qquad (4\text{-}17)$$

where

k_g = thermal conductivity of the gas

Pr = Prandtl number of the gas

4.3.3 Auxiliary equations

The gas mixture is considered as incompressible, which follows ideal gas law. The density is calculated as:

$$\rho = \frac{pM}{RT} \qquad (4\text{-}18)$$

where

ρ = density

p = pressure

M = molecular weight

R = universal gas constant

T = temperature

The specific heat (c_p) of the gas mixture is calculated as a mass fraction average of the specific heat of species and can be written as:

$$c_p = \sum_i Y_i c_{p,i} \qquad (4\text{-}19)$$

where

Y_i = mass fraction of species i

$c_{p,i}$ = specific heat of the species i

The enthalpy (H) and entropy (S) of the gas mixture are calculated as:

$$H = \sum_i m_i \left[H_i^0 + \int_{T_{ref}}^{T} c_{p,i} \, dT \right] \tag{4-20}$$

$$S = \sum_i m_i \left[S_i^0 + \int_{T_{ref}}^{T} \frac{c_{p,i}}{T} \, dT \right] \tag{4-21}$$

where

H_i = enthalpy of species i

H_i^0 = enthalpy of species i at standard condition

S_i = entropy of species i

S_i^0 = entropy of species i at standard condition

T_{ref} = reference temperature

The diffusion flux of a chemical species i in turbulent flows is calculated as:

$$J_i = -\left(\rho D_i + \frac{\mu_t}{Sc_t} \right) \nabla Y_i \tag{4-22}$$

where

D_i = diffusion coefficient of species i

μ_t = turbulent viscosity

Sc_t = turbulent Schmidt number ($Sc_t = \mu_t / \rho D$)

The source of energy due to chemical reaction is calculated as:

$$S_{h,reac} = -\sum_i \frac{H_i^0}{M_i} R_i \tag{4-23}$$

where R_i is the net rate of production of species i produced by chemical reaction.

Equivalent emission of the particles (E_p), equivalent absorption coefficient (a_p) and equivalent particle scattering coefficient (σ_p) in the RTE are defined as follows:

$$E_p = \lim_{V_p \to 0} \sum_{n=1}^{n_p} \varepsilon_p A_p \frac{\sigma T_{pn}^4}{\pi V_p} \tag{4-24}$$

$$a_p = \lim_{V_p \to 0} \sum_{n=1}^{n_p} \varepsilon_p \frac{A_p}{V_p} \qquad (4\text{-}25)$$

$$\sigma_p = \lim_{V_p \to 0} \sum_{n=1}^{n_p} (1 - f_p)(1 - \varepsilon_p) \frac{A_p}{V_p} \qquad (2\text{-}26)$$

where

ε_p = particle emissivity

A_p = area of the coal particle

T_{pn} = temperature of the nth coal particle

n_p = number of coal particles

V_p = volume of coal particles

f_p = particle scattering factor

All physical properties of gas and coal particles including modeling constant used in the present calculation are shown in Table 4-1.

Table 4-1 Properties of gas/solid and modeling constants used in calculation

Parameter	Symbol	Remarks
Gas properties		
Thermal conductivity	k_g	0.0454 W/m·K
Viscosity	μ	1.72×10^{-5} kg/m·s
Specific heat	c_p	Eq. (4-19)
Absorption coefficient	a	1.5 m^{-1}
Scattering coefficient	σ_s	0 m^{-1}
Refractive index	φ	1
Diffusion coefficient	D	2.88×10^{-5} m^2/s
Turbulent model		
Turbulent Schmidt number	Sc_t	0.7
Turbulent model constant	$C_{1\varepsilon}$	1.44
Turbulent model constant	$C_{2\varepsilon}$	1.92
Turbulent model constant	C_μ	0.09
Turbulent Prandtl number for k	σ_k	1.0
Turbulent Prandtl number for ε	σ_ε	1.3
Coal particle properties		
Particle density	ρ_p	1400 kg/m^3
Particle specific heat	C_p	1680 J/kg·K
Particle Vaporization temperature	T_{vap}	400 K
Particle emissivity	ε_p	0.9
Particle scattering factor	f_p	0.9
Fraction of heat absorbed by particle	f_h	1.0
Devolatilization model		
Pre-exponential factor	$A_{f,1}$	200000 s^{-1}
Activation energy	$E_{ac,1}$	1.046×10^8 J/kmol
Pre-exponential factor	$A_{f,2}$	1.3×10^7 s^{-1}
Activation energy	$E_{ac,2}$	1.674×10^8 J/kmol

4.4 Reaction models

4.4.1 Devolatilization

Devolatilization is the first chemical process occurring as part of coal gasification. When the temperature of the coal particles reaches the vaporization temperature (400K), chemical reactions occur producing various amounts of gases, tar, and coke. The tar and gases are usually referred as volatiles. The volatiles are released according to Kobayashi model [8,9]. In this model, two competing overall reactions are considered as follows:

$$
\begin{array}{c}
\text{Volatiles}_1 + \text{Char}_1 \\
\alpha_1 \qquad (1-\alpha_1)
\end{array}
$$

Combustible in coal particle

$$
\begin{array}{c}
\text{Volatiles}_2 + \text{Char}_2 \\
\alpha_2 \qquad (1-\alpha_2)
\end{array}
$$

(4-27)
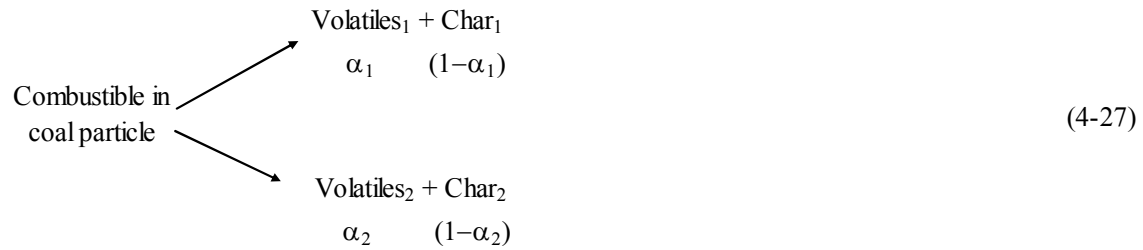
where α_1 and α_2 are the yields of the two competing reactions. α_1 is set to the fraction of volatiles determined by proximate analysis, because this rate represents devolatilization at low temperatures. The second yield parameter, α_2, is set to unity, which is the yield of volatiles at very high temperatures.

This model assumes two kinetic rates, $k_{kin,1}$ and $k_{kin,2}$, which may control the devolatilization over different temperature ranges, are given as:

$$
k_{kin,1} = A_{f,1} \exp^{-(E_{ac,1}/RT_p)}
\tag{4-28}
$$

$$
k_{kin,2} = A_{f,2} \exp^{-(E_{ac,2}/RT_p)}
\tag{4-29}
$$

where $A_{f,1}$ and $A_{f,2}$ are pre-exponential factors, $E_{ac,1}$ and $E_{ac,2}$ are activation energies for the two reactions.

These two kinetic rates are weighted, to yield an expression for the devolatilization as:

$$
\frac{m_p(t)}{(1-f_{w,0})m_{p,0} - m_a} = \int_0^t (\alpha_1 k_{kin,1} + \alpha_2 k_{kin,2}) \exp\left(-\int_0^t (k_{kin,1} + k_{kin,2})dt\right)dt
\tag{4-30}
$$

where

$m_p(t)$ = volatile yield up to time t

$m_{p,0}$ = initial coal particle mass

m_a = ash content in coal particle

$f_{w,0}$ = initial mass fraction of water in coal particle

4.4.2 Gas phase reactions

For the gas phase reactions, both the finite rate and the eddy dissipation models are used, and the smaller of the two is used as the reaction rate. Finite rate model computes the rate of gas phase reaction resulting from both forward and backward reaction as follows:

$$\hat{R}_{i,k}^{(A)} = (\upsilon_{i,k}^{"} - \upsilon_{i,k}^{'}) \left(k_{kin,f,k} \prod_{i=1}^{I} [X_i]^{\eta_{i,k}^{'}} - k_{kin,b,k} \prod_{i=1}^{I} [X_i]^{\eta_{i,k}^{"}} \right) \tag{4-31}$$

where

$\hat{R}_{i,k}^{(A)}$ = molar rate of creation or destruction for ith species in kth reaction

X_i = molar concentration of ith species

$\upsilon_{i,k}^{'}$ = stoichiometric coefficients for ith reactant species in kth reaction

$\upsilon_{i,k}^{"}$ = stoichiometric coefficients for ith product species in kth reaction

$k_{kin,f,k}$ = forward rate constant for kth reaction

$k_{kin,b,k}$ = backward rate constant for kth reaction

$\eta_{i,k}^{'}$ = rate exponents for ith reactant species in kth reaction

$\eta_{i,k}^{"}$ = rate exponents for ith product species in kth reaction

The forward rate constant for the kth reaction is assumed to follow the Arrhenius equation as follows:

$$k_{kin,f,k} = A_{f,k} T^{\alpha_k} \exp^{\frac{-E_{ac,k}}{RT}} \tag{4-32}$$

where

$A_{f,k}$ = pre-exponential factor for kth reaction

α_k = temperature exponent for kth reaction

$E_{ac,k}$ = activation energy for kth reaction

T = temperature

R = universal gas constant

In calculation, it is assumed that the gas phase is a mixture of ideal gas. The backward rate constant, $k_{kin,b,k}$ is related to the forward rate constant as follows:

$$k_{kin,b,k} = \frac{k_{kin,f,k}}{\exp\left(\dfrac{\Delta S_k^0}{R} - \dfrac{\Delta H_k^0}{RT}\right)\left(\dfrac{P}{RT}\right)^{\sum_{i=1}^{I} \upsilon_{i,k}'' - \upsilon_{i,k}'}} \tag{4-33}$$

where

ΔS_k^0 = change of standard state molar entropy in kth reaction

ΔH_k^0 = change of standard state molar enthalpy in kth reaction

P = pressure

Eddy dissipation model takes into account the turbulent mixing of the gases [10]. It assumes that the chemical reaction is faster than the time scale of the turbulence eddies. Thus, the reaction rate is determined by the turbulence mixing of the species. The reaction is assumed to occur instantaneously when the reactants meet. The net rate of production or destruction of a species is given by the smaller of the two expressions (Eqs. 4-34 and 4-35):

$$\hat{R}_{i,k}^{(R)} = \upsilon_{i,k}' M_i A_R \rho \left(\frac{\varepsilon}{k}\right) \min_R \left(\frac{Y_R}{\upsilon_{R,k}' M_R}\right) \tag{4-34}$$

$$\hat{R}_{i,k}^{(P)} = \upsilon_{i,k}' M_i A_R B_P \rho \left(\frac{\varepsilon}{k}\right) \left(\frac{\sum_P Y_P}{\sum_j^N \upsilon_{j,k}'' M_j}\right) \tag{4-35}$$

where

Y_R = mass fractions of reactant species

Y_p = mass fractions of product species

A_R = Magnusen constant for reactants (4.0)

B_P = Magnusen constant for products (0.5)

M_i = molecular weight of species i

The net source of chemical species i due to reaction is computed as the sum of the reaction sources over the K reactions as:

$$R_i = M_i \sum_{k=1}^{K} \hat{R}_{i,k} \qquad (4\text{-}36)$$

All the hydrogen, oxygen and nitrogen are assumed to be released as volatiles. Volatiles are assumed as a single hypothetical component, $C_{\alpha1}H_{\alpha2}O_{\alpha3}N_{\alpha4}$. The values of $\alpha1$, $\alpha2$, $\alpha3$ and $\alpha4$ are calculated from the coal's ultimate and proximate analyses. Once the volatiles component is released, it is converted into CO, CO_2, H_2O, H_2, CH_4 and N_2 according to reaction R9. All gas phase reactions considered in calculation are summarized in Table 4-2.

Table 4-2 Gas phase reactions considered in calculation

		ΔH [MJ/kmol]	A_f [m³/kmol·s]	E_a [J/kmol]	References
$CO + \tfrac{1}{2}O_2 \rightarrow CO_2$	(R1)	- 283.24	2.2×10^{12}	1.67×10^8	[8,11]
$CO + H_2O \leftrightarrow CO_2 + H_2$	(R2)	- 41.10	2.75×10^2	8.38×10^7	[8,11]
$CH_4 + H_2O \leftrightarrow CO + 3H_2$	(R3)	+ 206.00	4.4×10^{11}	1.68×10^8	[8,11]
$CH_4 + \tfrac{1}{2}O_2 \leftrightarrow CO + 2H_2$	(R4)	- 35.7	3.0×10^8	1.26×10^8	[8,11]
$H_2 + \tfrac{1}{2} O_2 \rightarrow H_2O$	(R5)	- 242.00	6.8×10^{15}	1.68×10^8	[8,11]
$4C_6H_6 \rightarrow C_{24}H_{12} + 6H_2$	(R6)	- 9.15	1.50×10^{10}	4.70×10^5	[12]
$C_6H_6 + 4.5O_2 \rightarrow 6CO + 3H_2O$	(R7)	- 746.00	2.00×10^9	3.10×10^7	[13]
$C_{24}H_{12} + 15O_2 \rightarrow 24CO + 6H_2O$	(R8)	- 2357.00	2.00×10^9	3.10×10^7	[13]
$C_{\alpha1}H_{\alpha2}O_{\alpha3}N_{\alpha4} \rightarrow$ $\beta_1CO + \beta_2CO_2 + \beta_3H_2 +$ $\beta_4CH_4 + \beta_5H_2O + \beta_6C_6H_6 + \beta_7N_2$	(R9)		3.09×10^8	1.67×10^8	[14]

Nitrogen is assumed as inert to calculate the stoichiometric coefficient of product species for reaction R9. The pyrolysis data obtained from experimental work, which is reported in Chapter 2, is used to calculate the β values. In this assumption, all aliphatic and aromatic compounds are lumped into CH_4 and C_6H_6, respectively (Table 4-3).

Table 4-3 Volatiles species concentration produced from coal pyrolysis

Species	wt%	β
CO	0.2849	0.110
CO_2	0.2239	0.057
H_2	0.0502	0.342
H_2O	0.9643	0.470
(CH_4) Aliphatic compounds	0.4621	0.251
(C_6H_6) Aromatic compounds	1.4329	0.159
N_2	95.5817	Balanced with total N_2 present in coal

As reaction R9 contains six unknown variables (β_1 to β_6), it is necessary to use at least five equations. The following two equations together with three mass balance equations for three element (C, H and O) are used to develop the reaction R9.

$$\frac{Y_{d,CO}}{Y_{d,CO_2}} = 1.27 \tag{4-37}$$

$$\frac{Y_{d,C_6H_6}}{Y_{d,CH_4}} = 3.10 \tag{4-38}$$

where Y_d represents the mass yield for the corresponding species.

L. Chen et al. [15] explained the gas evolution from rapid pyrolysis of a bituminous coal at various pyrolysis temperatures ($500\text{-}900^0C$). It was found that the ratio of CO and CO_2 yield does not change with increasing the pyrolysis temperature. They also showed that the yield of higher hydrocarbon is approximately 3 times higher than that of CH_4. Therefore,

these two ratios obtained from Table 4-3 are used to calculate the stoichiometric co-efficient of product species for reaction R9.

4.4.3 Surface phase reactions

The surface phase reactions included in this calculation are shown in Table 4-4. A schematic of coal particle undergoing surface phase reaction is shown in Fig. 4-2. The black center region and the surrounding white region represent the solid coal particle and the gas phase, respectively. During surface reaction, it is assumed that the particle diameter will remain same while the density of the coal particle will be decreased.
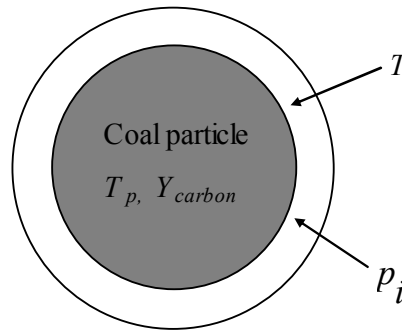
Figure 4-2 A schematic of particle surface reaction

Table 4-4 Surface reactions considered in calculation

		ΔH [MJ/kmol]	A_f [kg/m^2·s·Pa]	E_a [J/kmol]	Reference
$C + \frac{1}{2}O_2 \rightarrow CO$	(R1)	- 110.53	0.0520	1.30×10^8	[1, 8, 11]
$C + CO_2 \rightarrow 2CO$	(R2)	+ 172.44	0.0732	1.62×10^8	[1, 8, 11]
$C + H_2O \rightarrow CO + H_2$	(R3)	+ 131.28	0.0782	1.47×10^8	[1, 8, 11]

The burning rate of the carbon in coal particle is calculated using the finite rate model proposed by Smith [8, 13]. The rate of depletion of solid due to a surface reaction is given as:

$$\overline{R}_k = A_p \eta_k Y_{carbon} \widetilde{R}_k \tag{4-39}$$

$$\widetilde{R}_k = k_{kin,k} \left(p_{i,k} - \frac{\widetilde{R}_k}{D_k} \right)^{N_k} \tag{4-40}$$

where

$\overline{R}_k$ = rate of particle surface species depletion in kth reaction

$\widetilde{R}_k$ = rate of particle surface species reaction per unit area in kth reaction

η_k = effectiveness factor in kth reaction

D_k = diffusion co-efficient in kth reaction

$k_{kin,k}$ = kinetic rate of reaction for kth reaction

$p_{i,k}$ = partial pressure of the gas species i in kth reaction

A_p = surface area of coal particle

Y_{carbon} = mass fraction of carbon in coal particle

N_k = apparent order of reaction for kth reaction

The kinetic rate of the reaction and the diffusion co-efficient are computed as:

$$k_{kin,k} = A_{f,k} \exp^{-(E_{ac,k}/RT_p)} \tag{4-41}$$

$$D_k = D_{1,k} \frac{\left[(T_p + T)/2 \right]^{0.75}}{d_p} \tag{4-42}$$

where

$A_{f,k}$ = pre-exponential factor for kth reaction

$E_{ac,k}$ = activation energy for kth reaction

T_p = particle temperature

$D_{1,k}$ = diffusion rate constant for kth reaction

4.5 Boundary conditions

Uniform distributions of inlet mass flow rate and temperature are given for all inlet boundary surfaces. Turbulence quantities in terms of turbulence intensity and hydraulic diameter are specified for all inlet boundary surfaces. The turbulent intensity, I_t, and hydraulic diameter, D_H, are estimated as:

$$I_t = 0.16(\text{Re}_{D_H})^{-1/8} \tag{4-43}$$

$$D_H = \frac{4A}{P} \tag{4-44}$$

where A is the cross sectional area of the flow pipe and P is the wetted perimeter of the cross section.

The walls are assumed as stationary and smooth with no slip condition. A constant wall heat flux is assigned for wall boundary surfaces shown in Table 4-5. The boundary condition of the discrete phase at walls is assigned as "reflect", meaning the discrete phase elastically rebound off once reaching the wall. At the outlet, the discrete phase exits the computational domain. The surface injection model is used for all coal inlets.

Table 4-5 Heat loss at walls considered in calculation

Wall	Heat flux [w/m^2]	Remark
Combustor wall	3000	Assumption
Reductor wall	2400	Assumption

4.6 Numerical solution methods

The computation is carried out using the finite-volume-based commercial CFD software FLUENT (version 12.1) under steady state condition. The simulation uses the pressure-based solver, which employs an implicit pressure correction scheme and decouples the momentum and energy equations. SIMPLEC algorithm is used to couple the pressure and the velocity. First order upwind scheme is chosen for spatial discretization of the convective terms. In

pressure-based solver, the governing equations are solved sequentially (i.e., segregated from one another). Because the governing equations are non-linear and coupled, the solution loop must be carried out iteratively in order to obtain a converged numerical solution. The individual governing equations for the solution variables (e.g., u, v, w, p, T, k, ε etc.) are solved one after another. Each governing equation, while being solved, is "decoupled" or "segregated" from other equations. Each iteration consists of the steps illustrated in Fig. 4-3 and outlined below:

1. Solve the momentum equations, one after another, using the recently updated values of pressure and face mass fluxes.

2. Solve the pressure correction equation using the recently obtained velocity field and the mass-flux.

3. Correct mass fluxes, pressure, and the velocity field using the pressure correction obtained from Step 2.

4. Solve the equations for additional scalars such as turbulent quantities, energy, species, and radiation intensity using the current values of the solution variables.

5. Introduce the discrete phase by calculating the particle trajectories for each discrete phase injection.

6. Update fluid properties (e,g, density, viscosity, specific heat) including turbulent viscosity (diffusivity) based on the current solution.

7. Check for the convergence of the equations.

Repeat the above steps until a converged solution is achieved in which both the continuous phase flow field and the discrete phase particle trajectories are unchanged with each additional calculation.
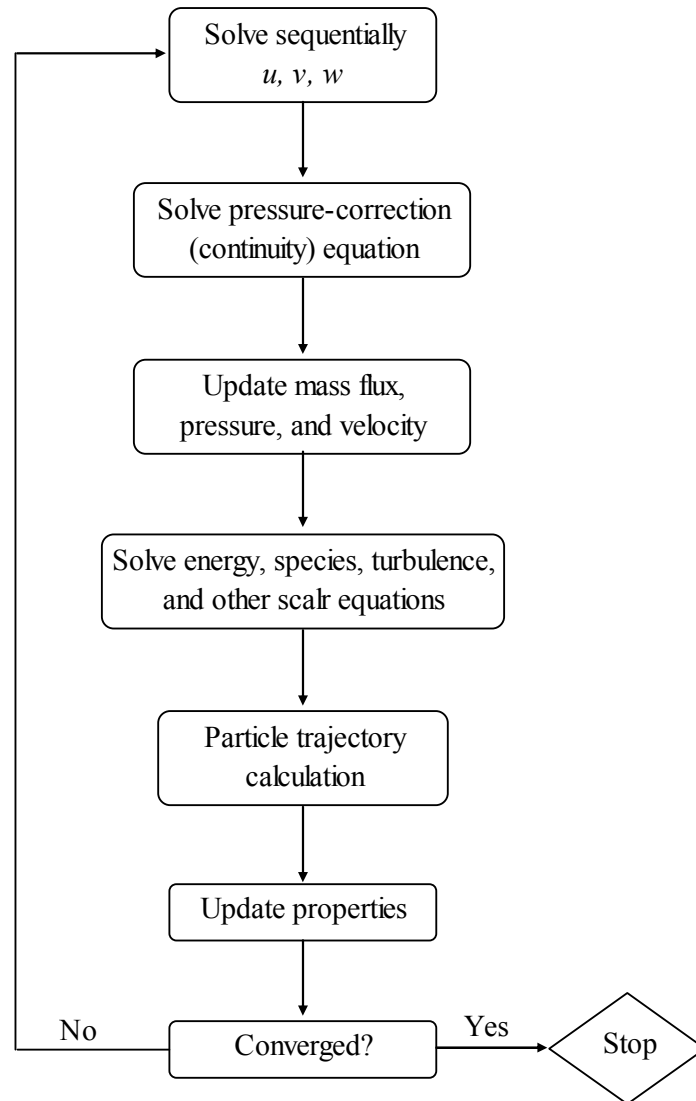
Figure 4-3 Overview of the pressure-based segregated solution methods

References

[1] Chen C., Masayuki H. and Toshinori K., "Numerical simulation of entrained flow coal gasifiers Part I: modeling of coal gasification in an entrained flow gasifier", *Chemical Engineering Science*, 55, 3861-3874 (2000).

[2] Hara S., Oki Y., Kajitani S., Watanabe H. and Umemoto S., "Examination of Gasification Characteristics of Pressurized Two-stage Entrained Flow Coal Gasifier

- Influence of Oxygen Concentration in Gasifying Agent", CRIEPI Energy Engineering Research Laboratory Report 2009, No. M08019.

[3] Jovanovic R., Milewska A., Swiatkowski B., Goanta A. and Spliethoff H., "Numerical investigation of influence of homogeneous/heterogeneous ignition/combustion mechanisms on ignition point position during pulverized coal combustion in oxygen enriched and recycled flue gases atmosphere", *International Journal of Heat and Mass Transfer*, 54, 921-931 (2011).

[4] Launder B.E. and Spalding D.B., "The numerical computation of turbulent flows", *Computer Methods in Applied Mechanics and Engineering*, 3, 269-289 (1974).

[5] ANSYS FLUENT 12.0 User's Guide, ANSYS Inc. 2009-01-29.

[6] Ranz W.E. and Marshall W.R., "Evaporation from drops part 1", *Chemical Engineering Progress*, 48(3), 141-146 (1952).

[7] Ranz W.E. and Marshall W.R., "Evaporation from drops part 2", *Chemical Engineering Progress*, 48(4), 173-180 (1652).

[8] Silaen A. and Wang T., "Effect of turbulence and devolatilization models on coal gasification simulation in an entrained-flow gasifier", *International Journal of Heat and Mass Transfer*, 53, 2074–2091 (2010).

[9] Kobayashi H., Howard J.B. and Sarofim A.F., "Coal Devolatilization at High Temperatures", *16th International Symposium on Combustion (The Combustion Institute)*, 1976.

[10] Magnussen B.F. and Hjertager B.H., "On mathematical models of turbulent combustion with special emphasis on soot formation and combustion", *Proceeding of combustion institute*, 16(1), 719-729 (1976).

[11] Watanabe H. and Otaka M., "Numerical simulation of coal gasification in entrained flow coal gasifier", *Fuel*, 85, 1935-1943 (2006).

[12] Massachusetts Ins. of Tech., Combustion Research Website (http://web.mit.edu).

[13] Kazakov A., Wang H. and Frenklach M., "Detailed modeling of soot formation in laminar premixed ethylene flames at a pressure of 10 bar", *Combustion and Flame*, 100, 111-120 (1995).

[14] Hashimoto N., Kurose R. and Shirai H., "Numerical simulation of pulverized coal jet flame employing the TDP model", *Fuel*, 97, 277-287 (2012).

[15] Chen L., Zeng C., Guo X., Mao Y., Zhang Y., Li W., Long Y. and Zhu H., "Gas evolution kinetics of two coal samples during rapid pyrolysis", *Fuel Processing Technology,* 91, 848-852 (2010).

[16] Smith I.W., "The Combustion Rates of Coal Chars: A Review", *19th International Symposium on Combustion (The Combustion Institute)*, 1045-1065 (1982).

CHAPTER 5

COAL GASIFICATION UNDER N_2/O_2 AND $CO_2/O_2/N_2$ CONDITIONS & SOOT FORMATION

5.1 Introduction

Gasification is the process of converting various carbon-based feedstocks to clean synthetic gas (syngas), which is primarily a mixture of hydrogen (H_2) and carbon-monoxide (CO) as fuels, through an incomplete combustion. Feedstock is partially combusted with O_2 and H_2O at high temperatures and pressures with only less than 30 wt% of the stoichiometric O_2 being provided [1]. Gas obtained by coal gasification can be used in many ways: for electricity production by employing the Integrated Gasification Combined Cycle (IGCC) (which is probably the most important use), in chemical industry for petrol, methanol and ammonia synthesis, for ore reduction, as an industrial fuel, as a town gas for domestic uses, for residential heating etc.

There are many research activities carried out on coal gasification under various gasification environments. Based on the reactor geometry, the studies on coal gasification are divided into two types. In one type, coal and coal carrying gas are injected from one side along the axial distance of the reactor. The product gases are collected from the other side. The other type of reactor includes injection of coal and coal carrying gas at normal direction to the axial distance at different levels of reactor height. This type of reactor configuration is more similar to the available commercial gasifier. This chapter will discuss the coal gasification behaviors including soot formation in two stage entrained flow coal gasifier under various gasification conditions.

5.2 Comparison of calculated results with experimental data

5.2.1 Calculation conditions

Two bituminous type coals MN coal (Malinau coal, Indonesia) and CV coal (Coal Valley, Canada) are used to conduct the simulation of coal gasification under N_2/O_2 and $CO_2/O_2/N_2$ gasification conditions, respectively. The proximate and ultimate analyses of coals are given in Table 5-1. The initial particle size distribution follows the Rossin-Rammler distribution which is based on the assumption that an exponential relationship exists between the coal particle diameter, d_p, and the mass fraction of particle with diameter greater than d_p, is expressed by

$$Y_{d_p} = e^{-(d_p/\overline{d_p})^{\phi}}$$

(5-1)

where $\overline{d}_p$ and ϕ represent mean diameter and spread parameter, respectively. The initial particle size distributions shown in Figs. 5-1 and 5-2 give particle size distributions with mean diameter of 40 μm and 60 μm for MN coal and CV coal, respectively. The inlet conditions for various calculations shown in Tables 5-2, 5-3, 5-4 and 5-5 are obtained from Central Research Institute of Electric Power Industry (CRIEPI), Japan in a personal communication.

Table 5-1 Analyses of coals [2,3]

Parameters	Malinau (MN) coal (Indonesia)	Coal Valley (CV) coal (Canada)
Proximate analyses(ad)		
Moisture [wt%]	4.74	6.22
Fixed carbon [wt%]	48.55	49.00
Volatile matter [wt%]	38.72	34.50
Ash [wt%]	7.98	10.28
Ultimate analyses(db)		
C [wt%]	74.30	69.90
H [wt%]	5.25	4.30
O [wt%]	10.10	13.70
N [wt%]	1.85	1.07
High heating value [MJ/kg]	29.40	26.40
Low heating value [MJ/kg]	29.00	26.02

ad: air dried db: dry base
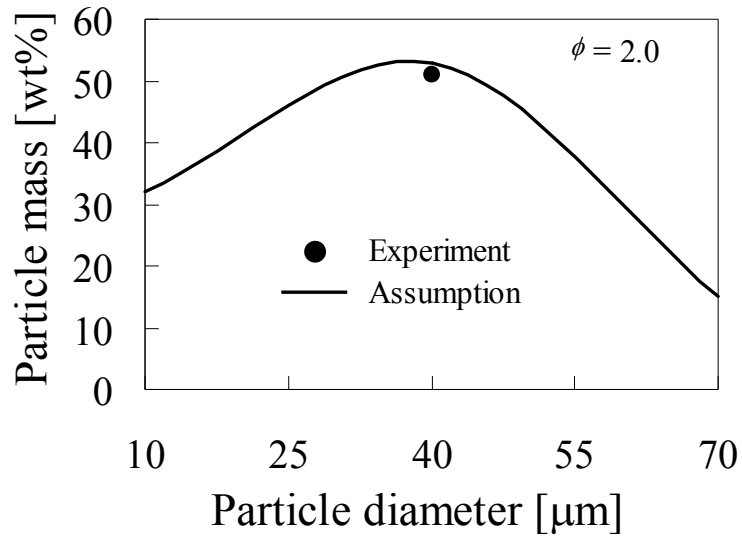
Figure 5-1 Initial particle size distribution for N_2/O_2 gasification (MN coal)

(Experimental value is from CRIEPI)
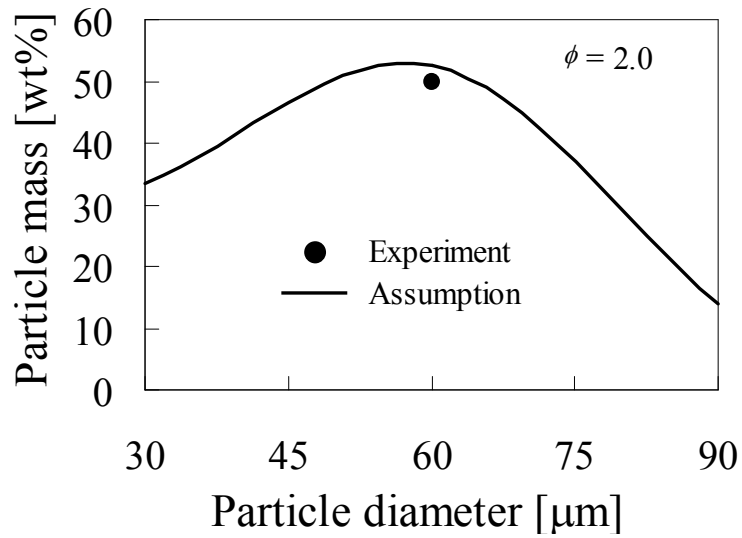
Figure 5-2 Initial particle size distribution for $CO_2/O_2/N_2$ gasification (CV coal)

(Experimental value is from CRIEPI)

Table 5-2 Inlet flow rates of coal and char for MN coal (From CRIEPI)

Parameters	Flow rate [kg/h]
Combustor coal	37.4
Combustor char	38.0
Reductor coal	63.5

Table 5-3 Inlet flow rates of coal and char for CV coal (From CRIEPI)

Parameters	Flow rate [kg/h]			
	Run 1	Run 2	Run 3	Run 4
Combustor coal	38.5	39.9	39.6	39.7
Combustor char	26.9	22.5	30.6	21.2
Reductor coal	60.8	59.4	61.6	59.1

Table 5-4 Experimental conditions of inlet gas for MN coal (From CRIEPI)

Parameters		value
Combustor coal	**Primary gas (PG) flow rate [kg/h]**	**92.9**
	PG CO_2 concentration [vol%]	0.0
	PG O_2 concentration [vol%]	21.0
	PG N_2 concentration [vol%]	79.0
	Secondary gas (SG) flow rate [kg/h]	**238.5**
	SG CO_2 concentration [vol%]	0.0
	SG O_2 concentration [vol%]	27.0
	SG N_2 concentration [vol%]	73.0
	SG temperature [K]	443.0
Combustor char	**Primary gas (PG) flow rate [kg/h]**	**66.3**
	PG CO_2 concentration [vol%]	0.0
	PG O_2 concentration [vol%]	0.0
	PG N_2 concentration [vol%]	100.0
Reductor coal	**Primary gas (PG) flow rate [kg/h]**	**70.8**
	PG CO_2 concentration [vol%]	0.0
	PG O_2 concentration [vol%]	21.0
	PG N_2 concentration [vol%]	79.0
Overall CO_2 concentration [vol%]		**0.0**
Overall O_2 concentration [vol%]		**21.0**
O_2 ratio [-]		**0.528**

Table 5-5 Experimental conditions of inlet gas for CV coal (From CRIEPI)

	Parameters	Run 1	Run 2	Run 3	Run 4
	Primary gas (PG) flow rate [kg/h]	**91.6**	**93.7**	**109.7**	**123.2**
	PG CO_2 concentration [vol%]	0.0	0.0	43.1	68.7
	PG O_2 concentration [vol%]	21.0	21.0	11.8	6.4
	PG N_2 concentration [vol%]	79.0	79.0	45.1	24.9
Combustor coal	**Secondary gas (SG) flow rate [kg/h]**	**224.3**	**165.2**	**160.2**	**129.4**
	SG CO_2 concentration [vol%]	0.0	0.0	0.0	0.0
	SG O_2 concentration [vol%]	25.8	33.6	43.9	59.6
	SG N_2 concentration [vol%]	74.2	66.4	56.1	40.4
	SG temperature [K]	488.0	447.0	421.0	355.0
	Primary gas (PG) flow rate [kg/h]	**60.3**	**91.5**	**89.8**	**90.2**
	PG CO_2 concentration [vol%]	0.0	100.0	100.0	100.0
Combustor char	PG O_2 concentration [vol%]	0.0	0.0	0.0	0.0
	PG N_2 concentration [vol%]	100.0	0.0	0.0	0.0
	Primary gas (PG) flow rate [kg/h]	**70.0**	**71.2**	**70.9**	**70.7**
	PG CO_2 concentration [vol%]	0.0	0.0	0.0	0.0
Reductor coal	PG O_2 concentration [vol%]	21.0	21.0	21.0	21.0
	PG N_2 concentration [vol%]	79.0	79.0	79.0	79.0
Overall CO_2 concentration [vol%]		**0.0**	**15.0**	**25.0**	**34.0**
Overall O_2 concentration [vol%]		**20.5**	**23.0**	**25.0**	**28.0**
O_2 ratio [-]		**0.528**	**0.514**	**0.526**	**0.531**

5.2.2 Comparison of experiment and calculation

The calculated outlet gas species concentrations are compared with experimental data obtained from CRIEPI. The comparisons of product gas species concentration are shown in Figs. 5-3 and 5-4 for coal gasification under N_2/O_2 and $CO_2/O_2/N_2$ conditions, respectively. The calculations show satisfactory agreement with the experimental results.

The concentration of CO increases with increasing inlet concentration of CO_2. Whereas a slight decrease in H_2 concentration is found if the inlet CO_2 concentration is increased. Increased CO_2 concentration promotes the char-CO_2 endothermic gasification reaction which in turn increases CO production (Fig. 5-4). H_2O concentration increases with increasing CO_2 concentration, because the relative extent of char-H_2O reaction compared to the char-CO_2 reaction decreases under rich CO_2 concentration. Increased CO_2 concentration also tends to increase the backward reaction rate, resulting in an increase in H_2O concentration and a decrease in H_2 concentration. Referring to the Fig. 5-4, it is found that coal gasification under condition of Run 1 results in CO concentration about 17 vol%. In contrast, coal gasification under condition of Run 2 can produce about 22 vol% of CO. A slight decrease in H_2 concentration from 4.86 vol% to 4.57 vol% is obtained, when the gasification condition is changed from Run 1 to Run 2. However, the syngas heating value will be increased due to significant rise in CO concentration under CO_2-rich gasification condition.

The calculated results show that the conversion of combustor coal shown in Fig. 5-5a is nearly 100 wt% for all calculated conditions. Whereas in experiment, the carbon conversion was increased from 90 to 100wt% when the inlet CO_2 concentration was increased from 0% to 15 vol%. With further increase in CO_2 concentration from 15 to 25 or 34 vol% resulted in carbon conversion of about 80 wt%. The carbon conversions of reductor coal for various gasification conditions are shown in Fig. 5-5b. It is found that the calculations overestimate the experimental carbon conversion for the reductor coal. The conversion of carbon increases with increasing the inlet concentration of CO_2. In experiment, the carbon conversion of

reductor coal was found in the range of 50 to 58 wt%. Whereas, the conversion becomes 90 wt% in calculation when the inlet CO_2 concentration is increased to 34 vol%.
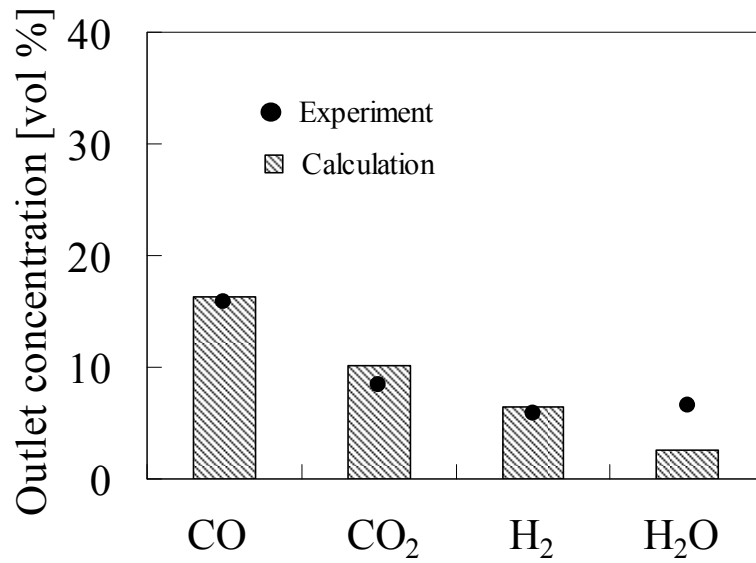

Figure 5-3 Comparison of calculated outlet species concentration with experimental data

(From CRIEPI) under N_2/O_2 gasification condition without soot (MN coal)
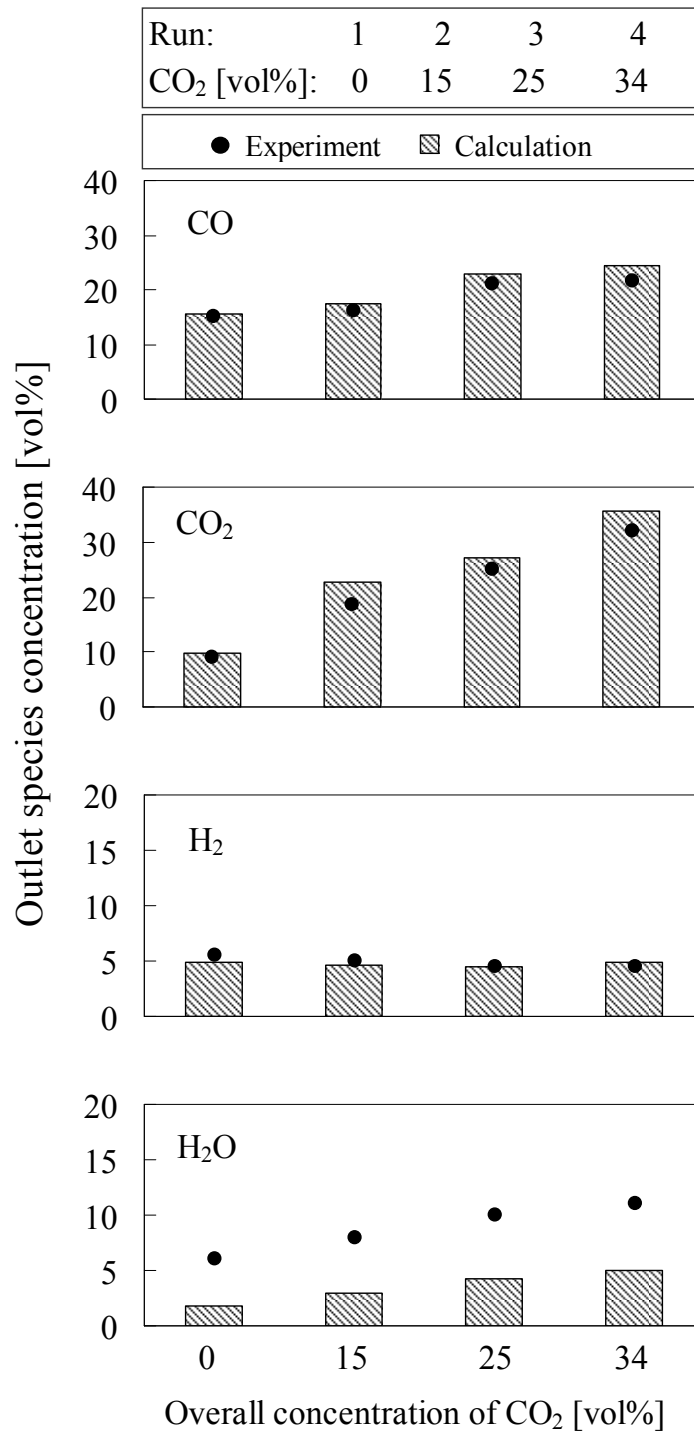
Figure 5-4 Comparison of calculated outlet species concentration with experimental data

(From CRIEPI) under various $CO_2/O_2/N_2$ gasification conditions without soot (CV coal)
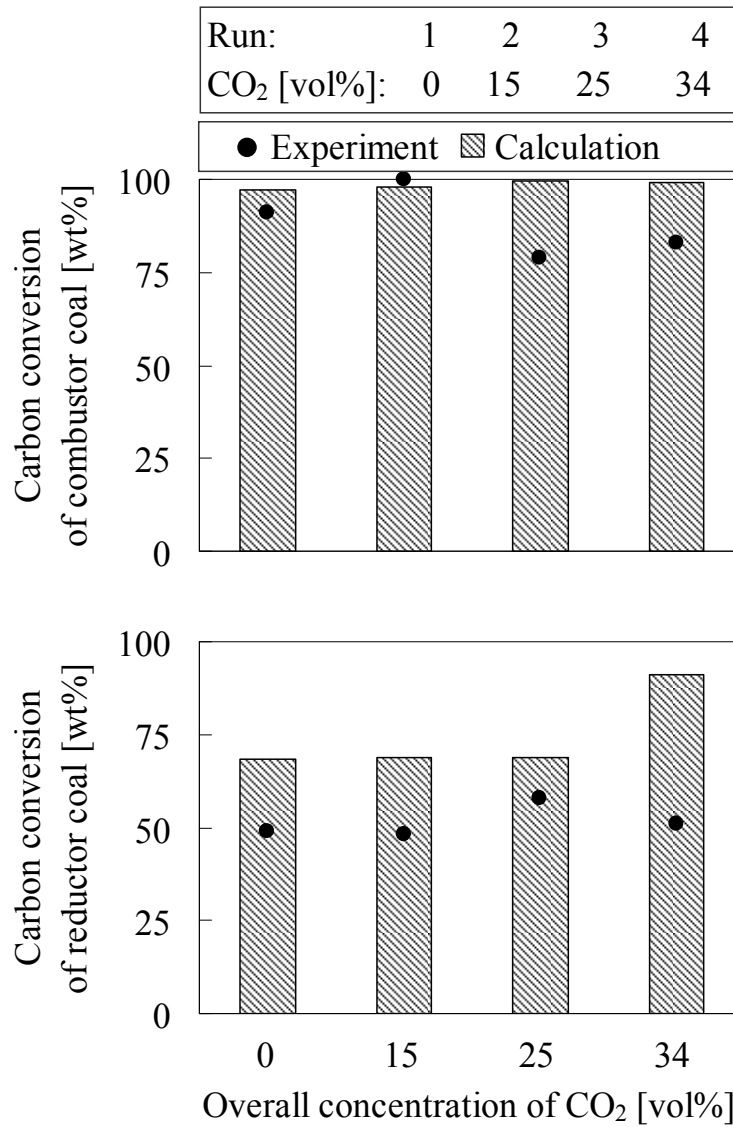
Figure 5-5 Comparison of calculated outlet carbon conversion with experimental data [3] under various $CO_2/O_2/N_2$ gasification conditions for combustor and reductor coal (CV coal)

5.3 Effect of soot formation

The comparison for two conditions of without soot and with soot shown in Fig. 5-6 indicates that there is no significant change in outlet species concentration. However, the gas temperatures much differ for the two conditions. The gas temperature profiles at centerline for experiment and calculations are shown in Fig. 5-7. In both, trends of gas temperature are found to be similar for experiment and calculations. However, calculation without soot formation over estimates the experimental gas temperature. In contrast, calculation with soot formation provides better agreement with the experiment. It indicates that the soot formation can affect the gas temperature significantly. In case of soot formation, the reaction of volatiles (R9) includes C_6H_6 which is considered as a soot precursor. This PAH molecules is then accumulated to produce a larger PAH, Coronene ($C_{24}H_{12}$), which is referred here as soot. The gas temperature for calculation with soot decreases significantly because of reducing the heat of reaction. The heat of reaction for R9 is calculated as:

$$\Delta H = \beta_1.\Delta H_f(CO)+\beta_2.\Delta H_f(CO_2)+\beta_4.\Delta H_f(CH_4)+\beta_5.\Delta H_f(H_2O)+\beta_6.\Delta H_f(C_6H_6)-\Delta H_f(vol)$$

It is clear from the above equation that with adding C_6H_6 molecules in the right side of reaction R9, a positive term for C_6H_6 (Table 5-6) is added to the calculation, resulting in a decrease in heat of reaction. The gas temperature also decreases due to the large heat capacity of PAH molecules considered in the soot formation mechanism. Table 5-6 shows that PAH molecules (C_6H_6 and $C_{24}H_{12}$) significantly differ in heat capacity than the other gas species.

For all conditions, the centerline gas temperature in the combustor is much higher than that in the reductor, because the combustor operates under relatively rich oxygen conditions. A small peak is found near the reductor burner at $z/H_{comb}=2.2$. This is because of combustion of coal fed near the reductor burner. The rise of gas temperature due to exothermic char-O_2 reaction is minimized because of increased endothermic char-CO_2 and char-H_2O reactions in the reductor.
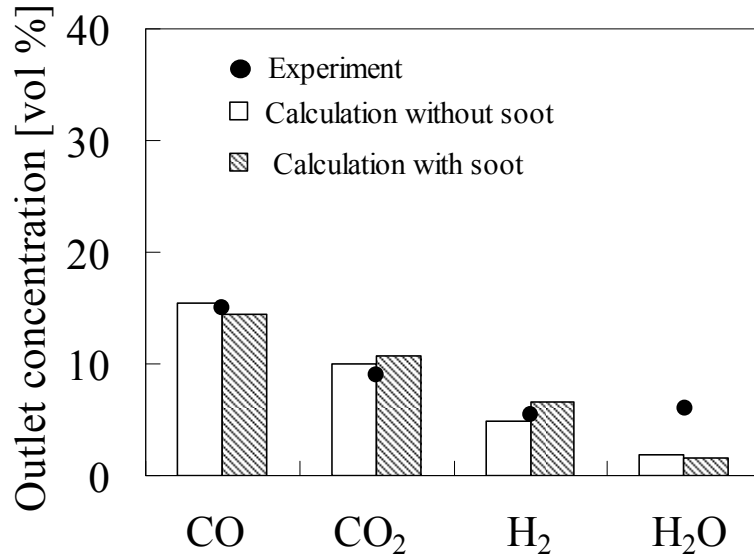
Figure 5-6 Comparison of calculated outlet species concentration with experimental data

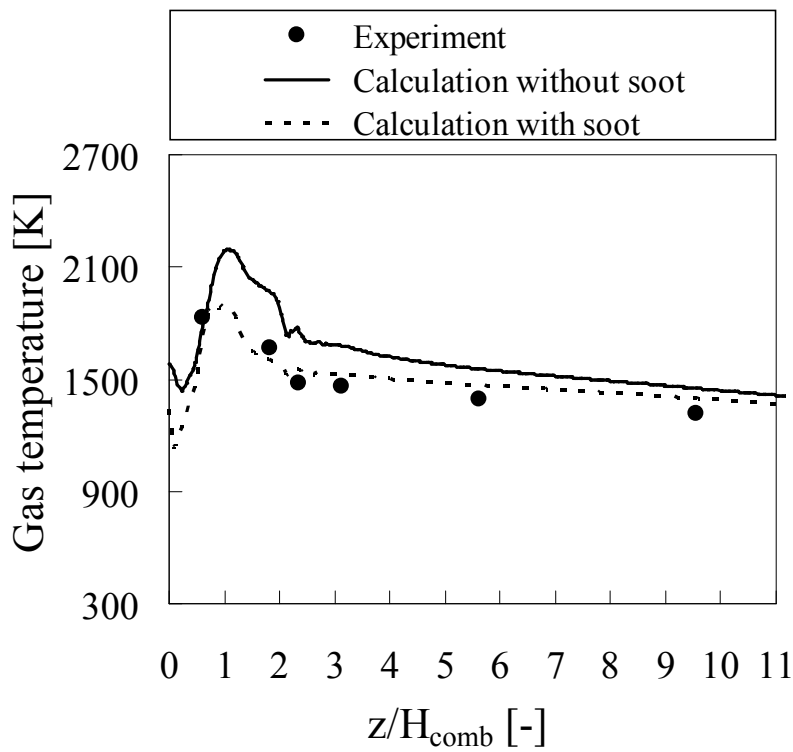(From CRIEPI) under N_2/O_2 gasification condition (CV coal Run 1)

Figure 5-7 Comparison of calculated centerline gas temperature profiles with experimental

data [3] under N_2/O_2 gasification condition (CV coal Run 1)

Table 5-6 Heat of formation and heat capacity of species

Species	ΔH_f [kJ/mol]	Heat capacity [J/mol·K]
CO	-110.5	20.2
CO_2	-393.5	28.4
H_2	0.0	20.1
CH_4	-74.8	35.6
H_2O	-241.8	28.0
C_6H_6	82.9	82.4
$C_{24}H_{12}$ (Soot)	295.0	287.0
Volatiles	78.6	-

Figure 5-8 shows that carbon conversion of combustor coal remains almost same, while a decrease in reductor carbon conversion from 63 wt% to 49 wt% is found if soot formation occurs. The significant reduction in reductor carbon conversion is due to the lowering of gas temperature in case of soot formation condition. The soot formation mechanism also includes the oxidation of PAH/soot (R7 & R8) with O_2 molecule. These reactions decrease the relative consumption of O_2 by carbon solid by reaction R10, resulting in a decrease in reductor carbon conversion.
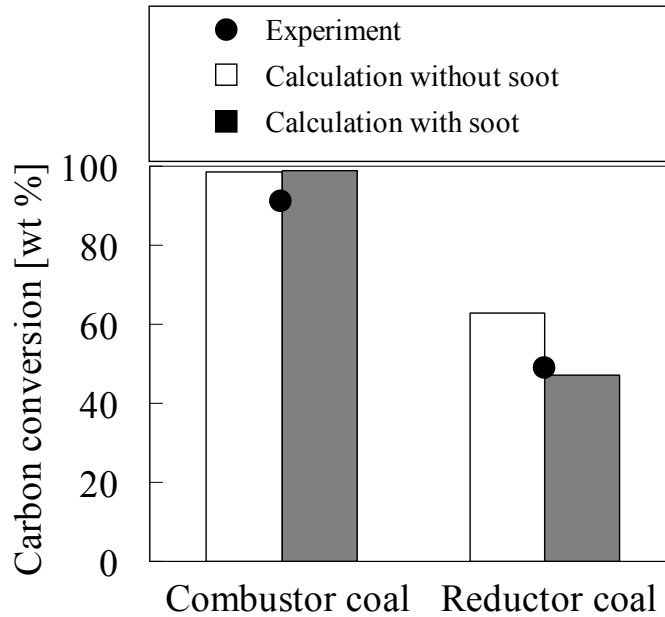
Figure 5-8 Comparison of calculated outlet carbon conversions with experimental data [3]

under N_2/O_2 gasification condition (CV coal Run 1)

Species concentration profiles for two calculated conditions are shown in Figs. 5-9 and 5-10. No soot is observed until z/H_{comb}=1.0. However, soot concentration increases after z/H_{comb}=1.0 and continues until z/H_{comb}=4.0 in the reductor. H_2 concentration also increases after z/H_{comb}=2.2 because of occurring soot formation reaction(R6). This means the concentration of H_2 will be increased if the soot formation advances in the gasifier. Therefore, it can be concluded that production of soot can increase the syngas heating value in this regard, in spite of having diverse effect of soot.

In the combustor, the concentrations of CO_2 and H_2O are much higher than that of CO and H_2. This indicates that the gas product at the combustor outlet is mainly composed of CO_2 and H_2O. This is because coal gasification occurs in the combustor under O_2-rich conditions. In the reductor, the concentrations of CO and H_2 increase whereas CO_2 and H_2O decrease. A prominent peak is observed near the reductor burner at z/H_{comb}=2.2 where CO_2 and H_2O concentrations increase suddenly. A significant peak for H_2O is visible because of the addition

of moisture released from coal. In the reductor, gasification reaction char-CO_2 and char-H_2O become dominant over the char-O_2 reaction, resulting in a decrease in gas temperature and an increase in CO and H_2 concentrations.
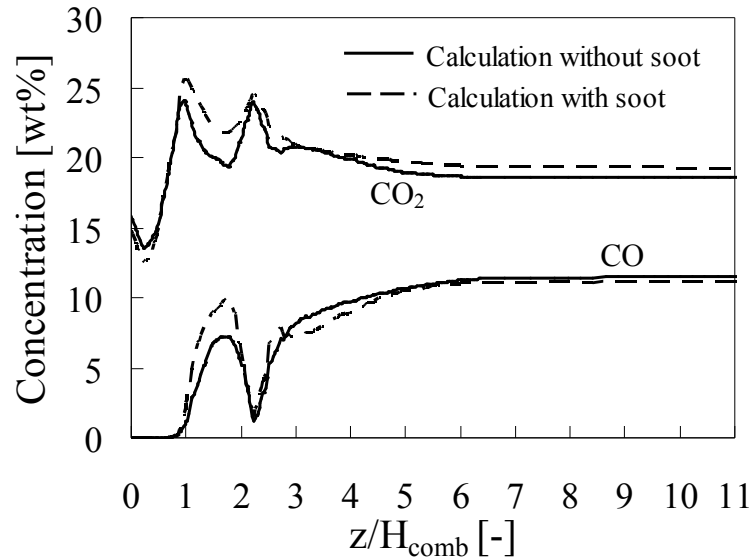

Figure 5-9 The change of CO and CO_2 concentration with axial distance calculated under

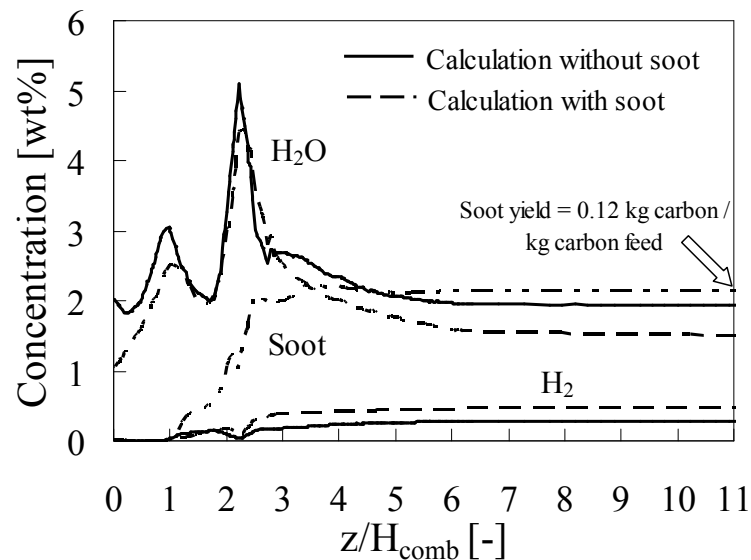N_2/O_2 gasification condition (CV coal Run 1)

Figure 5-10 The change of soot, H_2 and H_2O concentration with axial distance calculated

under N_2/O_2 gasification condition (CV coal Run 1)

5.4 Prediction of soot

Path lines of gas stream in terms of soot mass fraction are shown in Fig. 5-11. Helical flow of the gas stream indicates that most of the gas travels near the gasifier wall rather than in the center region of the gasifier. Thus the reaction for soot formation occurs near the wall, resulting in some higher soot concentration near the gasifier wall. It is also found that soot formation increases with increasing the reactor height. No significant soot is observed until z/H_{comb}=0.9. Because in the combustor more O_2 is fed, resulting in a reduced soot formation. Formation of soot starts near the combustor exit and continues to increase the soot concentration. The contours of soot, O_2, CO and H_2 concentration are shown in Fig. 5-12. It confirms that the soot concentration in the combustor is negligible where the O_2 concentration exists. It is also clear that there is some higher soot accumulation near the gasifier wall. Soot formation reaction (R6) also produces H_2 together with soot species. As a result, local H_2 concentration is also increased where soot is formed (Fig. 5-12).

The cross sectional views at various gasifier heights in terms of soot concentration and gas temperature are shown in Fig. 5-13.
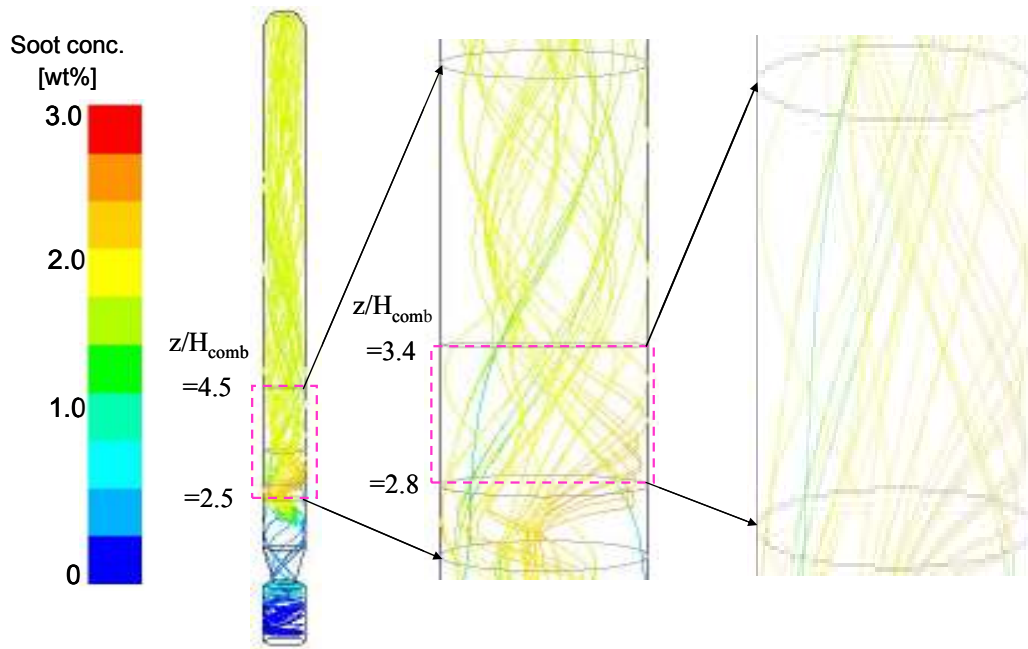
Figure 5-11 Streamlines colored by soot mass fraction calculated under N_2/O_2 gasification condition (CV coal Run 1)
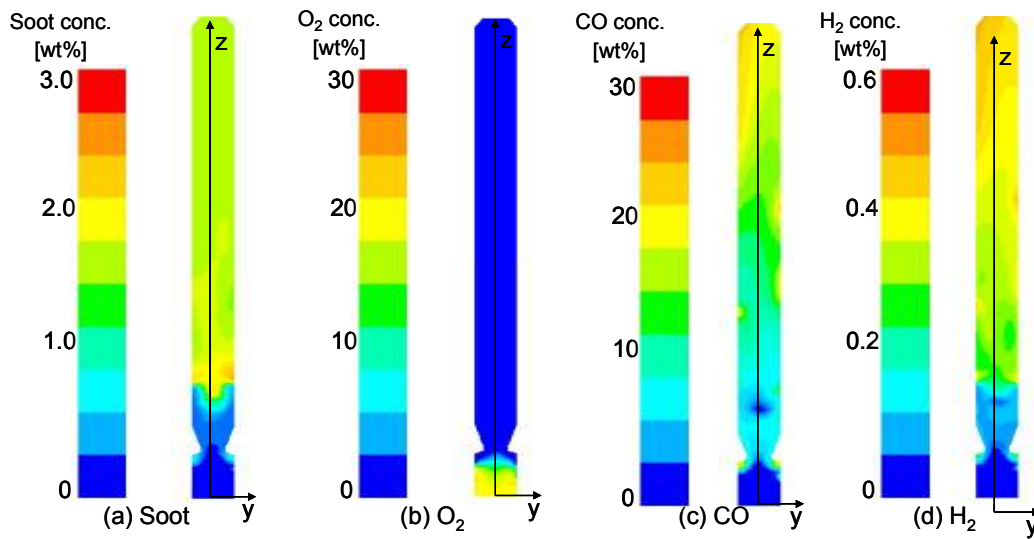

Figure 5-12 Contours of soot, O_2, CO and H_2 concentration on the z plane at center of the gasifier calculated under N_2/O_2 gasification condition (CV coal Run 1)
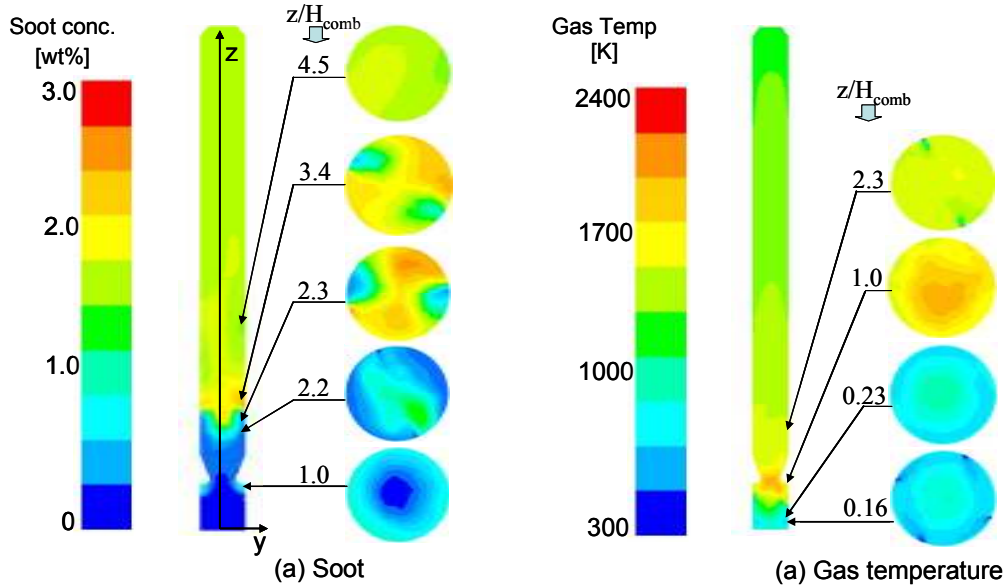
Figure 5-13 Contours of soot concentration and gas temperature at various cross sections

calculated under N_2/O_2 gasification condition (CV coal Run 1)

5.5 Behavior of gas and coal particle

The temperatures distribution near coal inlet levels in terms of velocity vectors are shown in Fig. 5-14. The left side figure represents velocity vectors near combustor coal burner. The right side figure shows the velocity vectors near reductor coal burner. It is found that combustor coal are injected in comparatively lower gas temperature region than the reductor coal. The gas temperature at center is higher than the region near the combustor wall because of occurring combustion reaction. The high temperature gas is then passed to the reductor region. As a result, endothermic char-CO_2 and char-H_2O gasification reactions occurs in the reductor. Figure 5-14 also shows that the swirling flow inside the combustor is very large compared to the reductor because of tangential fed of coal and conveying gas.

Particles tracking colored by particle temperature for the combustor and reductor coal are shown in Fig. 5-15. To provide a clear view, only one particle is shown in each track. Clearly, the combustor coal particles follow a helical flow in the combustor because of the

tangential feeding of gas and coal. The smaller particles follow the streamlines of the gas more easily than the larger particles. The larger particles possess higher inertia than the smaller particles. High inertia enables the larger particles to deviate from the streamlines of the gas. This increases the travel distance of coal particles in the combustor. The average path lengths calculated for 10, 40, and 70 μm particles in the combustor are 2.5, 7.2, and 15.5 m, respectively. In contrast, reductor coal particles tend easily to go upward with the continuous gas phase because of the absence of strong swirling flow; the swirling pattern disappears as the flow moves upward. Thus the reductor coal particles experience shorter residence times and path lengths than the combustor coal particles.
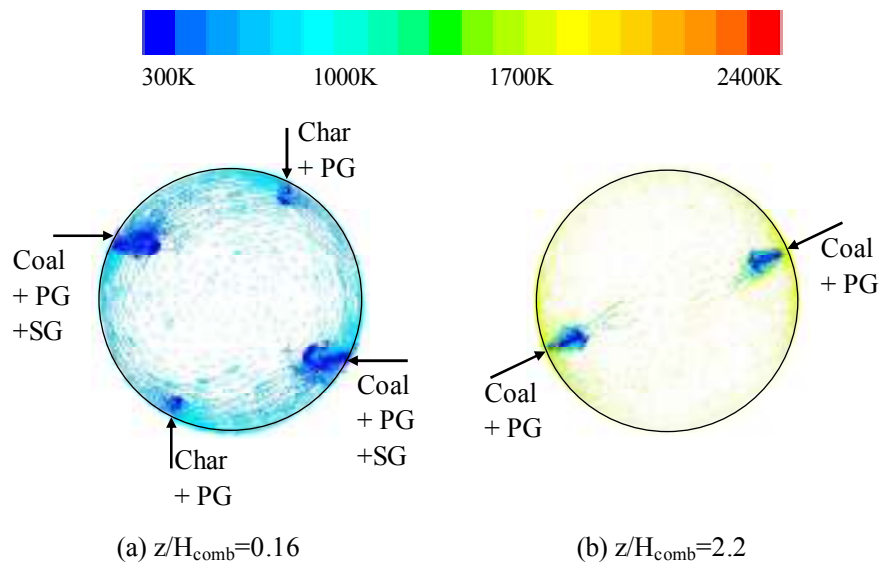

(a) z/H_{comb}=0.16　　　　　　(b) z/H_{comb}=2.2

Figure 5-14 Velocity vector colored by gas temperature calculated under N_2/O_2 gasification condition (MN coal) at: (a) combustor and (b) reductor
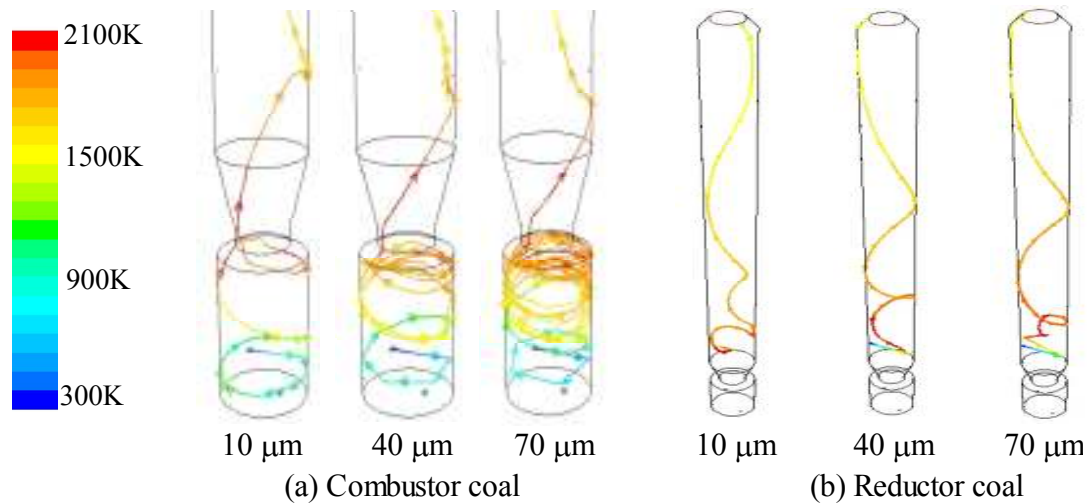
Figure 5-15 Particle track colored by particle temperature for different sizes of coal calculated under N_2/O_2 gasification condition (MN coal)

The conversion of coal particles with residence time for combustor and reductor coal is shown in Fig. 5-16. It shows that the conversion of coal particles sharply increases until about 60 wt%, which represents 100% completion of coal devolatilization. After that, each particle shows distinct differences. For 10-μm coal particles, conversions for both combustor and reductor coal rise to 100 wt% after a short residence time of 0.08 s. This is because the reaction rate for smaller particles is faster because of increased surface area than that for the larger particles. Although the gas temperature in the combustor is comparatively much higher than in the reductor, complete conversion of the 70-μm coal particles does not occur. Their conversion is very limited after complete devolatilization, although they cover a longer distance in the combustor. Therefore, to avoid unnecessary travelling, which can also cause ash deposition along the combustor wall, feeding of smaller-sized coal particles into the combustor is recommended. This will also increase the conversion of coal in the combustor.

The residence-time dependence of the z coordinate of coal particles for the combustor and reductor (Fig. 5-17) show that the residence times for the smallest particles (10μm) are minimum, where for the largest particles (70 μm) the residence time are maximum. This is

true for both combustor and reductor coal. The larger sized combustor coal particles (40 μm and 70 μm) reside longer near the combustor exit (z/H_{comb}=1.0), which confirms the lengthening of their path lengths. Because of increased inertia force, the larger particles are pinned to the combustor wall by centrifugation. This increases the probability of ash deposition at the combustor wall in the real gasifier.

The changes of particle temperatures are shown in Fig. 5-18. The temperature of the smaller size particle increases rapidly than the larger particles. This is because of fast carbon reaction due to increased surface area compared to larger particles.
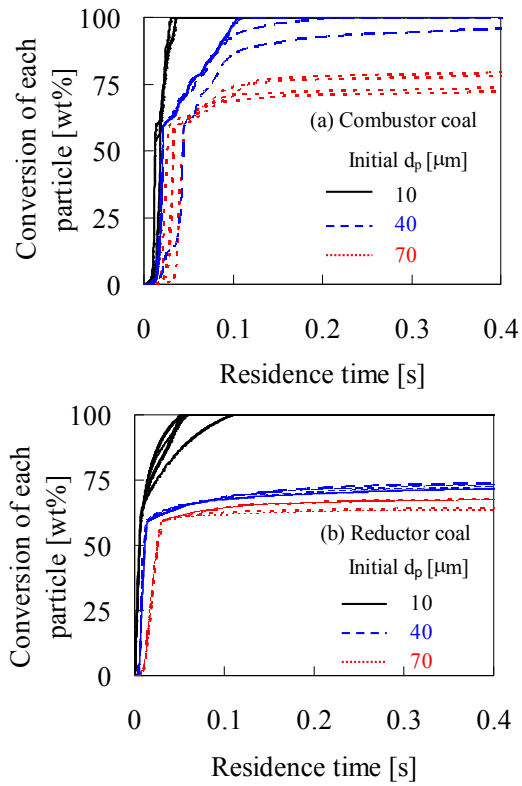
Figure 5-16 Conversion of (a) combustor and (b) reductor coal with residence time calculated under N_2/O_2 gasification condition (MN coal)
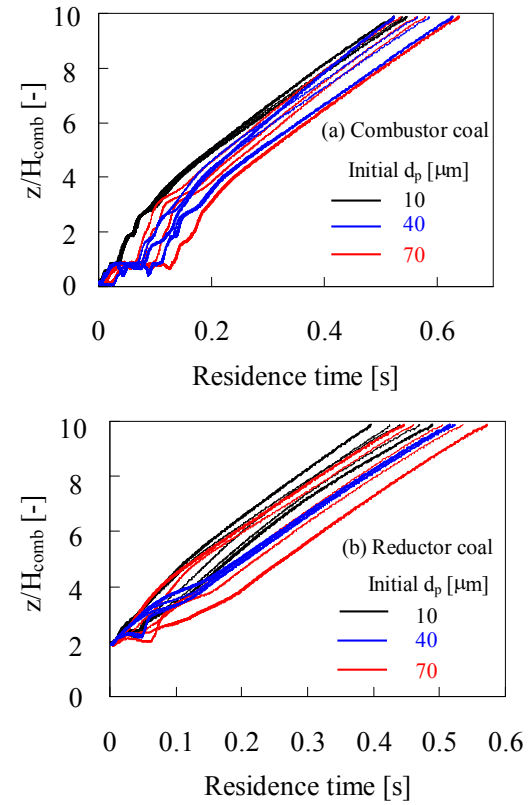
Figure 5-17 Change of particle z position with residence time for (a) combustor and (b) Reductor coal calculated under N_2/O_2 gasification condition (MN coal)
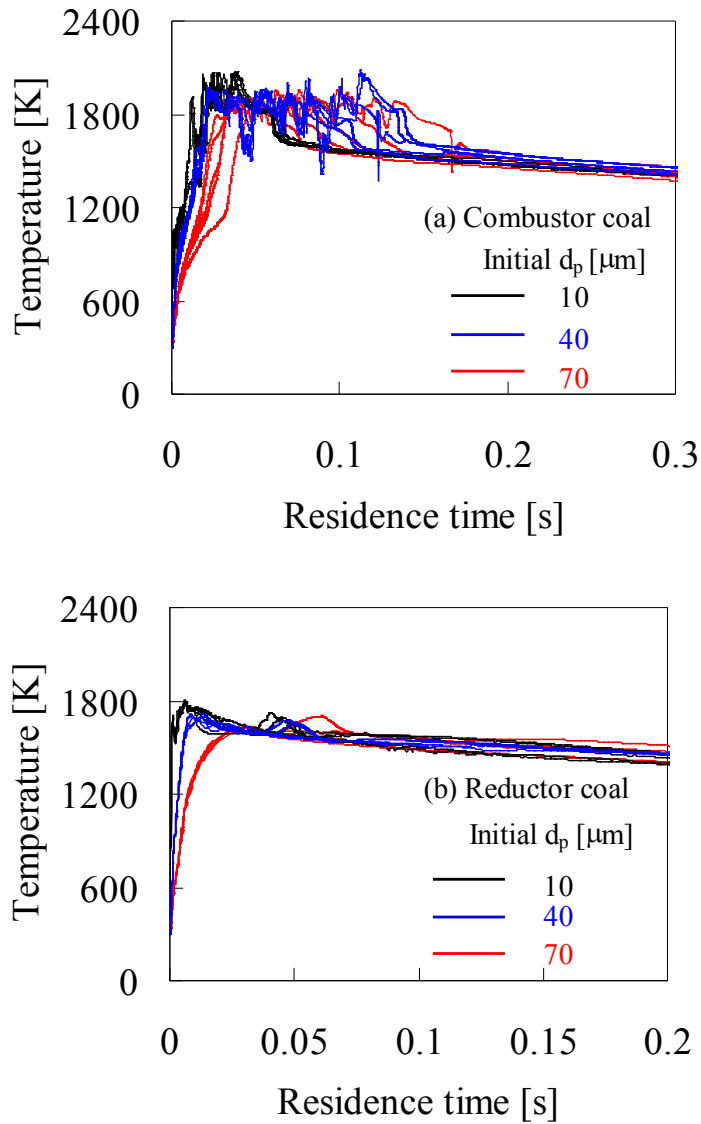
Figure 5-18 Change of particle temperature for (a) Combustor coal and (b) Reductor coal

with residence time calculated under N_2/O_2 gasification condition (MN coal)

5.6 Chapter conclusions

3D numerical simulation of coal gasification process in a two-stage entrained flow gasifier is investigated under various gasification conditions. Comparison of the calculated outlet species concentrations with those from experimental results showed a satisfactory

agreement confirming the validity of the current model. The calculated results are summarized as follows:

a) The comparatively higher CO_2 and H_2O concentrations relative to CO and H_2 concentrations in the combustor means that the contribution of the combustor to the overall CO and H_2 production is very small relative to the reductor. However, the combustor plays a major role in increasing gas temperature, which can enhance the endothermic char-CO_2 and char-H_2O reactions in the reductor.

b) Analysis of coal particles behaviors shows that to increase coal conversion and to decrease the probability of ash deposition at the combustor wall, smaller coal particles need to be used in the combustor during coal gasification.

c) $CO_2/O_2/N_2$ gasification provides higher CO concentration than N_2/O_2 gasification condition.

d) Existence of soot is obtained mainly in the reductor part of the gasifier.

References

[1] Silaen A. and Wang T., "Effect of turbulence and devolatilization models on coal gasification simulation in an entrained-flow gasifier", *International Journal of Heat and Mass Transfer*, 53, 2074–2091 (2010).

[2] Hara S., Oki Y., Kajitani S., Watanabe H. and Umemoto S., "Examination of Gasification Characteristics of Pressurized Two-stage Entrained Flow Coal Gasifier - Influence of Oxygen Concentration in Gasifying Agent", *CRIEPI Energy Engineering Research Laboratory Report*, M08019 (2009).

[3] Kidoguchi K., Kajitani S., Oki Y., Umemoto S., Umetsu H., Hamada H. and Hara S., "Evaluation of CO_2 Enriched Gasification Characteristics Using 3t/d Bench Scale Coal Gasifier - Influence of CO_2 Concentration in Gasifying Agent", *CRIEPI Energy Engineering Research Laboratory Report*, M11019 (2012).

CHAPTER 6

SENSITIVITY ANALYSIS

6.1 Introduction

Sensitivity analysis is the study of the variation in the predictions made by the model when a change occurs to a component of the model or if an input to the model is altered. In gasification the predictions made by a model can be a number of different variables including soot formation, carbon conversion, syngas composition and exit gas temperature. This chapter extends the study of sensitivity analysis on coal gasification under CO_2/O_2 gasification condition with the objective of predicting more carbon conversion and more syngas formation.

Chen et al. [1-2] performed a series of numerical simulation for a 200 T/D two-stage air blown entrained flow gasifier under various operating conditions such as heterogeneous reaction rate, particle size, and coal partitioning to the two stages. They reported that the carbon conversion decreases when the pre-exponential factor for the char-O_2, char-CO_2 and char-H_2O reaction rates are decreased. They also predicted that increasing the average coal particle size decreases the carbon conversion, which results in an increase in the exit gas temperature and a decrease in heating value of product gas. The air ratio showed a significant effect on gas composition. Increasing air ratio leads to increase CO_2 and decrease CO and H_2 concentration, and accordingly, had a strong effect on the heating value of the product gas. The partitioning of coal between the combustion stage and the reduction stage was investigated by changing the fraction of the total coal feed rate into the combustor, holding other parameters fixed. For a constant air ratio, the carbon conversion and the higher heating value of product gas were predicted to change very little with the coal partitioning between the combustor and reductor.

Silaen and Wang [3-5] conducted numerical simulation of the coal gasification process in two stage entrained flow gasifier. They investigated the effects of several parameters on gasification performance including coal mixture (slurry or dry powder), oxidant (oxygen-blown or air-blown), wall cooling, and various coal distributions between the two stages. They reported that coal-slurry feed is preferred over coal-powder feed to produce hydrogen. On the other hand, coal-powder feed is preferred over coal-slurry feed to produce carbon monoxide. The air-blown operation yields poor fuel conversion efficiency and the lowest syngas heating value due to air dilution. The effect of wall cooling has been shown insignificant on the exit gas composition and heating value. The fuel conversion efficiency of the case with coal distribution with 75% (first stage) vs. 25% (second stage) is better than the case with 50% vs. 50% coal distribution. Horizontal injection direction was compared to downward and upward direction. The results revealed that the horizontal injection direction gives the best gasifier performance. Changing the direction of the first-stage injectors downward resulted in a decrease of carbon conversion and an increase of H_2 production. Changing the direction of the second-stage injectors, however, did little affect the overall flow patterns due to the smaller-quantity of coal injection (25%) and hence the gasifier performance was essentially insignificantly affected.

From the previous discussion, it is found that the combustor is operated under higher temperatures (2000-2100 K) condition. In contrast, the temperature is about 1100-1200 K in the reductor. The low temperature in the reductor also retards the endothermic gasification reactions, resulting in reducing the carbon conversion.

The main objective of this study is to investigate the uncertainty of model parameters, effects of char reaction rates, effects operating conditions, effects of heat losses, effects of inlet concentration of CO_2 and O_2 ratio in an effort to increase the syngas heating value and carbon conversion in coal gasification. The O_2 ratio is defined here as the ratio of the amount of O_2 fed into the gasifier to the amount of O_2 required for complete combustion of carbon present in coal. The heating value of product syngas is the sum of energy release burning the component gas as follows:

$$Heating\ value = Heating\ value\ of\ CO \times Y_{CO} + Heating\ value\ of\ H_2 \times Y_{H_2} \tag{6-1}$$

where heating value of CO and H_2 are considered as 12372 and 141790 kJ/kg [6], respectively. CO_2 and H_2O are non combustible gases and therefore make no energy contribution.

6.2 Calculation conditions

A bituminous type coal CV coal (Table 5-1) is used to conduct the simulation of coal gasification for sensitivity analysis under CO_2/O_2 condition. The inlet conditions for coal/char and gas flow rate are shown in Tables 6-1 and 6-2. Properties of gas/solid and modeling constants are summarized in Table 6-3. The calculated results obtained under the conditions shown in Tables 6-1, 6-2 and 6-3 are referred to as the standard case (Case 1). The calculated results for various cases are summarized in Table 6-4.

Table 6-1 Inlet flow rates of coal and char (CV coal)

Parameters	
Combustor coal flow rate [kg/h]	38.5
Combustor char flow rate [kg/h]	26.9
Reductor coal flow rate [kg/h]	60.8

Table 6-2 Conditions of inlet gas under $CO_2/O_2/N_2$ gasification (CV coal)

Parameters		
	Primary gas (PG) flow rate [kg/h]	**91.6**
	PG CO_2 concentration [wt%]	0.0
	PG O_2 concentration [wt%]	23.0
	PG N_2 concentration [wt%]	77.0
Combustor coal	**Secondary gas (SG) flow rate [kg/h]**	**224.3**
	SG CO_2 concentration [wt%]	0.0
	SG O_2 concentration [wt%]	28.4
	SG N_2 concentration [wt%]	71.6
	SG temperature [K]	488.0
	Primary gas (PG) flow rate [kg/h]	**60.3**
	PG CO_2 concentration [wt%]	100.0
Combustor char	PG O_2 concentration [wt%]	0.0
	PG N_2 concentration [wt%]	0.0
	Primary gas (PG) flow rate [kg/h]	**70.0**
	PG CO_2 concentration [wt%]	0.0
Reductor coal	PG O_2 concentration [wt%]	23.0
	PG N_2 concentration [wt%]	77.0
Overall CO_2 concentration [wt%]		**14.0**
Overall O_2 concentration [wt%]		**23.0**
Overall O_2 ratio [-]		**0.528**

Table 6-3 Properties of gas/solid and modeling constants used for standard case

Parameter	Symbol	Remarks
Gas properties		
Thermal conductivity	k_g	0.0454 W/m·K
Viscosity	μ	1.72×10^{-5} kg/m·s
Absorption coefficient	A	1.5 m^{-1}
Scattering coefficient	σ_s	0 m^{-1}
Refractive index	φ	1
Mass diffusion coefficient	D	2.88×10^{-5} m^2/s
Turbulent model		
Turbulent Schmidt number	Sc_t	0.7
Turbulent model constant	$C_{1\varepsilon}$	1.44
Turbulent model constant	$C_{2\varepsilon}$	1.92
Turbulent model constant	C_μ	0.09
Turbulent Prandtl number for k	σ_k	1.0
Turbulent Prandtl number for ε	σ_ε	1.3
Coal particle properties		
Particle density	ρ_p	1400 kg/m^3
Particle specific heat	C_p	1680 J/kg·K
Particle Vaporization temperature	T_{vap}	400 K
Particle emissivity	ε_p	0.9
Particle scattering factor	f_p	0.9
Fraction of heat absorbed by coal particle	f_h	1.0
Devolatilization model		
Pre-exponential factor	$A_{f,1}$	2×10^5 s^{-1}
Activation energy	$E_{ac,1}$	1.046×10^8 J/kmol
Pre-exponential factor	$A_{f,2}$	1.3×10^7 s^{-1}
Activation energy	$E_{ac,2}$	1.674×10^8 J/kmol

Table 6-4 Summary of calculation for two stage entrained flow gasifier under $CO_2/O_2/N_2$ gasification condition (CV coal)

Case	Variable changes	Carbon conversion (combustor coal) [wt%]	Carbon conversion (reductor coal) [wt%]	Carbon conversion (overall) [wt%]	Outlet soot [wt%]	Outlet CO [wt%]	Outlet H_2 [wt%]	Outlet T [K]
1	Standard condition	99.36	49.29	77.03	1.79	16.46	0.46	1352
Uncertainty of model parameters								
2	Latent heat of water, L $0 \rightarrow 3.8 \times 10^5$ J/kg	99.26	48.88	76.55	1.77	16.53	0.44	1346
3	Fraction of heat absorbed by coal particle, f_h $1.0 \rightarrow 0.5$	98.52	48.16	76.27	1.81	16.86	0.45	1345
4	Diffusion rate constant, D_1 $5 \times 10^{-12} \rightarrow 10 \times 10^{-12}$	98.02	51.02	76.59	1.77	17.21	0.55	1340
5	Scattering coefficient, σ_s $0 \rightarrow 1.5$ m^{-1}	98.47	50.25	77.97	1.77	17.54	0.49	1358
6	Absorption coefficient, a $1.5 \rightarrow 3.0$ m^{-1}	98.89	52.06	79.31	1.82	20.10	0.53	1368

Effect of char kinetic rates

7	10 times char-O_2 rate, A_f 0.052 → 0.52	99.22	50.21	77.13	1.823	17.85	0.43	1346
8	10 times char-CO_2 rate, A_f 0.0732 → 0.732	99.67	51.83	78.67	1.777	18.35	0.45	1263
9	10 times char-H_2O rate, A_f 0.0782 → 0.782	98.32	52.01	78.21	1.854	19.05	0.63	1281

Effect of operating conditions

10	Reductor coal injection pattern Directly to the center of reactor → Tangentially (Refer to Fig. 6-7)	99.15	48.87	76.85	1.71	16.89	0.43	1358
11	Coal size distribution Particle diameter ranges: 10-70 μm → 10-50 μm (Refer to Fig. 6-8)	99.44	52.64	77.28	1.791	16.24	0.49	1346
12	Combustor secondary O_2 70.8 kg/h → 53 kg/h Reductor primary O_2 16.28 kg/h → 34 kg/h	97.17	56.89	78.02	1.68	16.70	0.48	1397

13	Combustor coal inlet 40 kg/h → 60 kg/h Reductor coal inlet 60 kg/h → 40 kg/h	83.16	54.47	75.03	1.66	15.89	0.39	1367
14	Coal type CV coal → Taiheiyo coal (Refer to Table 6-5)	99.42	67.64	83.12	2.21	15.14	0.40	1365

Effect of heat loss

15	Heat loss At combustor wall: 3000 w/m^2 → 3300 w/m^2 At reductor wall: 2400 w/m^2 → 2640 w/m^2	96.35	47.35	72.32	1.83	16.35	0.41	1328
16	Reductor wall boundary condition Heat loss (2400w/m^2) → Temperature (1673K)	99.44	77.32	89.55	1.55	32.31	0.58	1672

6.3 Results and discussion

6.3.1 Uncertainty of model parameters

In the modeling of coal gasification, there are many uncertain parameters used in the calculation. It is very difficult to get exact value of various model parameters for the specific problem especially in coal gasification. The use of unknown model parameters may causes a difference between calculation and experiment. The effects of some important model parameters such as latent heat of devolatilization, fraction of heat absorbed by coal particle, diffusion coefficient, absorption coefficient etc. on carbon conversion, syngas production and the product gas temperature are numerically investigated.
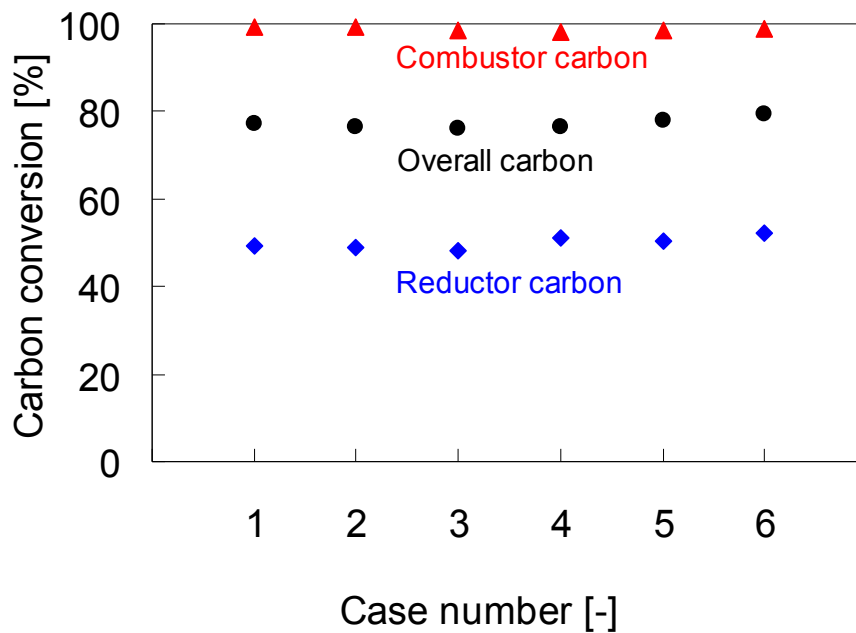
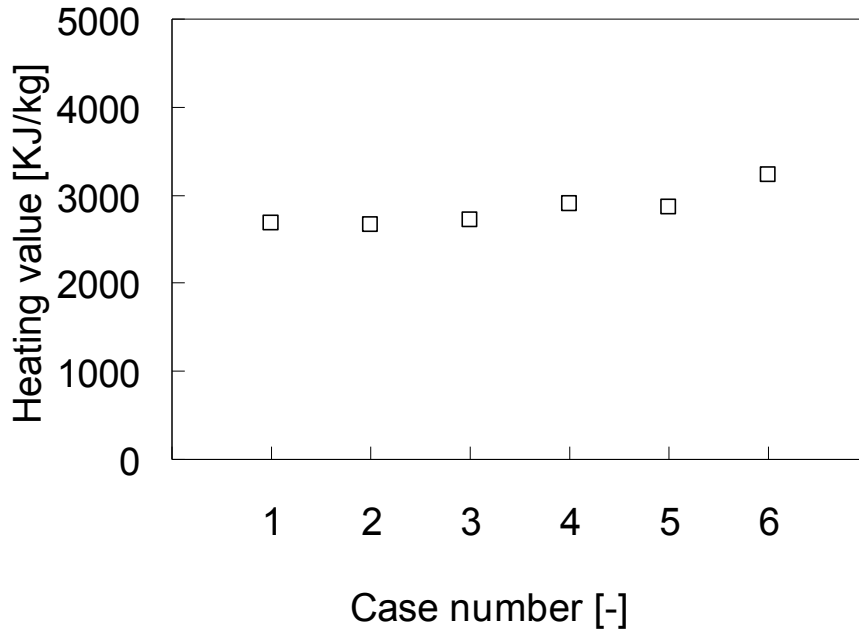**Figure 6-1** Effects of model parameters on carbon conversion

Figure 6-2 Effects of model parameters on product gas heating value

The latent heat of water present in coal is neglected in the standard case (Case 1). For the Case 2, it is considered that 0.38 MJ (see Table 5-1) heat is required for evaporation of water present in 1 kg coal. This heat is approximately 1.5% of the high heating value of coal (26.40 MJ/kg). A small decrease in gas temperature at outlet is found because of heat consumed in evaporation of water during devolatilization. However, no significant changes in carbon conversion and syngas production is obtained if latent heat is considered. In other hand, it can be concluded that a small difference in coal heating value will not significantly affect the carbon conversion and syngas production.

The surface reaction consumes or produces energy during the char gasification reactions (R10-R12) shown in Table 4-4. The fraction of heat absorbed/released by solid coal particle is represented here as f_h. The default value of 1.0 (Case 1) implies that the entire heat of reaction is absorbed/released by solid phase. To investigate the effect of this heat distribution to the solid and gas phase, another calculation with a value $f_h =0.5$ (Case 3) is carried out. This means the heat required for surface reaction will be contributed equally by

both solid and gas phases. There are no significant changes in carbon conversion and syngas heating value found for the two cases. Since the coal gasification is carried out under $CO_2/O_2/N_2$ gasification condition, a slight decrease in gas temperature for case 3 is obtained because of consuming energy from gas phase during char-CO_2 endothermic reaction (R11).

The effects of radiation parameters on carbon conversion, gas temperature and species concentration are numerically investigated by changing the radiation parameters; scattering coefficient and absorption coefficient. The scattering coefficient is changed from 0 m^{-1} (Case 1) to a value of 1.5 m^{-1} (Case 5). In another calculation, the absorption coefficient is increased from a value 1.5 m^{-1} to a value 3.0 m^{-1} (Case 6). Carbon conversion, syngas production and product gas temperature increase with increasing scattering coefficient and absorption coefficient. It is noticeable that increasing the absorption coefficient results in a significant change in syngas production. It indicates that endothermic char-CO_2 and char-H_2O reactions enhance under higher value of absorption coefficient. Interestingly, the gas temperature increases, although endothermic reactions occur. This temperature rise is due to absorption of more heat by gas species. Since the absorption capacity of CO_2 is higher than the other species, CO_2 can play a significant role to absorb heat from radiation energy under $CO_2/O_2/N_2$ gasification condition.

Referring to the Table 6-4, it is found that the productions of soot under various changes in model parameters remain unchanged.

6.3.2 Effects of char kinetic rates

Calculations are performed under Case 7: increasing the pre-exponential for the char-O_2 by a factor of 10, Case 8: increasing the pre-exponential for the char-CO_2 by a factor of 10 and Case 9: increasing the pre-exponential for the char-H_2O by a factor of 10. The calculated carbon conversions and syngas heating values are shown in Figs. 6-3 & 6-4.

It is found that with increasing the reaction rate of carbon the reductor carbon conversion increases, while the conversion of combustor carbon remains unchanged. The effect of reaction rate of char-O_2 on gas temperature is very small. In contrast, the gas temperatures at outlet for Cases 8 and 9 are decreased much compared to the standard case. This means endothermic reactions, char-CO_2 and char-H_2O, increase under calculated conditions. Therefore, by increasing the rate of reaction of char-CO_2, it is possible to get more CO, resulting in an increase in syngas heating value. The reaction rate of carbon by CO_2 will be also increased if CO_2 concentration is increased in the gasifier. Since $CO_2/O_2/N_2$ gasification operates under CO_2-rich condition than the conventional air blown gasification, it can be concluded that $CO_2/O_2/N_2$ gasification will be able to produce high heating value gas, resulting in an increase in gasification efficiency. On the other hand, char-H_2O reaction rate also plays a significant role to increase the syngas heating value. The concentration is increased from 16wt% to 19wt% and 0.46wt% to 0.63wt% for CO and H_2, respectively.
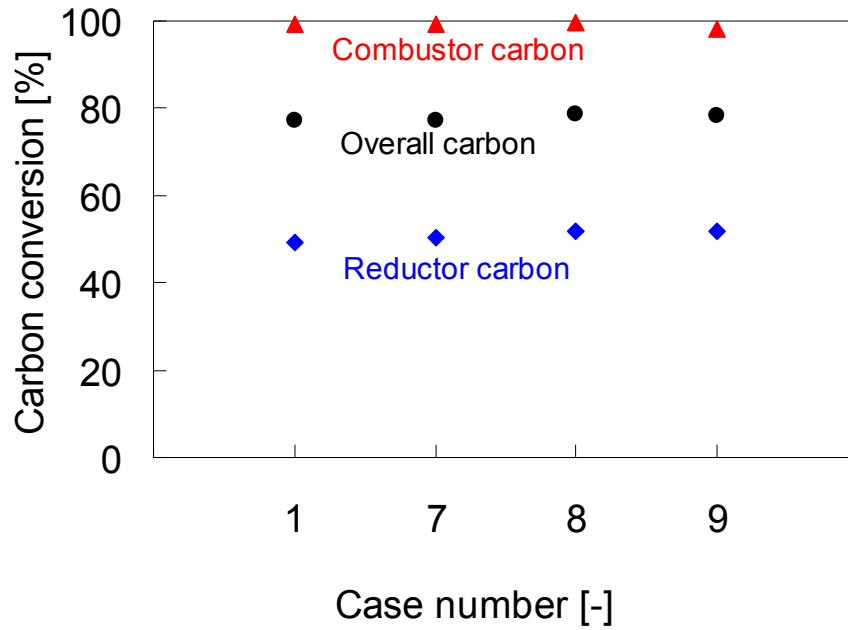
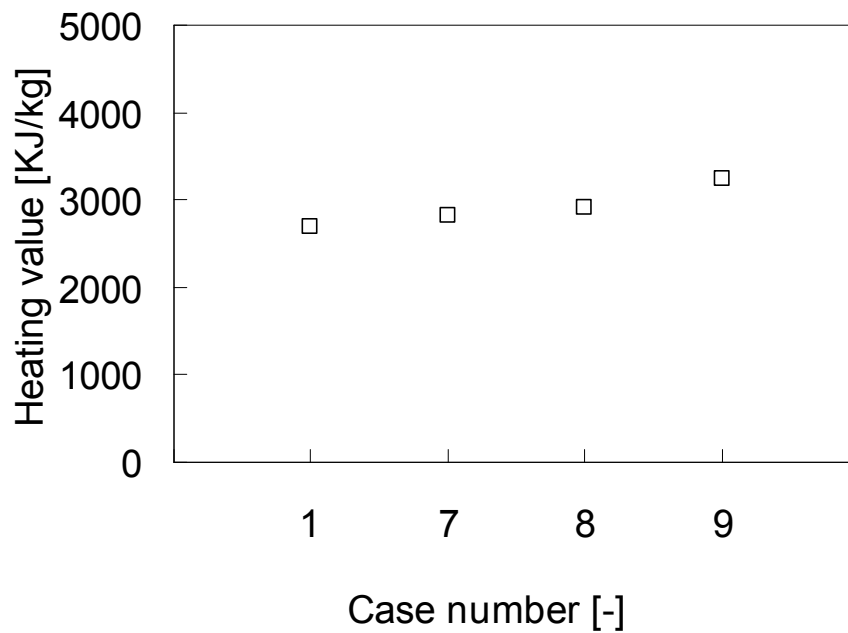**Figure 6-3** Effects of kinetic parameters of char reaction rate on carbon conversion

Figure 6-4 Effects of kinetic parameters of char reaction rate on product gas heating value

6.3.3 Effects of operating conditions

The effects of operating conditions on carbon conversion, syngas heating value and gas temperature are numerically investigated in an effort to increase the carbon conversion and syngas heating value without changing the total gas and coal flow rates. The calculations are carried out by changing the coal injection pattern, coal particle size, coal distribution in the two stages, O_2 distribution in the two stages and coal type.

In standard case (Case 1), the combustor injectors are placed similar to a tangential firing system to create swirling flow inside the gasifier. The reductor injectors are directed towards the center of the gasifier. To investigate the effect of reductor coal injection pattern, the reductor injectors are also placed similar to a tangential firing system. This condition will be referred as Case 10. To make a clear understanding, cross sectional views of velocity vectors at z/H_{comb}=2.2 for Cases 1 and 10 are shown in Fig. 6-7. The results show that reductor coal injection pattern does not affect the coal gasification significantly.
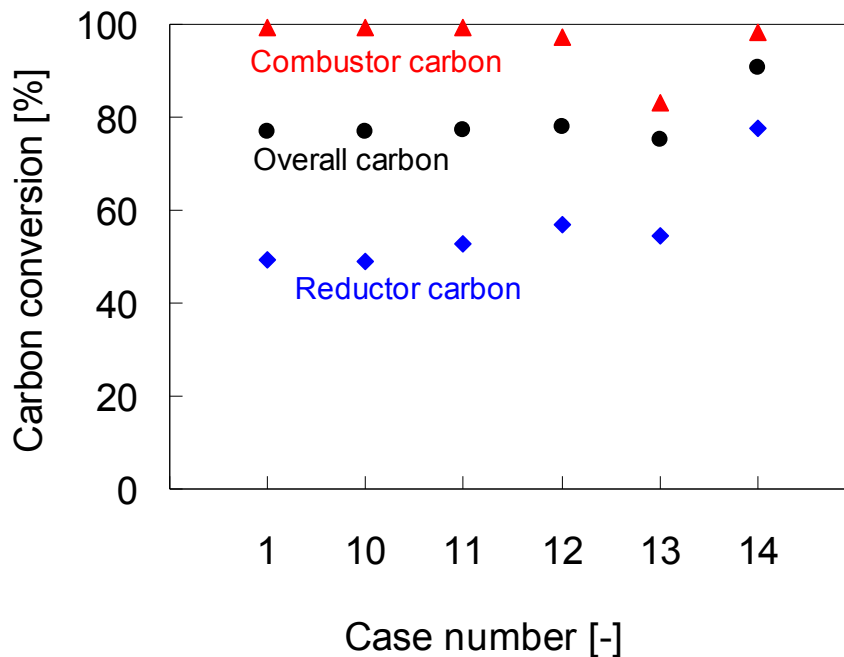

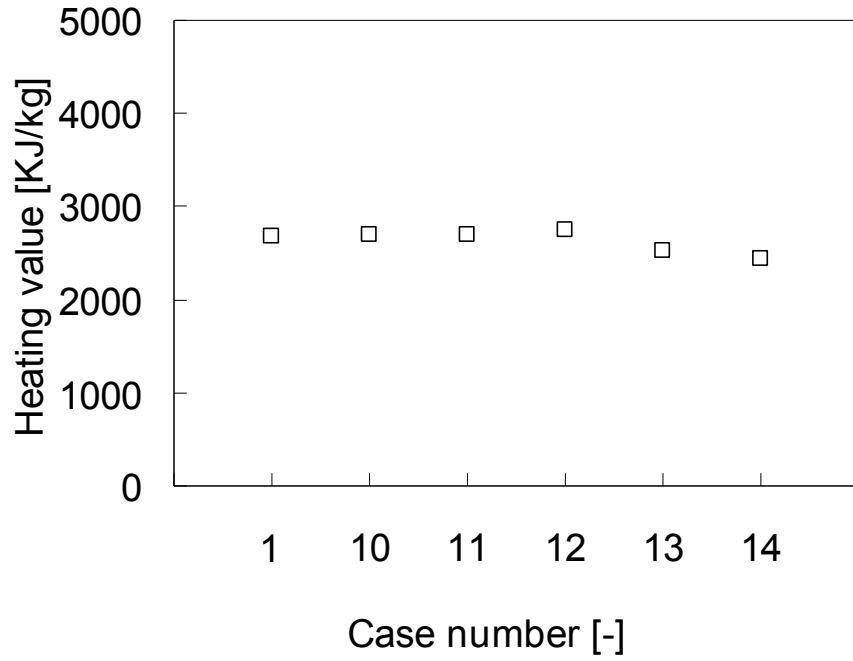**Figure 6-5** Effects of operating conditions on carbon conversion

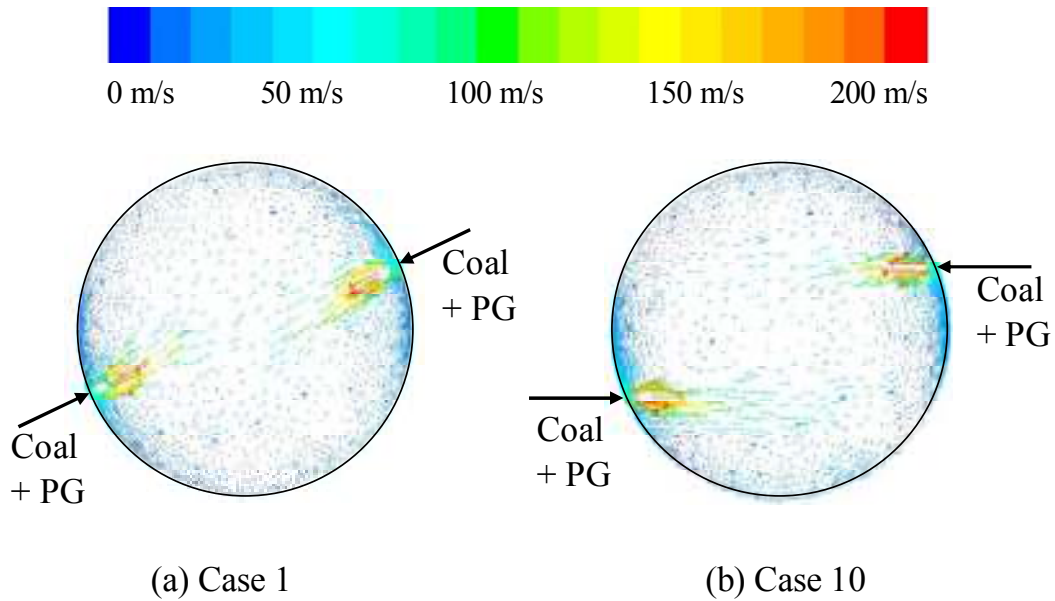**Figure 6-6** Effects of operating conditions on product gas heating value

(a) Case 1   (b) Case 10

Figure 6-7 Cross sectional views of velocity vectors colored by velocity magnitude at

z/H$_{comb}$=2.2 for Cases 1 and 10

131

To investigate the effect of coal particle diameter on the gas temperature and carbon conversion, a smaller initial particle size distribution is considered in the calculation. The calculation is carried out for coal with a mean diameter of 30μm. The initial particle size distributions for Cases 1 and 11 are shown in Fig. 6-8. No significant change in calculated results is observed if the coal particle size distribution is changed from the Case 1 to Case 11.
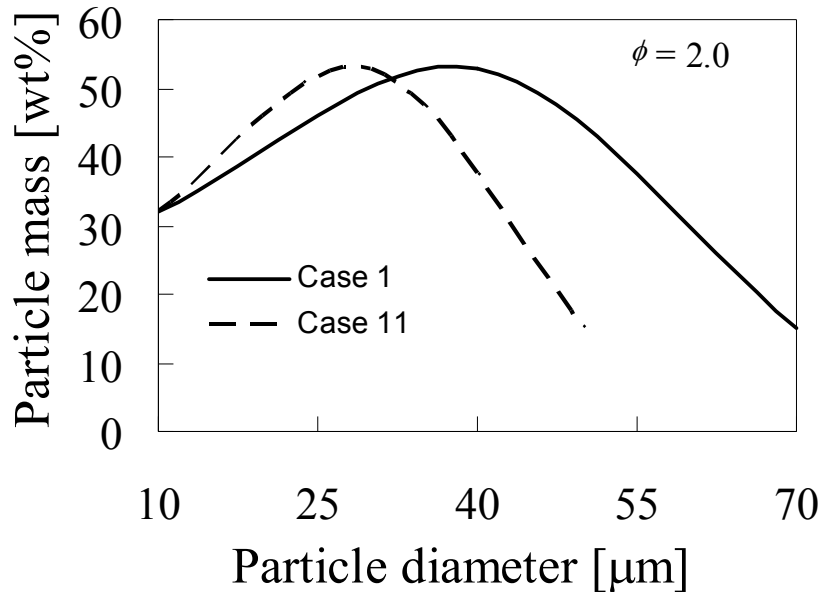

Figure 6-8 Initial coal particle size distributions considered for Cases 1 and 11

The partitioning of O_2 between the combustion stage and the reduction stage is investigated by changing the fraction of the total O_2 feed into two stages, keeping other parameters fixed. Calculation is carried out under condition where reductor coal primary N_2 is replaced by 25wt% of combustor secondary O_2 (Case 12). The gas temperatures profiles for Cases 1 and 12 are shown in Fig. 6-9. Case 12 predicts lower gas temperatures in the combustor and higher gas temperatures in the reductor compared to Case 1. A significant gas temperature difference between two cases about 300K is recorded near reductor burner at z/H_{comb}=2.2. This suggests that the partitioning of O_2 between two stages plays a significant role to control the gas temperature.

The carbon conversion for combustor coal decreases from 99 wt% to 97 wt%, while the reductor coal shows an increase in carbon conversion from 49 wt% to 57 wt%, if the gasification condition is changed from Case 1 to Case 12. Reductor carbon conversion increases due to increase in O_2 concentration in the reductor. However, the overall carbon conversion does not change significantly although the reductor gas temperature is higher for Case 12 than the Case 1. It indicates that the gas temperature is still not enough to advance char gasification reactions in the reductor under calculated condition.

The outlet concentration of soot decreases if the O_2 supply in the reductor is increased. Higher gas temperature in the reductor also increases the soot oxidation, resulting in a decrease in soot concentration in the gasifier. Instead char-CO_2 and char-H_2O reaction rate increases, producing higher carbon conversion and higher syngas heating value.
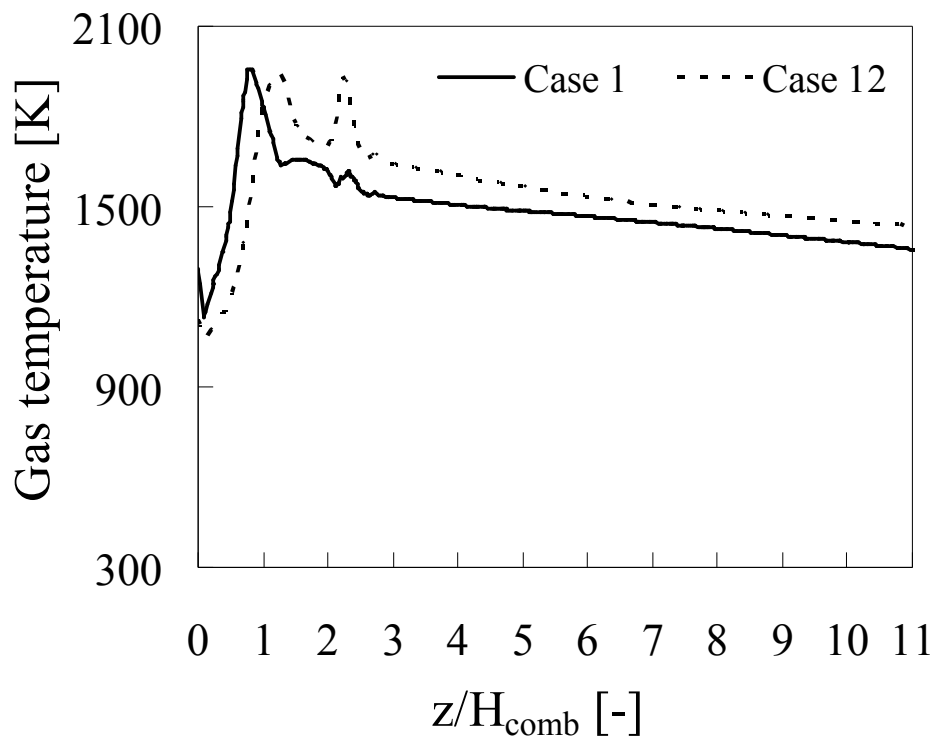

Figure 6-9 Effect of O_2 distribution between two stages on gas temperature profiles

The partitioning of coal between the combustion stage and reductor satge is numerically investigated by changing the fraction of the total coal feed rate into the combustor, holding other parameters fixed. The fraction of the combustor coal fed to the combustor is increased from 40 kg/h (Case 1) to 60 kg/h (Case 13). The carbon conversion for combustor coal decreases from 99 wt% to 83 wt% if combustor coal fed increases from 40 kg/h to 40 kg/h (Table 6-4). In contrast, reductor carbon conversion increases from 49 wt% to 54 wt% while decreasing the coal feed rate into the reductor. Table 6-4 also shows that outlet mass fraction of soot decreases from 1.79 wt% to 1.66 wt% if combustor coal fed increases from 40 kg/h to 60 kg/h. The production of volatiles component C_6H_6, which is precursor of soot formation, increases in the combustor due to increased coal feed rate. Since combustor is operated under higher temperatures and under higher O_2 concentrations, soot oxidation in the combustor increases, resulting in reducing soot concentration in the gasifier. The concentration of CO and H_2 decrease with decreasing coal feed rate into the reductor. Since the gasification reaction mainly occurs in the reductor zone, it is not recommended to decrease the feed rate of reductor coal although soot concentration is low for Case 13.

The effect of coal type on gas temperature and species concentration is numerically investigated. Another bituminous type coal, Taiheiyo coal (Case 14), is used to compare the results with the standard coal CV. The volatile matter is higher and the fixed carbon is lower in Taiheiyo coal than those in CV coal. The comparisons are shown in Table 6-5. Soot concentration increases from 1.79 wt% to 2.21 wt% due to increased volatile matter in Taiheiyo coal. CO concentration decreases from 16 wt% to 15 wt% because of lower fixed carbon in Taiheiyo coal.

Table 6-5 Analyses of CV coal (Canada) [7] and Taiheiyo bituminous coal [2]

Parameters	CV coal	Taiheiyo coal
Proximate analyses(ad)		
Moisture [wt%]	6.22	5.30
Fixed carbon [wt%]	49.00	35.80
Volatile matter [wt%]	34.50	46.70
Ash [wt%]	10.28	12.10
Ultimate analyses(db)		
C [wt%]	69.90	77.60
H [wt%]	4.30	6.50
O [wt%]	13.70	13.90
N [wt%]	1.07	1.13
Heating value [MJ/kg]	26.40	27.40

ad: air dried db: dry base

6.3.4 Effects of heat losses

The effects of heat losses are numerically investigated by changing the reductor wall boundary surface condition. For all cases (1 to 14), it is found that by changing various model parameters, kinetic reaction rates and operating conditions, it is possible to increase the carbon conversion of redcutor coal to a maximum value of 57 wt% (Case 12). One common reason for this limit is due to low gas temperature in the reductor. For this reason, a high temperature reductor wall at 1673K is considered here to ensure high gas temperature in the gasifier. Although it is an unusual condition for the real gasifier, this condition is applied to check what happen if the gasification occurs under higher temperatures condition. The calculated results are shown in Figs. 6-10 & 6-11.
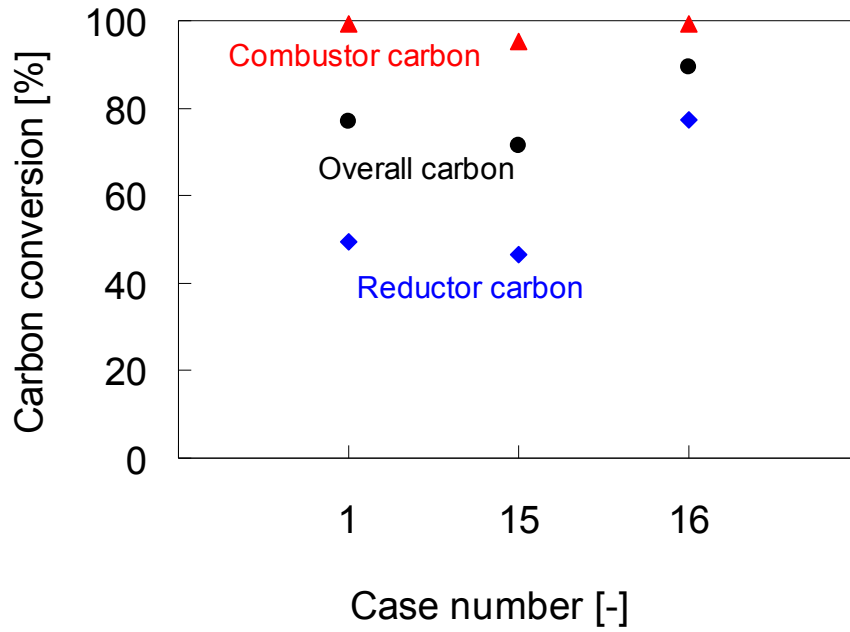
Figure 6-10 Effects of heat losses on carbon conversion
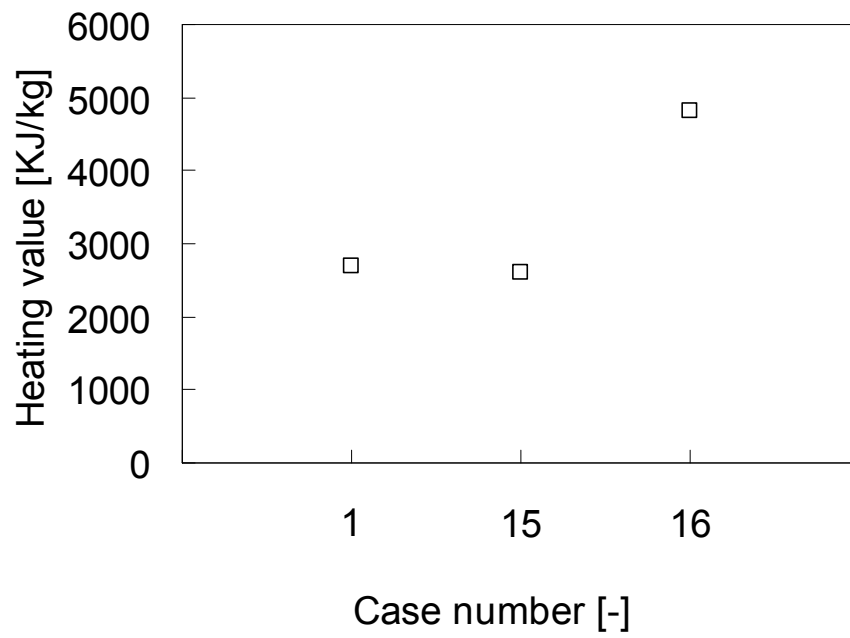

Figure 6-11 Effects of heat losses on product gas heating value

The effect of heat loss to the reactor wall on carbon conversion and species concentration is numerically studied. The heat loss for Case 15 is increased by 10% of the standard Case 1. With increasing heat loss to wall results in a decrease in carbon conversion from 77 wt% to 72 wt%. The gas temperature decreases with increasing heat loss to wall, while soot formation, CO and H_2 concentration remain unchanged.

In standard case, a constant heat flux to wall is given (Table 4-5). The reductor wall boundary condition is changed from a constant heat loss to a constant wall temperature. A constant reductor wall temperature at 1673K (Case 16) is set to ensure high gas temperature in the gasifier. A high wall temperature in the reductor produces higher gas temperatures in the gasifier, result in a significant rise in carbon conversion of reductor coal from 49 wt% to 77 wt%. Noticeable outlet concentrations about 32 wt% and 0.58 wt% are obtained for CO and H_2, respectively. Therefore, it can be concluded that to get higher carbon conversion from coal gasification it is necessary to increase the gas temperature in the reductor. Besides this the inlet concentration of gasification agents ($CO_2/O_2/H_2O$) should be increased. The effects of CO_2 and O_2 concentration on carbon conversion, syngas production and soot formation are discussed in next paragraphs.

6.3.5 Effect of CO_2 concentration

The effect CO_2 concentration on gas temperature, species concentration, carbon conversion etc. is numerically investigated by changing the inlet concentration of CO_2 at constant O_2 ratio (=0.528). CO_2 concentration is increased by decreasing the N_2 concentration in the primary and secondary gas inlet at combustor. Inlet conditions are shown in Table 6-6. The aim of this numerical study is to increase the production of syngas and carbon conversion from coal gasification.

Table 6-6 Conditions of inlet gas for various CO_2 concentration

Parameters				
Combustor coal: 38.5 kg/h				
Primary gas (PG) flow rate [91.6 kg/h]				
PG CO_2 concentration [wt%]	0.0	20.0	60.0	60.0
PG O_2 concentration [wt%]	23.0	23.0	23.0	23.0
PG N_2 concentration [wt%]	77.0	57.0	17.0	17.0
Secondary gas (SG) flow rate [224.3 kg/h]				
SG CO_2 concentration [wt%]	0.0	0.0	0.0	50.0
SG O_2 concentration [wt%]	28.4	28.4	28.4	28.4
SG N_2 concentration [wt%]	71.6	71.6	71.6	21.6
Combustor char: 26.9 kg/h				
Primary gas (PG) flow rate [60.3 kg/h]				
PG CO_2 concentration [wt%]	100.0	100.0	100.0	100.0
PG O_2 concentration [wt%]	0.0	0.0	0.0	0.0
PG N_2 concentration [wt%]	0.0	0.0	0.0	0.0
Reductor coal: 60.8 kg/h				
Primary gas (PG) flow rate [70.0 kg/h]				
PG CO_2 concentration [wt%]	0.0	0.0	0.0	0.0
PG O_2 concentration [wt%]	23.0	23.0	23.0	23.0
PG N_2 concentration [wt%]	77.0	77.0	77.0	77.0
Overall CO_2 concentration [wt%]	**14.0**	**18.0**	**26.0**	**50.0**
Overall O_2 concentration [wt%]	**23.0**	**23.0**	**23.0**	**23.0**

The average gas temperature profiles for various CO_2 concentrations at constant O_2 ratio are shown in Fig. 6-12. It is found that the gas temperature decreases with increasing the overall concentration of CO_2 at gasifier inlet. The gas temperature decreases with increasing the CO_2 concentration due to increased char-CO_2 reaction rate. Under CO_2-rich concentration, endothermic reaction (Reverse reaction of R2) also increases, resulting in a decrease in gas temperature.
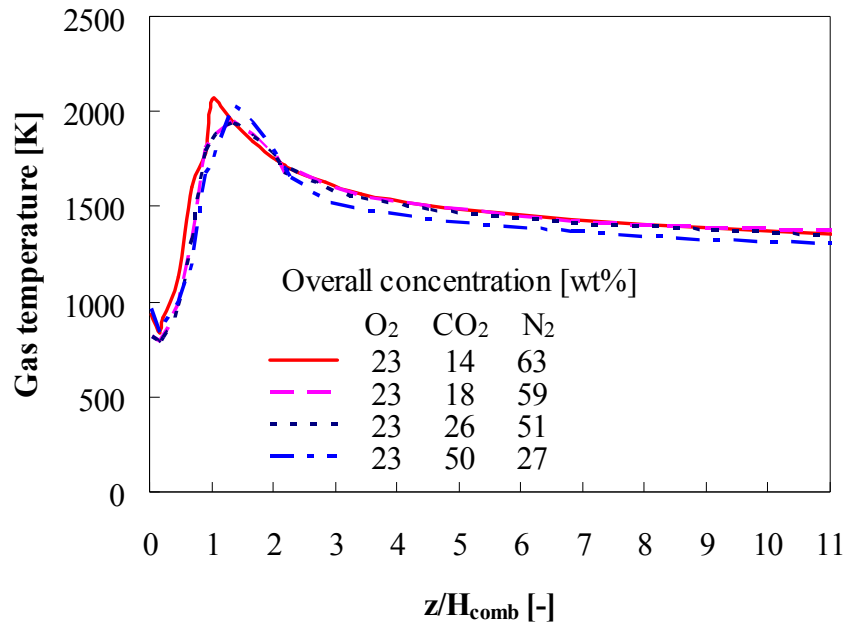

Figure 6-12 Effect of overall concentration of CO_2 on average gas temperature profiles

The syngas (CO and H_2) concentration profiles for various cases are shown in Figs. 6-13 and 6-14. It clearly shows that CO concentration increases with increasing the CO_2 concentration. The significant difference for various cases is obtained in the reductor zone. If the inlet concentration of CO_2 is increased to 50wt%, outlet CO concentration becomes 23 wt%. H_2 concentration decreases slightly when the CO_2 concentration is increased. This reduction in H_2 concentration does not affect the syngas gas heating value (Fig. 6-15) due to significant rise in CO concentration.

Carbon conversions for various cases are shown in Fig. 6-16. It is found that the reductor carbon conversion gradually increases with increasing the CO_2 concentration, while the combustor carbon conversion initially increases and then decreases at a high CO_2 concentration (50 wt%). Reductor carbon conversion increases from 49 wt% to 57 wt% if the inlet concentration of CO_2 is increased from 14 wt% to 50 wt%. This means the effect of CO_2 concentration is very small in the reductor at higher CO_2 concentrations. On the other hand, in the combustor the carbon conversion decreases from 99 wt% to 92 wt%, resulting in a decrease of overall carbon conversion. Therefore, it is not recommended to use more CO_2 to get efficient carbon conversion in coal gasification. Since high CO_2 concentration also causes the gasifier temperature down and affects the gasification characteristics, a very high CO_2 concentration may not be suitable in the real gasification process. Considering the carbon conversion and the limitation of CO_2 concentration in the gasifier, it can concluded that the use of 20 to 25 wt% CO_2 will be enough to produce optimum syngas heating value for the present calculation.

The changes of outlet concentration of species (CO, CO_2, H_2, H_2O and soot) with increasing the CO_2 concentration in the gasifier are shown in Figs. 6-17 and 6-18. The concentration of CO, CO_2 and H_2O increase, while a decrease in H_2 concentration is found if the inlet concentration of CO_2 is increased. The trends in species concentrations are similar to the results explained in Chapter 5. Soot concentration increases slightly with increasing the CO_2 concentration. At higher CO_2 concentrations, since the gas temperature and the relative diffusion of O_2 decrease, the oxidation of soot also decreases. This results in an increase in soot concentration. Therefore, to decrease the soot concentration, it is necessary to increase the gas temperature as well as O_2 concentration. The effect of O_2 concentration is discussed in the following section.
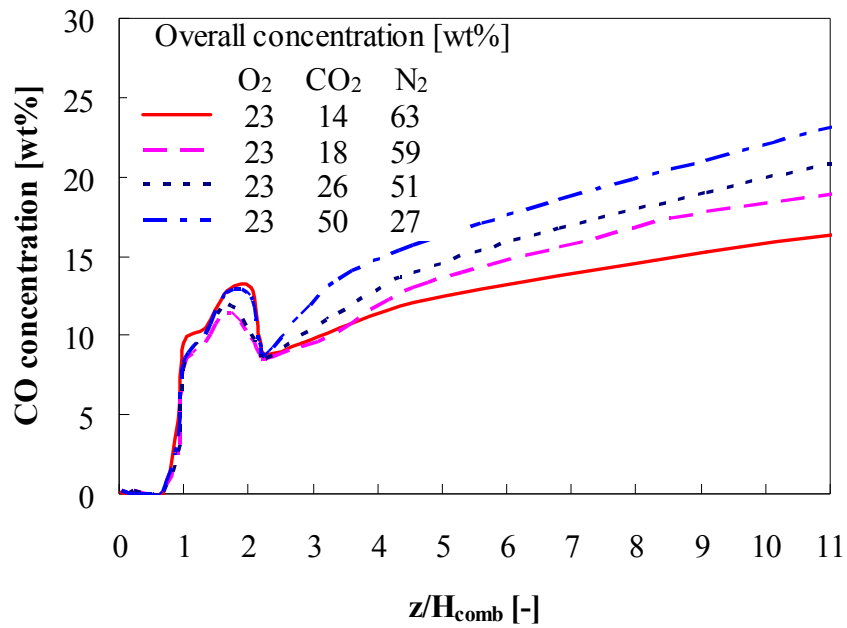
Figure 6-13 Effect of overall CO_2 concentration on average CO concentration profiles

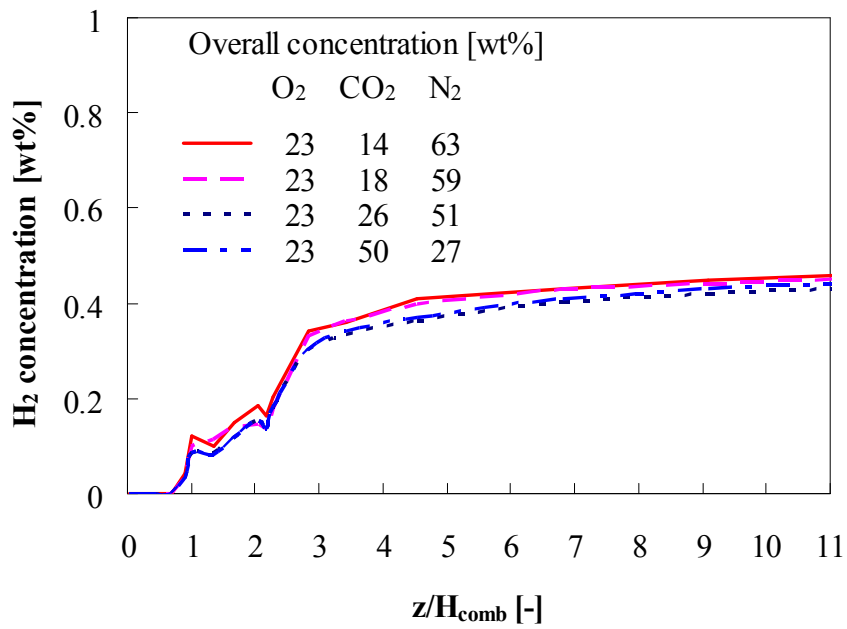**Figure 6-14** Effect of overall CO_2 concentration on average H_2 concentration profiles
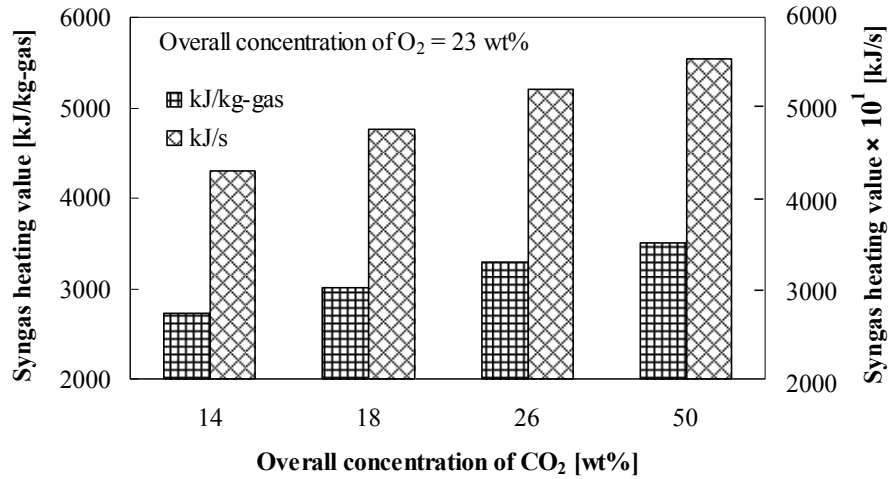
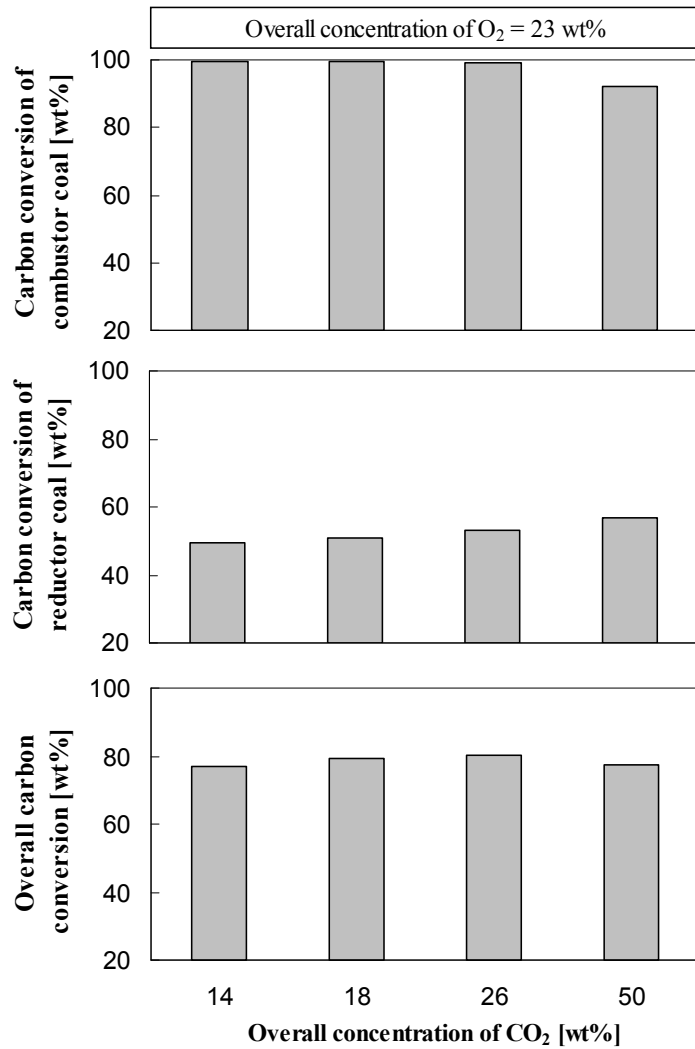**Figure 6-15** Effect of overall CO_2 concentration on syngas heating value

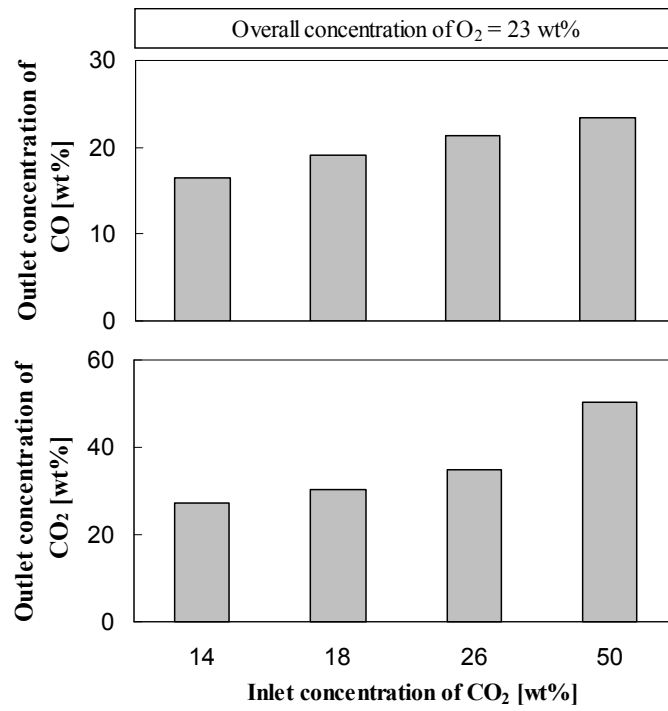**Figure 6-16** Effect of overall CO_2 concentration on carbon conversions

142

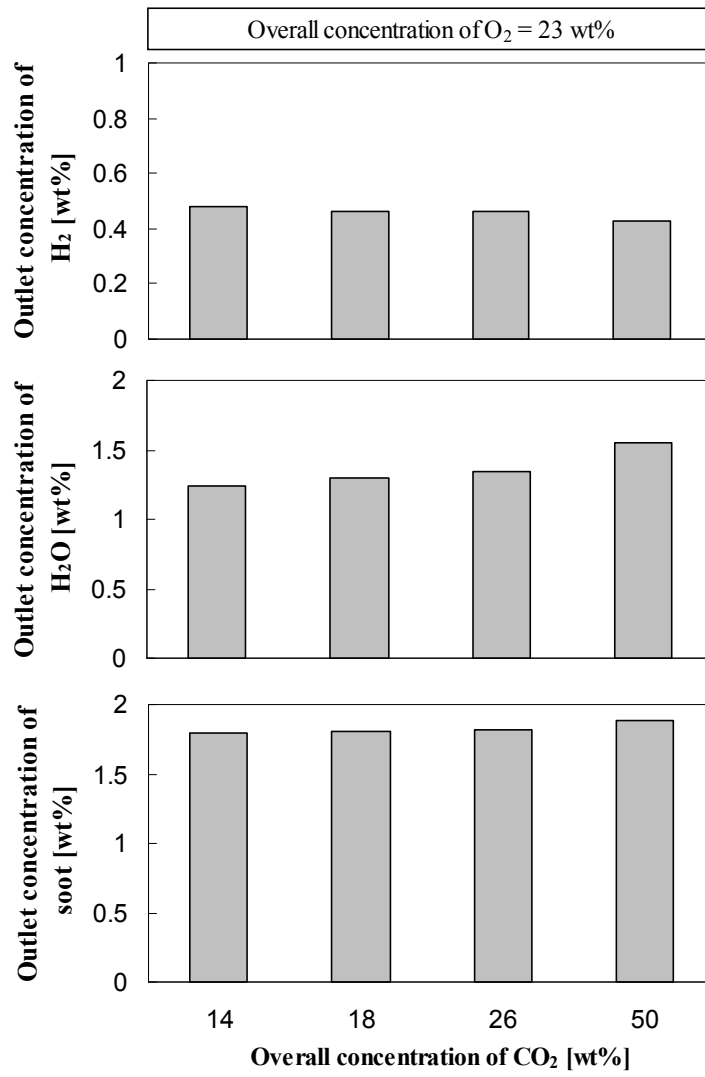**Figure 6-17** Effect of overall CO_2 concentration on outlet CO and CO_2 concentrations

Figure 6-18 Effect of overall CO_2 concentration on outlet H_2, H_2O and soot concentration

144

6.3.6 Effect of O_2 ratio

The effect of O_2 ratio on syngas heating value, carbon conversion and soot formation is numerically investigated under CO_2/O_2 gasification condition. The O_2 ratio is increased by increasing the O_2 concentration in the secondary gas inlet at combustor, keeping all other parameters fixed.

The average gas temperature profiles for various O_2 ratios under constant CO_2 concentration are shown in Fig. 6-19. It clearly shows that with increasing the O_2 ratio in the gasifier the gas temperature increases significantly. At higher O_2 ratios, the oxidation reaction increases, resulting in a significant rise in gas temperature. The average species concentration profiles for CO and H_2 are shown in Figs. 6-20 and 6-21.
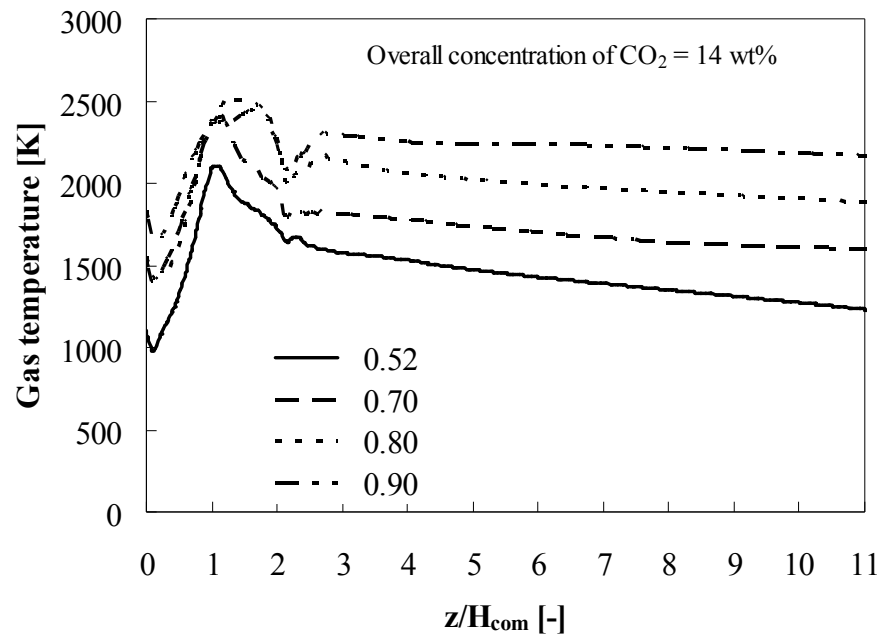

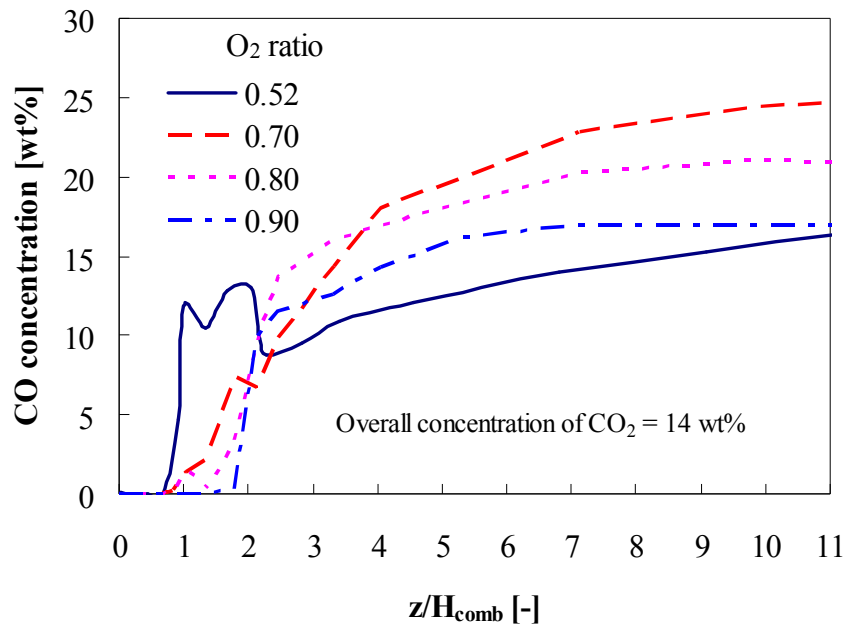**Figure 6-19** Effect of O_2 ratio on average gas temperature profiles

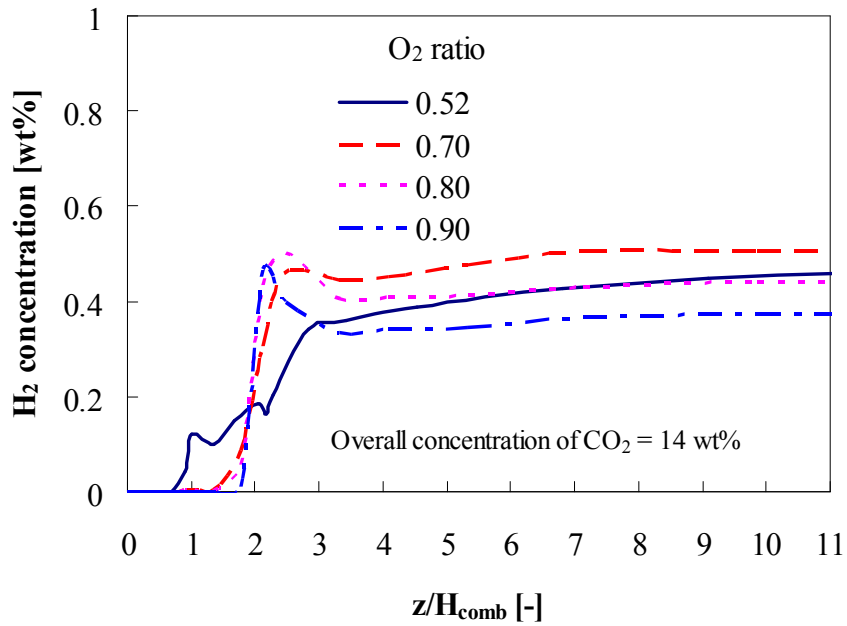**Figure 6-20** Effect of O_2 ratio on average CO concentration profiles

Figure 6-21 Effect of O_2 ratio on average H_2 concentration profiles

The syngas heating value increases with increasing the O_2 ratio, and reaches a maximum value of 3800 KJ/kg when the O_2 ratio is increased to 0.7 [Fig. 6-22]. After this limit heating value decreases with increasing O_2 ratio.

The changes of outlet species concentration with increasing O_2 ratio are shown in Figs. 6-23 & 6-24. It is found that CO and H_2 concentrations initially increase with increasing the O_2 ratio and then decrease. An increase in CO concentration indicates that oxidation of char tends to increase under higher O_2 ratios. At the same time when CO concentration increases, CO_2 and H_2O concentration decrease. This means char-CO_2 and char-H_2O reaction also enhances if O_2 ratio is increased. Although these two reactions are endothermic, the gas temperature increases due to significant rise in char-O_2 oxidation reaction. Figure 6-25 shows that carbon conversion increases with increasing the O_2 ratio, reaches a complete (100%) conversion when the O_2 ratio becomes 0.8. However, the maximum syngas heating value (3800 KJ/kg) is obtained when the carbon conversion becomes 94 wt%. If the target is to get a complete conversion of carbon, a lower heating value gas will be produced from the coal gasification.

It is also noticeable that the point where the syngas heating value or syngas concentration reaches a maximum value, CO_2 concentration becomes minimal at that condition. This indicates that if the gasification is carried out with O_2 ratio at 0.7, it is possible to get maximum heating value gas with the minimum CO_2 production, under the present condition.

The formation of soot slightly decreases with increasing the O_2 ratio until 0.7. After that a sharp decrease in soot formation is obtained if the O_2 ratio is increased. This indicates that soot oxidation reaction becomes noticeable under high gas temperature and high O_2 ratio.
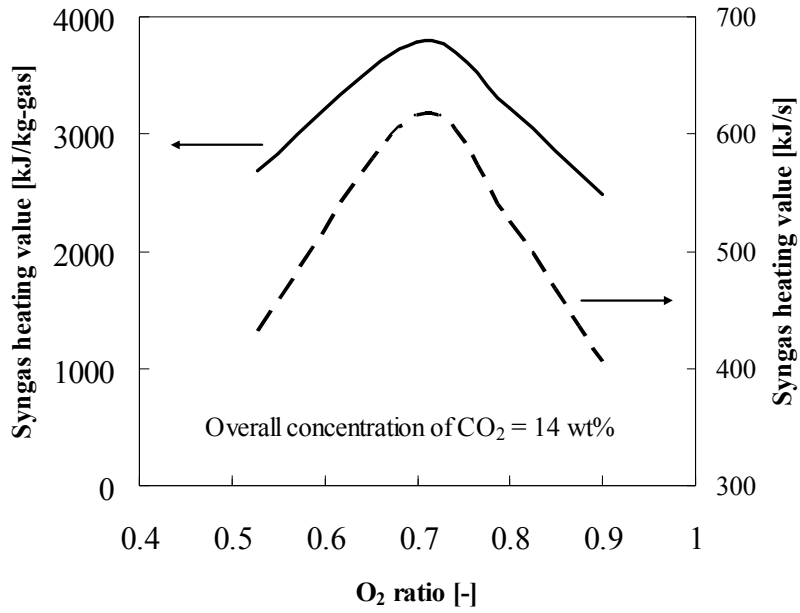
Figure 6-22 Effect of O_2 ratio on syngas heating value
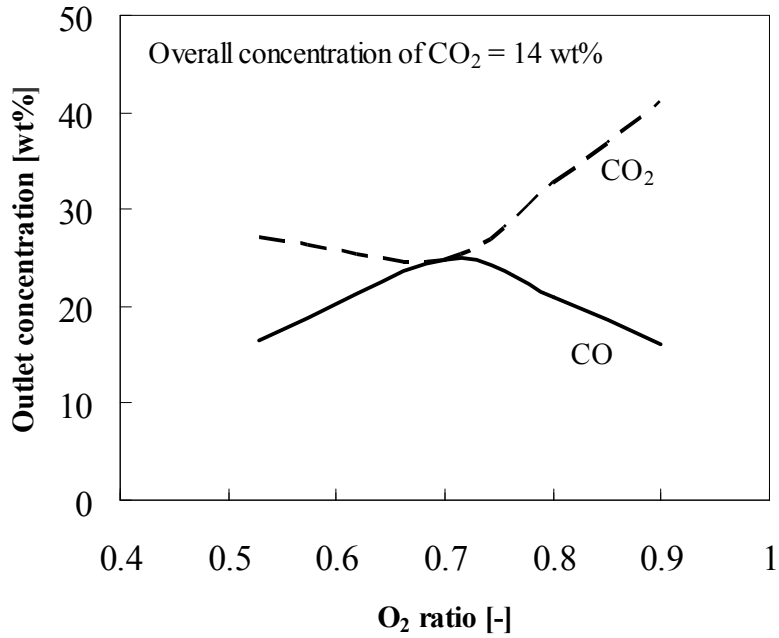

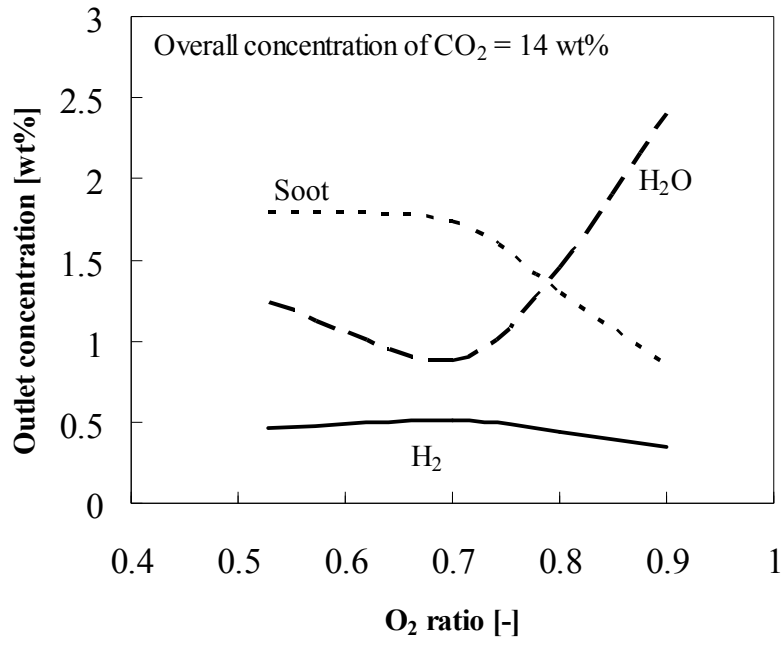**Figure 6-23** Effect of O_2 ratio on outlet average CO and CO_2 concentrations

Figure 6-24 Effect of O_2 ratio on outlet average soot, H_2 and H_2O concentrations
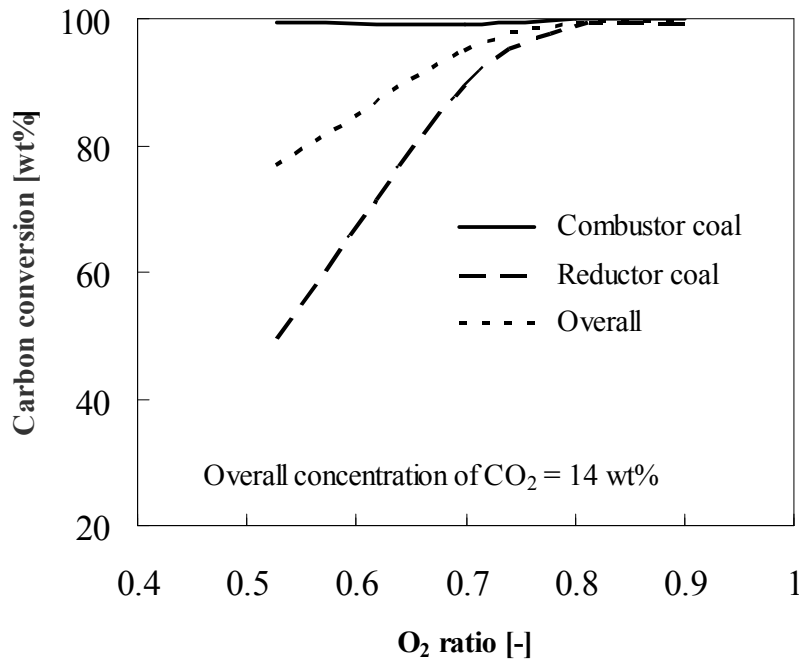

Figure 6-25 Effect of O_2 ratio on carbon conversion

6.4 Chapter conclusions

The numerical simulations of coal gasification in two stage entrained flow gasifier are carried out under various gasification conditions listed in Table 6-4. It is found that the carbon conversions of combustor coal lie in the ranges from 97 wt% to 99 wt% for most of the calculated conditions. While the carbon conversion of reductor coals varies from 45 wt% to 57 wt%. A noticeable change is obtained when the gasification occurs under a high temperature condition (Refer to Case 16). The major results are summarized as:

a) The carbon conversion of reductor coal is comparatively lower than the combustor coal, because reductor is operated under lower temperatures.

b) Remarkable outlet concentrations about 32 wt% and 0.58 wt% are obtained for CO and H_2, respectively if high temperature is maintained in the reductor. At a high temperature (1673K), the overall carbon conversion becomes 89 wt%.

c) High CO_2 concentration can produce high heating value syngas. However, a very high inlet concentration of CO_2 lowers the carbon conversion in combustor.

d) To get efficient coal conversion, coal gasification should be carried out with higher O_2 ratio under CO_2/O_2 gasification condition.

References

[4] Chen C., Masayuki H. and Toshinori K., "Numerical simulation of entrained flow coal gasifiers Part I: modeling of coal gasification in an entrained flow gasifier", *Chemical Engineering Science*, 55, 3861-3874 (2000).

[5] Chen C., Masayuki H. and Toshinori K., "Numerical simulation of entrained flow coal gasifiers Part II: effects of operating conditions on gasifier performance", *Chemical Engineering Science*, 55, 3875-3883 (2000).

[6]   Silaen A. and Wang T., "Effect of turbulence models on gasification simulation", *Proceedings of the 25th International Pittsburgh Coal-Gen Conference*, Pittsburgh, Pennsylvania, September (2008).

[7]   Silaen A. and Wang T., "Effects of fuel injection angles on performance of a two stage coal gasifier", *Proceedings of the 23rd Pittsburgh Coal Conference*, Pittsburgh, Pennsylvania, September (2006).

[8]   Silaen A. and Wang T., "Effect of turbulence and devolatilization models on coal gasification simulation in an entrained-flow gasifier", *International Journal of Heat and Mass Transfer*, 53, 2074–2091 (2010).

[9]   National Institute of Standards and Technology (NIST) chemistry web book.

[10]   Kidoguchi K., Kajitani S., Oki Y., Umemoto S., Umetsu H., Hamada H. and Hara S., "Evaluation of CO_2 Enriched Gasification Characteristics Using 3t/d Bench Scale Coal Gasifier - Influence of CO_2 Concentration in Gasifying Agent", *CRIEPI Energy Engineering Research Laboratory Report*, M11019 (2012).

CHAPTER 7

CONCLUSIONS

7.1 Concluding remarks

This thesis systemically conducted the numerical simulation of coal volatiles gasification, soot formation in coal volatiles gasification and coal gasification including soot formation under various gasification conditions. From this thesis, the following conclusions are drawn:

Chapter 1 gave an introduction to the contribution of coal to the global energy demand. The energy production from coal fired power plant is increasing day by day, which result in increased CO_2 emission from the existing power plant. However, CO_2 emission from coal gasification can be reduced if an efficient $CO_2/O_2/N_2$ coal gasification is implemented in IGCC system.

Chapter 2 discussed the study of reaction mechanism in coal volatiles gasification under various conditions. In this chapter, the detailed reaction mechanism (255 species and 1095 elementary reactions) is reduced by using the rate of production analysis under $CO_2/O_2/N_2$ gasification condition. The derived reduced mechanism consists of 46 chemical species and 165 elementary chemical reactions, which is validated under various gasification conditions. The effect of CO_2/O_2 mixtures is evaluated under $CO_2/O_2/N_2$ gasification conditions in an effort to increase syngas and decrease soot and CO_2 emissions. Higher temperatures result in an increase in CO and H_2 concentrations and a decrease in PAHs and soot concentrations compared with lower temperatures. CO_2 inlet mass fraction shows a large effect on PAHs/soot reduction at higher temperatures. At lower temperatures, the O_2 input becomes important in reducing PAHs/soot.

Chapter 3 discussed the effect of various types of reaction mechanism (detailed and overall) on product gas concentration. The large number of species and reactions sometimes make difficulty to run the simulation especially for the complex flow system. One step soot model is proposed in here to implement it in coal gasification simulation for predicting soot in two stage entrained flow coal gasifier. The calculated trend of species concentration shows a reasonable agreement with those of the detailed mechanism with soot.

Chapter 4 explained various models and sub-models used for the simulation of coal gasification in this study.

Chapter 5 explained the results for the numerical simulation of coal gasification with soot formation in two stage entrained flow gasifier under various gasification conditions. It is found that the contribution of the combustor to the overall CO and H_2 production is very small relative to the reductor. However, the combustor plays a major role in increasing gas temperature. In contrast, soot formation decreases the gas temperature in the gasifier because of high heat capacity of PAH/soot produced in the gasification process. Some higher soot is formed in the reductor part near the gasifier wall which may be similar to the deposition of soot at real gasifier wall. Coal gasification under CO_2-rich environment shows that higher inlet CO_2 concentrations enhance the char-CO_2 reaction, result in an increase in CO concentration.

Chapter 6 discussed the sensitivity analysis of coal gasification in two stage coal gasifier under $CO_2/O_2/N_2$ gasification condition. The carbon conversion of reductor coal is comparatively lower than the combustor coal, because reductor is operated under lower temperatures. Remarkable outlet concentrations about 32 wt% and 0.58 wt% are obtained for CO and H_2, respectively if a high temperature is maintained in the reductor. Higher CO_2 concentrations can produce high heating value syngas. However, a high inlet concentration of CO_2 reduces the carbon conversion in combustor. On the other hand, with increasing the O_2 ratio, it is possible to increase the carbon conversion and syngas heating value. A maximum

153

heating value gas with the minimum CO_2 production can be obtained if the gasification is carried out with O_2 ratio at 0.7. The change of soot concentration under various gasification conditions is found to be limited. However, at higher O_2 ratios soot concentration disappears significantly.

7.2 Significant results

To predict the soot formation from coal gasification, a one step soot model is proposed which is capable of predicting similar trends in outlet species concentrations to the detailed soot formation mechanism (276 species, 2158 gas phase and 1635 surface phase elementary reactions).

Higher CO_2 concentrations can produce high heating value syngas. However, a very high inlet CO_2 concentration reduces the carbon conversion in the combustor. To get maximum syngas heating value from the coal gasification, O_2 ratio needs to be increased to 0.7.

7.3 Future works

Conduct the numerical simulation of coal gasification in a large scale coal gasifier by using the proposed one step soot model. After analyzing the calculated results for laboratory and large scale gasifier, required modification in one step soot model will be done.